The Role of microRNAs in the Regulation of Human UDP-glucuronosyltransferases (UGTs)

Dissertation

zur

Erlangung des Doktorgrades (Dr. rer. nat.)

der

Mathematisch-Naturwissenschaftlichen Fakultät

der

Rheinischen Friedrich-Wilhelms-Universität Bonn

vorgelegt von

Stefan Paulusch

aus

Bautzen

Bonn

November, 2020

Angefertigt mit Genehmigung der Mathematisch-Naturwissenschaftlichen Fakultät der Rheinischen Friedrich-Wilhelms-Universität Bonn

1. Gutachter: Prof. Dr. Christian Strassburg, Universitätsklinikum Bonn
2. Gutachter: Prof. Dr. Uwe Deppenmeier, Rheinische Friedrich-Wilhelms-Universität Bonn

Tag der Promotion: 29.04.2021
Erscheinungsjahr: 2021

Acknowledgments

Firstly, I would like to express my sincere gratitude to my advisor Professor Dr. Christian Strassburg for giving me the chance to carry out my doctorate in such a pleasant and welcoming atmosphere in the Department of Internal Medicine I, University Hospital Bonn.

My sincere thanks also go to Prof. Dr. Uwe Deppenmeier, Prof. Dr. Jörg Höhfeld and Prof. Dr. Ian Brock for the excellent supervision, as part of the Doctoral Committee.

I am equally grateful to my supervisor Dr. Sandra Kalthoff for the excellent guidance, insightful comments, and encouragement, but also for the hard questions which incented me to widen my research from various perspectives. Dr. Kalthoff's extensive experience in science and exceptional skills in the development of scientific experiments made a significant contribution towards the success of my doctorate project. A special thanks goes to my fellow PhD student Steffen Landerer, who was a guiding tutor and a friend who helped me to strive for excellence in research due to valuable discussions, suggestions, and advice in and around the lab. I am also very thankful to Master student Lena Menßen for the many funny talks in the office, and her helpful contribution in improving my writing skills. I will particularly miss the time having dinner all together and the hot wine gatherings at the Christmas market.

Very special gratitude goes to the next-door lab group AG Chang, in particular to Jennifer Söhne and AG Trebicka, currently working at the University Hospital Frankfurt for providing material, lab devices and the patient samples that helped to fulfill experimental requirements and supported the success of this project. I would also like to emphasize the excellent correspondence with Dr. Fernando Magdaleno and Gudrun Hack, their insight is kindly regarded.

Finally, I would like to express my gratitude to all maintenance and cleaning staff at Internal Medicine I, their active daily contribution guarantees a smooth and proper working environment at the Laboratories. Personally, I would like to thank my wife Judith Cruz-Espinoza for her limitless support, care and love throughout this project that helped me to be resilient, to remain motivated and passionate in scientific research. I will forever be thankful to my parents for supporting me in any possible way throughout my life and my Biotechnology studies.

Summary

The liver is the central organ of the body involved in endo- and xenobiotic metabolism. By activity of drug-metabolizing enzymes such as UDP-glucuronosyltransferases (UGTs) residing in the liver as well as other tissues of the gastrointestinal tract and beyond, lipophilic substances are conjugated with a sugar moiety rendering substances highly hydrophilic and easily excretable via bile or urine. Oxidative stress is a major inducer of liver injury and is associated with the development of liver diseases. UGTs metabolize a wide array of hazardous compounds and reactive metabolites and, therefore, contribute to the reduction of oxidative stress.

Transcriptional regulation of the *UGT1A* gene locus has been studied in detail. However, its post-transcriptional regulation has not been fully elucidated to date. MicroRNAs (miRNAs) are short (~22 nucleotides) endogenous, regulatory RNAs involved in the post-transcriptional regulation of target genes. MiRNAs bind to miRNA Recognition Elements (MREs) in the 3'-untranslated region (3'-UTR) of the target mRNA that forms a region of high complementarity (seed match), which results in mRNA degradation or translational inhibition. In this work, the role of miRNAs in the post-transcriptional regulation of *UGT1A* expression was investigated. A variety of miRNAs dysregulated in hepatocellular carcinoma were studied in UGT1A 3'-UTR luciferase assays and were overexpressed in HepG2, Kyse-70, and Caco-2 cell lines to evaluate a potential reduction of UGT1A mRNA and protein expression. Interestingly, two miRNAs (miR-214-5p and miR-486-3p) inhibited luciferase activity, UGT1A mRNA, and protein expression. The bioinformatic analysis within the UGT1A 3'-UTR revealed miRNA-binding sites. The mutation of putative responsible nucleotide sequences was able to recover luciferase activity demonstrating post-transcriptional regulation of miR-214-5p/486-3p via the beforehand identified MREs. Additionally, the application of antisense oligonucleotides inhibited miRNA functionality and restored luciferase activity. The study of the potential contribution of the identified miRNAs in the development of liver cirrhosis resulted in an upregulation of miR-486-3p within the serum of cirrhotic patients. Moreover, miR-486-3p was shown to be upregulated in male fibrotic *htgUGT1A*-WT mice leading to reduced UGT1A mRNA expression. This indicates a possible impact of miR-486-3p on glucuronidation capacity in fibrotic mice. The transfection of miR-486-3p into mice hepatocytes suggested a reduction of UGT enzymatic activity. In summary, miR-214-5p and miR-486-3p were discovered as two novel miRNAs regulating *UGT1A* expression by binding to target sites in the common UGT1A 3'-UTR resulting in the downregulation of UGT1A

mRNA and protein expression. Moreover, miR-486-3p is hypothesized to be a potential risk factor for the development or progression of liver fibrosis/cirrhosis due to a reduced UGT1A-mediated glucuronidation activity towards reactive metabolites and the potential disruption of the metabolic antioxidative balance in the liver.

Keywords:

- UDP-glucuronosyltransferases
- MicroRNAs
- Oxidative stress

Table of Contents

List of Figures

List of Tables

Abbreviations

Aqua dest.	Aqua destillata
AA	Amino Acid
AhR	Aryl Hydrocarbon Receptor
ALD	Alcoholic Liver Disease
ARE	Antioxidant Response Element
bp	base pair
ca	circa
CAR	Constitutive Androstane Receptor
°C	degree Celsius
CCl_4	Carbon tetrachloride
CRC	Colorectal Cancer
C-terminal	Carboxy-terminal
CYP	Cytochrome P-450
Da	Dalton
DMSO	Dimethyl Sulfoxide
DNA	Deoxyribonucleic acid
dNTP	Deoxynucleoside triphosphate
ds	double-stranded
ECM	Extracellular Matrix
E. coli	*Escherichia coli*
EDTA	Ethylenediaminetetraacetic Acid
e.g.	exempli gratia
et al	*et altera*
EtOH	Ethanol
FCS	Fetal Calf Serum
FXR	Farnesoid X Receptor
g	gram
GST	Glutathione S-Transferase
h	hour
HCC	Hepatocellular Carcinoma
HCV	Hepatitis C Virus
IgG	Immunoglobulin G

kb	kilobase
kDA	kilodaltons
kg	kilogram
LB-medium	Luria-Bertani medium
M	molar
MFE	Minimum Free Energy
mg	milligram
min	minute
miR/miRNA	MicroRNA
mL	milliliter
mM	millimolar
MRE	MicroRNA Recognition Element
nt	nucleotide
µg	microgram
µL	microliter
NAD(P)H	Nicotinamide Adenine Dinucleotide Phosphate Hydrogen
NAFLD	Non-Alcoholic Fatty Liver Disease
NASH	Non-Alcoholic Steatohepatitis
Nrf2	Nuclear factor erythroid 2-related factor 2
N-terminal	Amino-terminal
OD	Optical Density
ORF	Open Reading Frame
OS	Oxidative Stress
PBS	Phosphate Buffered Saline
PCR	Polymerase Chain Reaction
Pen/Strep	Penicillin/Streptomycin
PhiP	2-Amino-1-methyl-6-phenylimidazol[4,5-β] pyridine
PPAR	Peroxisome Proliferator-Activated Receptor
PXR	Pregnane X Receptor
RNA	Ribonucleic Acid
rpm	revolutions per minute
ROS	Reactive Oxygen Species
RT	Room Temperature

RXRα	Retinoid X Receptor alpha
SDS	Sodium Dodecyl Sulfate
SNP	Single Nucleotide Polymorphism
SOD	Superoxide Dismutase
s	second
siRNA	small interfering RNA
ss	single-stranded
Taq	*Thermus aquaticus*
TAE	Tris-Acetate-EDTA
TAMRA	Tetramethylrhodamine
U	Unit
UDP	Uridine Diphosphate
UGT	UDP-Glucuronosyltransferase
UTR	Untranslated Region
UV	Ultraviolet
WT	Wildtype
XRE	Xenobiotic Response Element

1 Introduction

1.1 Detoxification of Endo- and Xenobiotics by the Liver

The detoxification and elimination of endo- and xenobiotics is an essential part of human metabolism, which ameliorates substance-driven biological effects and their potentially harmful impacts. Many organs contribute to metabolism such as the lungs, kidneys, and intestines. However, the liver is one of the most metabolically active tissues [1]. The liver is the largest gland and the central metabolic organ of the body. Substances released from the intestine into the bloodstream are transported to the liver and its associated cells (hepatocytes) via the portal vein to be stored, utilized, converted, or detoxified. The liver stores polysaccharides, lipids, amino acids, and vitamins. It is the relevant synthesis site for coagulation factors, albumin, C-reactive protein, endogenous cholesterol, and bile. With the aim of eliminating toxins and other potentially hazardous compounds, about 2000 liters of blood are pumped through the liver daily. This allows the liver to convert toxic ammonia to non-toxic urea, and metabolize about 1 gram of alcohol per hour and per 10 kilograms body weight [2].

For detoxification purposes, the liver expresses a variety of drug-metabolizing enzymes that catalyze reactions in two major steps of biotransformation. These two enzymatically catalyzed phases of biotransformation are distinguished into: 1) functionalization and 2) conjugation reactions. In phase I, functional groups are added to, or unmasked within the target compound by oxidation, reduction, and hydrolysis reactions to increase the polarity of the compound. Typical functional groups include hydroxyl (-OH), sulfhydryl (-SH), carboxyl (-COOH), and amino (-NH_2) groups. Among others, cytochrome P-450 (CYP) enzymes are central to the catalysis of oxidation and reduction reactions accompanied by hydrolases to complete functionalization reactions [3]. In the second phase, the functionalized metabolite can be enzymatically conjugated with a polar group such as a sugar moiety (uridine diphosphate [UDP]-glucuronosyltransferases), sulfate (sulfotransferases), amino acids (N-acetyltransferases) or glutathione (glutathione S-transferases) to render the hydrophobic compound water-soluble and excretable [4]. Subsequently, the hydrophilic conjugates undergo carrier-associated transport from the cell into the water phase and are thereby eliminated from the body [5]. Therefore, CYP-mediated phase I reactions are associated with the generation of reactive oxygen species (ROS), whereas phase II reactions play an essential role for cellular defense against oxidative stress (OS)-related tissue injury [6].

1.2 Oxidative Stress

OS represents the cellular imbalance of oxidants and the antioxidant response [7]. The crucial component of OS are free radicals, which are molecules with an unpaired electron in their valence orbital [8]. Oxygen-containing free radicals with an unpaired electron are superoxide anion ($O_2^{\bullet -}$) or the hydroxyl radical ($OH^{\bullet}$), whereas oxygen derivates without an unpaired electron are hydrogen peroxide (H_2O_2), singlet oxygen ($^1O_2$) or hypochlorous acid (HOCl). Both types of oxygen-derived radicals can be summarized and are collectively termed as ROS. ROS are part of aerobic life and involved in the manifestation of vital cellular functions, including signal transduction, gene expression, and cellular growth or death [9]. ROS can be produced by the mitochondrial respiratory chain [10], CYP-derived oxidative metabolism [11], and auto-oxidation of endogenous substrates such as catecholamines, quinones, or heme proteins [12].

The primary goal of cellular redox homeostasis is to restrict ROS at levels that are not harmful for the organism. This is achieved by low-molecular-weight antioxidants (glutathione, vitamin E, beta-carotene, melatonin, etc.) or antioxidative enzymes (glutathione peroxidase, catalase or superoxide dismutase), which can remove or deactivate ROS [13-15]. However, when ROS levels become excessively high, this generates a redox imbalance, potentially leading to ROS-mediated oxidation of DNA, proteins, and lipids that may contribute to the pathogenesis of diabetes, cardiovascular and neurodegenerative disorders, or to severe liver diseases [8, 16-20].

1.3 Oxidative Stress-Induced Liver Diseases

OS is a driving force in many chronic liver diseases such as chronic hepatitis, liver fibrosis/cirrhosis, and hepatocellular carcinoma (HCC) [8]. Ethanol is a highly potent hepatotoxin and its metabolism generates increased hepatic levels of ROS. Under chronic alcohol consumption, high levels of ROS are generated by the various cell types of the liver, including hepatocytes, Kupffer cells (liver-specific macrophages), and hepatic stellate cells [21-24]. Hepatocytes are the major source of ROS through enzymatic activities of cytosolic alcohol dehydrogenase, NAD(P)H oxidase, or microsomal CYP2E1 enzymes that can release $O_2^{\bullet -}$ due to uncoupling of the catalytic cycle [25-27]. Among the consequences of alcoholic liver disease (ALD) are hepatic lipid accumulation (hepatic steatosis) and/or Kupffer cell-driven liver inflammation (alcoholic hepatitis) resulting in hepatocyte necrosis or apoptosis

that eventually activates profibrotic mechanisms leading to fibrosis. This pathological condition constitutes a highly dynamic scarring process of the liver characterized by the excessive accumulation of extracellular matrix (ECM) proteins and collagen [28-30] (Figure 1).

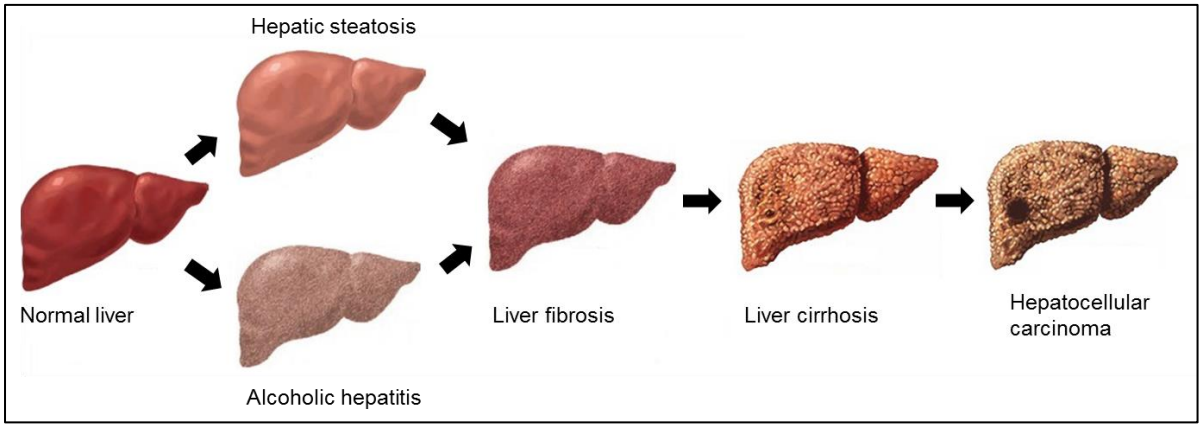

Figure 1. Stages of Liver Damage due to Excessive Alcohol Intake. Among others, alcohol is a detrimental hepatotoxin that induces chronic liver injury. It is metabolized in hepatocytes by alcohol dehydrogenase and cytochrome P450 2E1, which results in elevated production of reactive oxygen species (ROS). Ethanol-induced dysregulation of profibrotic signaling pathways, chemokines, and inflammatory cytokines lead to fatty liver (hepatic steatosis) and/or hepatocyte inflammation (alcoholic hepatitis). Hepatocyte apoptosis/necrosis and macrophages (Kupffer cells) release high levels of ROS, which leads to the activation of hepatic stellate cells that form scar tissue by the deposition of extracellular matrix proteins and collagen (liver fibrosis). The irreversible end-stage of chronic liver injury is cirrhosis that most often ends in HCC. The figure was modified from [31].

If the deleterious stimuli persist, liver fibrosis may progress to liver cirrhosis, which may result in liver failure or HCC [32]. Other conditions that can cause liver cirrhosis are viral hepatitis, cholestasis, and non-alcoholic steatohepatitis (NASH), which are all inevitably associated with OS [33-35]. Antioxidant enzymes actively remove ROS and thereby maintain a balance between the oxidant and antioxidant response [36]. The identification of molecular mechanisms, capable of influencing antioxidative enzymes involved in the protection against reactive metabolites is of crucial importance to counteract the OS-induced development of liver diseases. Together with other cytoprotective enzymes, UDP-glucuronosyltransferases (UGTs) play an essential role for cellular defense against reactive metabolites and are consequently functionally classified to act as indirect antioxidants [4, 37].

1.4 UDP-glucuronosyltransferases

UGTs are a superfamily of transferases (EC 2.4.1.17) localized in the smooth endoplasmic reticulum (ER) involved in the covalent linkage of lipophilic endo- and xenobiotics with glucuronic acid provided by UDP-glucuronic acid. UGTs render the hydrophobic parent compound water-soluble, biologically inactive, and readily excretable via bile or urine (Figure 2). A plethora of endobiotic (bile- and fatty acids, bilirubin, steroids, thyroid hormones) and xenobiotic substances (therapeutic drugs, carcinogens, environmental pollutants) are removed from the body via glucuronidation [38]. UGTs catalyze the transfer of glucuronic acid to many commonly occurring functional groups (-OH, -COOH or -NH_2), whereby structurally diverse compounds can be subjected to glucuronidation [6].

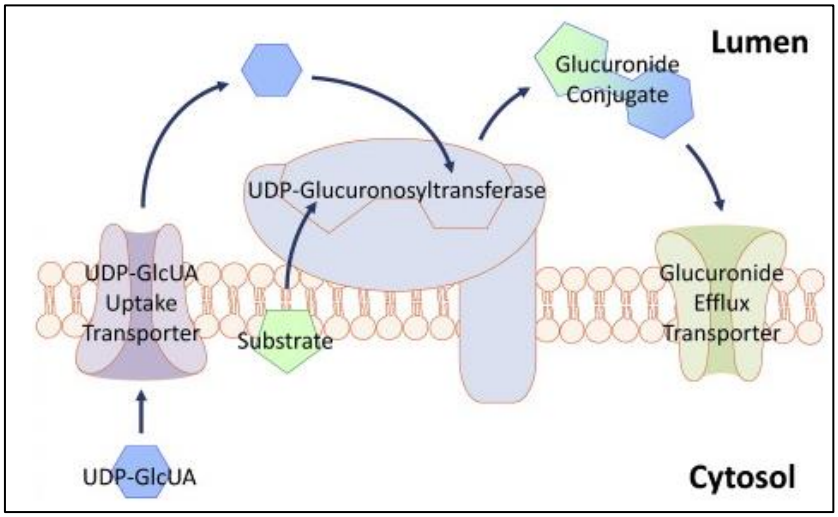

Figure 2. Subcellular Localization and Catalytic Activity of UDP-glucuronosyltransferases (UGTs). UGTs are anchored by their C-terminal transmembrane domain to the smooth endoplasmic reticulum (ER) membrane, whereas the N-terminal domain with the active site is located in the ER lumen. Co-substrate UDP-glucuronic acid (UDP-GlcUA) is imported by UDP-GlcUA uptake transporters, lipophilic substrates diffuse through the membrane and are both covalently linked by UGTs. The resulting water-soluble glucuronide is exported by glucuronide efflux transporters to the cytosol to be finally removed by biliary or renal elimination. The figure was modified from [6].

UGTs are synthesized as multi-domain proteins, transported, and inserted into the ER by an amino (*N*)-terminal signal peptide and anchored by a carboxy (*C*)-terminal transmembrane domain and an ER retention signal. Hybrid protein synthesis and sequence analysis found that the conserved *C*-terminal domain is involved in UDP-glucuronic acid binding, whereas the variable *N*-terminal half provides substrate binding [39, 40]. Comparative human cDNA analysis confirmed UGTs to consist of a set of 285-289 variable *N*-terminal and 246 identical *C*-terminal amino acids (AAs) domains [41].

To date, 22 human UGT proteins have been identified, distributed across four UGT families (UGT1, UGT2, UGT3, and UGT8) [42]. However, the most catalytically active subfamilies are UGT1A, UGT2A, and UGT2B [43].

The human *UGT1A* locus is located on chromosome 2q37, spans about 200 kb, and encodes nine functional isoenzymes of 50–60 kDa [44, 45]. UGT1A messenger RNAs (mRNAs) are generated by combining an individual isoform-specific exon 1 with the common exons 2-5, including 3'-untranslated region (UTR) (Figure 3). Every *UGT1A* gene is regulated by its own promoter, which leads to isoform-specific expression mediated by different transcription factors (TFs) [46]. Nevertheless, the prevalence of single nucleotide polymorphisms (SNPs) in *UGT1A* promoters or coding sequences was described to alter *UGT1A* transcriptional induction and enzymatic properties, and SNPs exhibit frequencies up to 40 % in the white population [45].

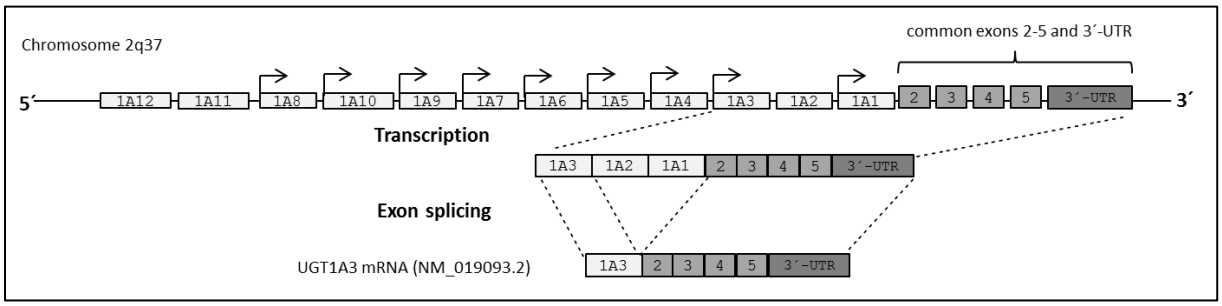

Figure 3. Generation of UGT1A Transcripts by Exon Sharing. The *UGT1A* locus is located on chromosome 2q37 and is composed of nine isoform-specific first exons (1A1-1A10; *UGT1A2*, *UGT1A11* and *UGT1A12* are pseudogenes) and four shared exons 2-5, including a common 3'-untranslated region (3'-UTR). Transcription of each *UGT1A* gene is tissue-specific and inducible by its own promoter. Transcripts are generated by exon sharing outlined for UGT1A3 mRNA (NCBI, NM_019093.2). The figure was modified from [45, 47].

1.5 Transcriptional Regulation of the *UGT1A* locus

UGT1A genes are subject to constitutive and inducible expression regulated by TFs targeting their binding sites in the 5'-upstream promoter regions [48]. For instance, the constitutive expression of UGTs is regulated by TF hepatocyte nuclear factors (HNF) 1α and 4α in hepatic or extrahepatic tissues, in combination with intestine-specific TF caudal-related homeodomain protein 2 [49, 50]. On the other hand, the inducible *UGT1A* expression is regulated by tissue-specific (ligand-activated) TFs. Among others, these TFs involve nuclear receptors, including farnesoid X receptor (FXR), constitutive androstane receptor (CAR), and pregnane X receptor (PXR) [48]. A common feature of FXR-, CAR- and PXR-regulated DNA binding is the dependence on heterodimerization with retinoid-X-receptor alpha (RXRα) likewise a TF and a member of the nuclear receptor superfamily [51, 52]. The aryl

hydrocarbon receptor (AhR), which is not part of the nuclear receptor superfamily, is a ligand-dependent TF capable of inducing drug metabolizing enzyme gene (e.g. *CYP450* or *UGT1A*) expression in response to xenobiotic stress [53].

After ligand binding to AhR (e.g. polycyclic aromatic hydrocarbon such as benzo(α)pyrene), AhR translocates into the nucleus and forms a heterodimer together with AhR nuclear translocator (ARNT) [54]. The AhR-ARNT heterodimer binds to 5'-regulatory regions such as xenobiotic response elements (XRE) identified in the promoters of *UGT1A* genes that induces their transcription [55]. The intracellular OS sensor nuclear factor erythroid 2-related factor 2 (Nrf2) is a TF that underlies cullin 3 (CUL3)-Kelch-like ECH-associated protein 1 (Keap1)-mediated ubiquitination and degradation under normal conditions [56]. In response to OS, Keap1 is inactivated releasing Nrf2 from cytoplasmic sequestration. Activated Nrf2 translocates into the nucleus, binds to antioxidant response elements (ARE), which results in the transcription of cytoprotective genes [57]. A coordinated Nrf2- and AhR-dependent transcriptional regulation of *UGT1A* genes has been described [58]. A brief explanation of the individual UGT1A isoforms is provided in the following sections.

1.5.1 UGT1A1

UGT1A1 is highly expressed in the liver and the gastrointestinal (GI) tract, including the small intestine, colon, and stomach [59]. It is involved in the detoxification of endogenous bilirubin (a degradation product of heme-containing proteins) and a myriad of xenobiotics such as therapeutic agents, 2-hydroxyestrone, oestradiol, irinotecan metabolites, and mutagenic xenobiotics [43, 60, 61]. *UGT1A1* transcription is induced by HNF1, upstream stimulating factor, AhR, CAR, PXR, or peroxisome proliferator-activated receptor (PPAR). However, *UGT1A1* transcription is reduced by SNPs in the *UGT1A1* promoter and coding sequence [62].

1.5.2 UGT1A3

UGT1A3 is expressed in the intestine, and at lower levels in the liver and extrahepatic tissues such as the colon, and stomach [63]. It is involved in the glucuronidation of bile acids, estrogens, and vitamin D derivatives. Xenobiotic substances include benzo(α)pyrene metabolites or non-steroidal anti-inflammatory drugs (e.g. ibu-, flurbi- or ketoprofen), which induce *UGT1A3* transcription mediated by AhR [45, 64, 65]. The *UGT1A3* gene shares high homology in the coding (> 90 %) and promoter (> 80 %) region with the *UGT1A4* gene [66], which commonly leads to the shared *N*-glucuronidation of primary, secondary, and tertiary

amines [67]. *UGT1A3* transcription can be induced by FXR or PPAR, while respective binding sites are lacking in the *UGT1A4* promoter [48].

1.5.3 UGT1A4

UGT1A4 is expressed in the liver and various other tissues, including the bile ducts, colon, and small intestine [45]. As outlined in section 1.5.2, the human *UGT1A4* gene is closely related to *UGT1A3* and it catalyzes the glucuronidation of a variety of endo- and exogenous compounds, including antidepressants, anticonvulsants, and environmental mutagens [68]. In return, xenobiotics induce *UGT1A4* transcription via AhR that is able to access two XRE elements located in the *UGT1A4* promoter [69].

1.5.4 UGT1A6

UGT1A6 is widely expressed in human tissues at different levels, including the liver, small intestine, and colon [70]. It is described as “phenol UGT” due to its ability to catalyze the glucuronidation of planar phenols (e.g. 1-naphthol or 4-nitrophenol), phenolic benzo(α)pyrene metabolites, and carcinogenic arylamines [45, 71]. It glucuronidates endogenous serotonin and the therapeutic drug paracetamol [72, 73]. These compounds serve as ligands for tissue-dependent and xenobiotic-derived transcriptional regulation by either AhR or Nrf2, as well as PXR and CAR [70].

1.5.5 UGT1A7

The *UGT1A7* gene product is highly expressed in extrahepatic tissue (the small intestine, colon, and kidneys) and at minute amounts in the liver, if at all biologically relevant [59]. Therefore, UGT1A7 was suggested to provide initial glucuronidation at the entry point of xenobiotics, i.e. aerodigestive tract (e.g. esophagus, stomach, and trachea) [48]. UGT1A7 catalyzes the glucuronidation of a spectrum of xenobiotics, including mutagens, phenols, anthraquinones, flavones or naphthol structures [45, 48]. A higher affinity for irinotecan metabolites (SN-38) has also been observed in UGT1A7 compared to UGT1A1 [74]. A number of *UGT1A7* genetic variants were identified, for instance *UGT1A7*3*, resulting in AA substitutions of exon 1 causing a lowered catalytic activity of UGT1A7 [75]. *UGT1A7*3* encodes a protein with low detoxification activity and represents a risk factor for the development of HCC [76].

1.5.6 UGT1A9

UGT1A9 is primarily expressed in the liver [48]. Additionally, it is highly expressed in the kidney, and at variable levels in other tissues such as colon, adrenal, and bladder [77]. Its broad substrate specificity encompasses anticancer agents, catechol estrogens, fatty acids, and mutagenic arylamines [78-80]. *UGT1A9* expression is induced by HNF1α/ 4α, AhR, Nrf2, and PPAR [48, 50, 81-83].

1.6 MicroRNAs as Post-Transcriptional Regulators of Gene Expression

In 1993, the new era of small, endogenous RNA molecules named microRNAs (miRNAs) began when it was discovered that the developmental transition of larval stages in *Caenorhabditis elegans* (*C. elegans*) is regulated by miRNAs [84, 85]. These single-stranded (ss), short (~ 22 nucleotides [nt]) RNA stretches function as post-transcriptional regulators of gene expression. Mammalian miRNAs exert their effects primarily by imperfect binding to the 3'- UTR of the target mRNA [86]. Together with other small RNAs, the formed level of sequence complementarity with the target mRNA can induce gene silencing, a process collectively termed as RNA interference [87]. MiRNAs were found to be expressed in numerous living organisms. They are involved in a large variety of cellular processes such as cell proliferation and cell death, carcinogenesis, immune response, lipid metabolism, differentiation of mammalian hematopoietic lineages, and plant leaf development [88-91]. In humans, miRNAs are further involved in xenobiotic metabolism, were they have been reported to regulate the expression of CYPs and other drug-metabolizing enzymes [92, 93]. Approximately 1,527 miRNAs have been reported to be encoded in the human genome [94]. Based on a computational search considering miRNA-based binding properties with the target mRNA, it was proposed that miRNAs repress more than 60 % of mammalian protein-coding genes [95]. In this process, a single miRNA may be capable of regulating hundreds of target genes [96, 97].

1.7 The Biogenesis of miRNAs

Although miRNAs can originate from pre-mRNA-derived intron-splicing ("mirtrons") [98], their primary biogenesis is the canonical or "linear" pathway (Figure 4). Therein, miRNAs are transcribed by RNA polymerase II or III from their genomic loci, which generates 5'-capped, poly(A) tailed (RNA polymerase II) primary miRNA (pri-miRNA) transcripts several

kilobases long [99, 100]. The pri-miRNA is cleaved by the microprocessor complex (Drosha-DGCR8), which is RNase III enzyme Drosha and its cofactor DiGeorge Critical Region 8 (DGCR8) into the ~70 nt precursor miRNA (pre-miRNA) hairpin that is exported from the nucleus into the cytoplasm by Exportin-5 (Exp-5)-Ran-Guanosine-5'-triphosphate (GTP) [101, 102]. However, the Drosha-mediated cleavage is not obligatory for miRNA derived from introns [98].

The pre-miRNA is cleaved into a miRNA duplex of mature length (~ 22 nt) by further RNA-induced silencing complex (RISC) loading complex subunit TAR-RNA binding protein (TRBP) and endoribonuclease Dicer [86, 103-105]. The RISC is formed by the incorporation of the mature miRNA into the Argonaute 2 (Ago2) protein, whereas the miRNA passenger strand is degraded [106, 107]. The ~100 kDa Ago2 protein is suggested as the catalytically active key component of the RISC involved in "slicing" of the complementary mRNA target [108]. Finally, the mature miRNA guides the RISC to the target mRNA's (typically 3'-UTR) miRNA Recognition Element (MRE) to form perfect base pairing between the miRNA 5'-end nts 2–8 (called the "seed region") and the target mRNA. Perfect base pairing in this region initiates the Ago2-mediated target mRNA cleavage, rapid deadenylation or translational inhibition [109, 110]. In addition, other miRNA-mediated mechanisms of eukaryotic gene expression regulation have been described [111]. Moreover, it has been suggested that additional base pairing between the miRNA 3'-end and the target mRNA increases the specificity of the RNA duplex and compensates for weak base pairing at the miRNA 5'-end [112].

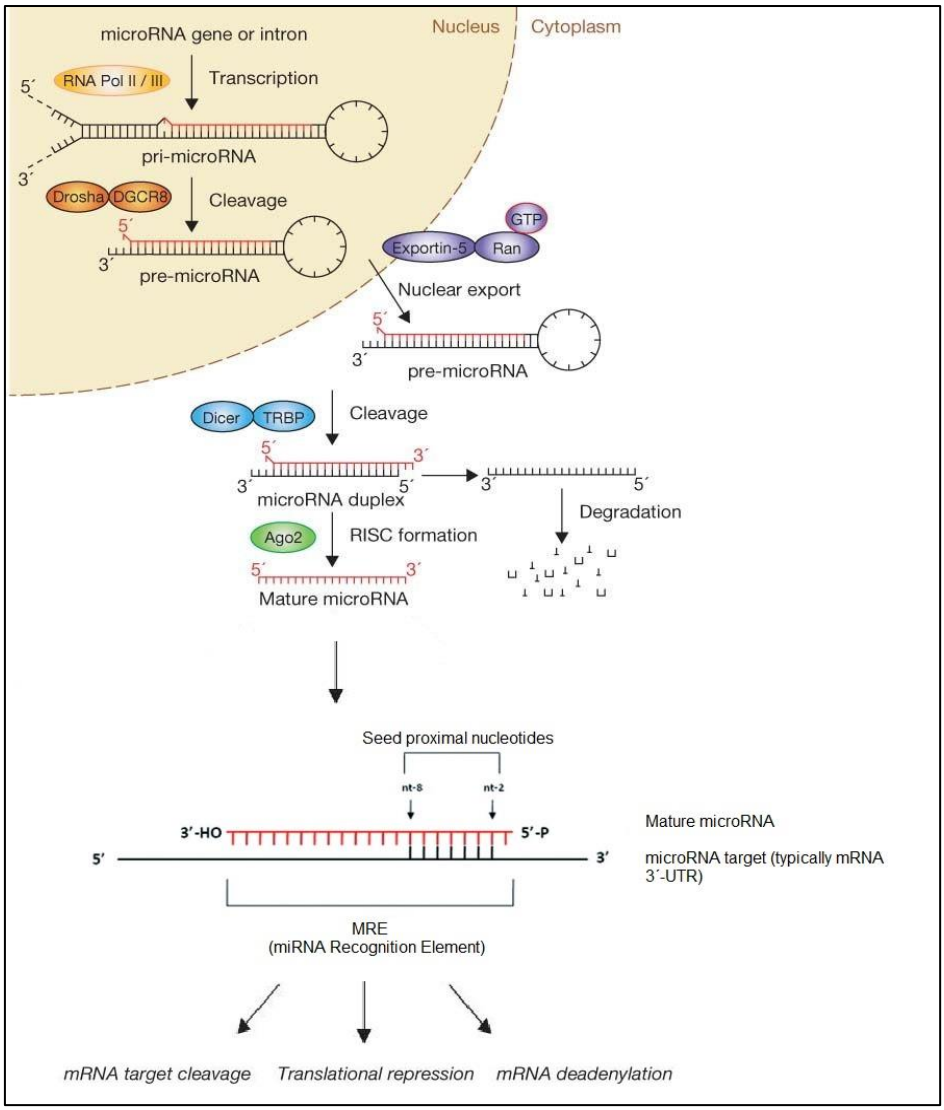

Figure 4. Biogenesis Pathway of Mammalian MicroRNAs. The transcription of microRNA genes in the nucleus and multiple steps of post-transcriptional processing are required to generate a mature single-stranded microRNA that can be incorporated into the RNA-induced silencing complex (RISC). The microRNA guides the RISC to the target mRNA, which induces mRNA degradation, deadenylation, or translational inhibition. The figure was modified from [109, 110].

1.8 MicroRNAs and the Development of Liver Diseases

MiRNAs are considered as relevant regulators of liver function during the onset of liver diseases [113], including fibrosis or cirrhosis [114], non-alcoholic fatty liver disease (NAFLD)/ NASH [115], and HCC [116]. Recently, it has been reported that miRNAs interfere with the expression of enzymes involved in the hepatic drug and xenobiotic metabolism [93].

In 2013, Vuppalanchi and collaborators found that miR-155 is significantly associated with decreased hepatic CYP3A activity and doubles the rate at which liver cirrhosis develops [117]. Previous studies have indicated that miR-155 regulates inflammation and is

upregulated in other chronic liver diseases such as ALD and HCC [118, 119]. In 2014, Dluzen *et al*. were the first to report a miR-491-3p-mediated negative regulation of UGT1A1, UGT1A3, and UGT1A6 mRNA expression in the liver cancer cell line Huh-7 [120]. Dluzen and colleagues found that the overexpression of miR-491-3p resulted in a reduced UGT1A1-mediated glucuronidation of a chemotherapeutic agent in Huh-7 cells, which suggested an intervention of miRNAs in drug metabolism. Moreover, post-transcriptional regulation of a number of TFs (outlined in section 1.5) was described to be affected by miRNAs leading to an impaired transcriptional activation of CYP or UGT1A enzyme genes [121-124].

1.9 Circulating miRNAs as Promising Biomarkers

In recent years, miRNAs have been found to serve as stable, prognostic, and diagnostic biomarkers for the detection of cancers [125]. In 2004, Calin *et al*. discovered that miRNA genes were located in fragile sites of the genome or cancer-associated genomic regions [126]. The investigators also found that miRNA genes could be located in breakpoint regions or minimal regions associated with loss of heterozygosity and amplification, linking the altered expression patterns of miRNAs with the development of cancer [126, 127]. When bound to lipid proteins or encapsulated in extracellular vesicles (microvesicles or exosomes), mirtrons are considered to be the stable form of circulating miRNA, detectable in circulating body fluids such as peripheral blood, including plasma or serum [128-131]. In many aspects, circulating miRNAs are pointed as promising biomarkers, for instance, the early detection of drug-induced liver injury [132], the prediction of HCC risk in cirrhotic patients with viral hepatitis [133] or the distinctive prediction of a particular liver disease such as fibrosis/cirrhosis, NAFLD, NASH or ALD [134].

1.10 Objectives of this Dissertation

MiRNAs are known to modulate the expression of target genes by binding to partially complementary sequences in the 3'-UTR of the target mRNA. It is well known that the increase of OS leads to the development of liver diseases. A reduced expression of drug-metabolizing enzymes (e.g. UGT1A7) is associated with an increased risk for the development of HCC due to reduced endo- and xenobiotic detoxification. This suggests that miRNAs and their associated potential of silencing *UGT1A* expression are likely effectors of

the metabolic antioxidative balance in the liver, and thereby contribute to OS-induced liver damage.

To date, little is known about the post-transcriptional regulation of *UGT1A* expression by miRNAs and their potential contribution to the pathogenesis of liver fibrosis/cirrhosis. For a better understanding of these processes, this thesis aimed to adress the following five issues:

1. To investigate a potential negative regulatory effect on the common UGT1A 3'-UTR, luciferase reporter gene assays will be carried out on 30 miRNAs differentially expressed in HCC [135].
2. To examine a potential reduction of UGT1A mRNA and protein expression after miRNA transfection in cell culture, comprehensive Real-Time PCR (UGT1A mRNA) and Western blot (UGT1A protein) analyses will be conducted covering the 30 miRNAs mentioned in objective 1.
3. To analyze a miRNA and UGT1A 3'-UTR base pairing and to reveal a potential post-transcriptional regulation of *UGT1A* expression through the common 3'-UTR, a computational analysis for MREs with the highest thermodynamic stability will be performed using online databases. To test the loss of miRNA functionality, the predicted nucleotide stretches responsible for seed matching will be mutated in the UGT1A 3'-UTR and verified by luciferase reporter gene assays.
4. An aberrant miRNA expression profile has frequently been linked to human cancer types [126]. In consequence, miRNAs from plasma or serum are often used as valuable prognostic/diagnostic biomarkers to predict tissue-derived malignant changes [131, 136]. The 4th objective of this project is to determine the expression levels of circulating miRNAs in the serum of 60 cirrhotic patients and 42 healthy controls performing quantitative polymerase chain reaction analysis. The miRNAs identified in objectives 1-3 will be further examined in this analysis. This experiment may evaluate miRNAs as potential risk factors for the development or perpetuation of liver fibrosis/cirrhosis due to a reduced UGT1A-mediated detoxification capacity.
5. The dysregulation of miRNAs is often associated with the pathogenesis of liver diseases such as fibrosis/cirrhosis, NAFLD/NASH, and HCC [114-116]. Therefore, the 5th objective of this project is to translate the findings from the human analysis (objective 4) to the animal model, where the expression of the previously identified miRNAs will be studied at simulated conditions of ALD. A humanized transgenic mouse model of alcoholic liver fibrosis will be established and the miRNA expression

levels in livers of treated mice will be determined by quantitative polymerase chain reaction at the end of the experiment.

2 Materials and Methods

2.1 Materials

2.1.1 RNA from Serum of Cirrhotic Patients Underwent TIPS Procedure

All patient and control RNA samples were collected by the lab group Trebicka at the Medical Clinic I, University Hospital Bonn. The RNA was isolated from serum obtained from the liver vein of cirrhotic patients underwent transjugular intrahepatic portosystemic shunt (TIPS) placement (n=60) or peripheral blood of healthy individuals (served as controls; n=42) [137, 138]. Prior to the RNA isolation procedure 2 pmol/200 µL SV40-miRNA (Qiagen, Hilden, Germany) was added to the serum samples, for later normalization of circulating miRNA levels. The miRNA was reverse transcribed using a stem-loop primer for generation of the first product of reverse transcription (RT). For amplification of the RT product during end-point PCR, a SV40-miRNA or miRNA of interest specific forward primer and a universal reverse primer (complementary to a nucleotide sequence of the stem-loop) was used. The miRNA expression levels were measured in a quantitative Real-Time PCR (TaqMan-qPCR, section 2.2.16).

2.1.2 Humanized Transgenic *UGT1A* Mice

A humanized transgenic (htg) *UGT1A* mouse model was used, where mice contain the entire human *UGT1A* gene locus apart from *UGT1A8*, *UGT1A10* and pseudogenes (*UGT1A11* and *UGT1A12*) illustrated in
Figure **3** [139]. A quantitative Real-Time PCR confirmed six gene copy numbers in *htgUGT1A*-WT mice, and fluorescence *in situ* hybridization (FISH) analysis demonstrated their localization on the same chromosome [139].
Transgenic *htgUGT1A*-WT mice were generated by breeding transgenic mice with non-transgenic C57BL/6J-mice (Jackson Laboratories, Maine, USA) and the offsprings were PCR-tested for the human *UGT1A3* gene. The positively tested transgenic mice were used for experiments in the age of 8-12 weeks, housing in individually ventilated cages in a temperature-controlled environment with a 12-hour light-dark cycle in the Central Animal Facility of the University Hospital Bonn. All experiments were performed in accordance with the "German Animal-Protection Law" and approved by the North Rhine-Westphalia state-agency for Nature, Environment and Consumer Protection (LANUV, Germany).

As outlined in the objective 5 (section 1.10), the generation of a *htgUGT1A*-WT mouse model of alcoholic liver fibrosis was pursued by applying a two-hit model. Ethanol exposure causes direct oxidative attack on the liver tissue ("first hit") [140], but is not sufficient to generate liver fibrosis. Thereby, a "second hit" was performed by carbon tetrachloride (CCl_4) treatment. This treatment was reported to develop steatosis, perisinusoidal and portal fibrosis or bridging fibrosis [141]. Therefore, *htgUGT1A*-WT mice were administered drinking water containing 5 % (v/v) ethanol for 8 weeks (or water without ethanol as a control) and additionally, received 5 % (v/v) CCl_4 dissolved in corn oil intraperitoneal injection (2 mL/kg body weight) twice a week. The total duration of the experiment was 8 weeks. The CCl_4 intraperitoneal injection was administrated in the last 4 weeks. Mice were sacrificed and livers immediately frozen in liquid nitrogen followed by storage at -80 °C in a freezer until required.

2.1.3 Human Cell Lines

In this work the following human cell lines were used:

- Kyse-70: esophageal squamous cell carcinoma (DSMZ no. ACC 363)
- Caco-2: colon adenocarcinoma (DSMZ no. ACC 169)
- HepG2: HCC (DSMZ no. ACC 180)
- Hek293: human embryonal kidney (DSMZ no. ACC 305)

2.1.4 Bacterial Strains and Plasmids

Table 1. Bacterial Strains and Plasmids Used in this Work.

Strain or Plasmid	Relevant Genotype	Reference
Strain		
Escherichia coli (*E.coli*) JM109	e14-(McrA-)*rec*A1 *end*A1 *gyr*A96 *thi*-1 *hsd*R17 (rK-mkt) *sup*E44 *rel*A1 Δ(*lac-pro*AB) [F'tra D36 *pro*AB *lac*I^qZΔM15]	Lab collection
Plasmids		
pGL3-Basic Vector	Firefly luciferase reporter vector, *Amp*^{r}	Promega

pRL-TK Vector	*Renilla* luciferase transfection control vector, *Amp*^{r}	Promega
pGL3-UGT1A-3'-UTR	pGL3-Basic Vector with 679 bp of common UGT1A 3'-UTR, cloned into *SnaBI*-site after mutagenesis of *XbaI*- to *SnaBI*-site	Lab collection
pGL3-UGT1A-3'-UTR ΔmiR-486-3p binding site	pGL3-UGT1A-3'-UTR with 8 nt mutation at position nt 340 from stop codon in UGT1A 3'-UTR	This work
pGL3-UGT1A-3'-UTR ΔmiR-214-5p binding site	pGL3-UGT1A-3'-UTR with 8 nt mutation at position nt 258 from stop codon in UGT1A 3'-UTR	This work

2.1.5 Oligonucleotides

Table 2. Oligonucleotides for Amplification and Mutagenesis. All primers used in this work were purchased at MWG Eurofins.

Oligonucleotide	Orientation	Restriction Site	Sequence (5' > 3')
pGL3 vorXba F	Forward		CAGAGAGATCCTCATAAAGGCCA
pGL3 hinXba R	Reverse		CTCATCAATGTATCTTATCATG
UGT 3'UTR SnaBI F	Forward	*SnaBI*	GATACGTAGAAGTGGGTGGGAAATAAGGTAAAATTTTGAACC
UGT 3'UTR SnaBI R	Reverse	*SnaBI*	AATACGTACTTGCCCAGCACTTCATAGCTG
3'UTR WT 340bp mut fw	Forward		GGTCCCACCAAATTTAATACTGCAAATGG
3'UTR WT 340bp mut rv	Reverse		CCATTTGCAGTATTAAATTTGGTGGGACC
miR-214-5p seed del fw	Forward		GAGGACGTGCTTTAAATTTGGCATTCTAGA
miR-214-5p seed del rv	Reverse		TCTAGAATGCCAAATTTAAAGCACGTCCTC

2.1.6 miRNA Mimics, Primers, and Probes

Table 3. List of Selected Double-Stranded miRNA Mimics Used in this Work. The miRNAs are distinguished in -5p or -3p depending on the 5' or 3' arm of the pre-miRNA hairpin they derive from. miR-control was purchased at MWG Eurofins and all other miRNA mimics were obtained from Sigma-Aldrich.

miRNA Mimic	Sequence (5' > 3')
miR-control	UAAUGUAUUGGAACGCAUATT
hsa-miR-15a-5p	UAGCAGCACAUAAUGGUUUGUG
hsa-miR-16a-5p	UAGCAGCACGUAAAUAUUGGCG
hsa-miR-17-5p	CAAAGUGCUUACAGUGCAGGUAG
hsa-miR-18a-5p	UAAGGUGCAUCUAGUGCAGAUAG
hsa-miR-20a-5p	UAAAGUGCUUAUAGUGCAGGUAG
hsa-miR-21-5p	UAGCUUAUCAGACUGAUGUUGA
hsa-miR-25-5p	AGGCGGAGACUUGGGCAAUUG
hsa-miR-29a-5p	ACUGAUUUCUUUUGGUGUUCAG
hsa-miR-34a-5p	UGGCAGUGUCUUAGCUGGUUGU
hsa-miR-93-5p	CAAAGUGCUGUUCGUGCAGGUAG
hsa-miR-106b-5p	UAAAGUGCUGACAGUGCAGAU
hsa-miR-122-5p	UGGAGUGUGACAAUGGUGUUUG
hsa-miR-148a-5p	AAAGUUCUGAGACACUCCGACU
hsa-miR-151-5p	UCGAGGAGCUCACAGUCUAGU
hsa-miR-155-5p	UUAAUGCUAAUCGUGAUAGGGGUU
hsa-miR-181a-5p	AACAUUCAACGCUGUCGGUGAGU
hsa-miR-183-5p	UAUGGCACUGGUAGAAUUCACU
hsa-miR-199a-5p	CCCAGUGUUCAGACUACCUGUUC
hsa-miR-199a-3p	ACAGUAGUCUGCACAUUGGUUA
hsa-miR-200b-3p	UAAUACUGCCUGGUAAUGAUGA
hsa-miR-214-5p	UGCCUGUCUACACUUGCUGUGC
hsa-miR-214-3p	ACAGCAGGCACAGACAGGCAGU
hsa-miR-216a-5p	UAAUCUCAGCUGGCAACUGUGA
hsa-miR-221-5p	ACCUGGCAUACAAUGUAGAUUU
hsa-miR-222-5p	CUCAGUAGCCAGUGUAGAUCCU
hsa-miR-224-5p	UCAAGUCACUAGUGGUUCCGUUUAG
hsa-miR-330-5p	UCUCUGGGCCUGUGUCUUAGGC
hsa-miR-4321	UUAGCGGUGGACCGCCCUGCG
hsa-miR-486-3p	CGGGGCAGCUCAGUACAGGAU
hsa-miR-519d-5p	CCUCCAAAGGGAAGCGCUUUCUGUU

Table 4. List of Oligonucleotides and Probes for Gene Expression Analysis by TaqMan-qPCR. A list of primers and TaqMan-probes was used in this work [142]. Primers and TAMRA-probes were purchased at MWG Eurofins; MGB- and all other probes were purchased at Applied Biosystems.

Gene	Primer and Probes

UGT1Aall	Forward: GCTATGGCAATTGCTGATGCTTT Reverse: CGATGGTCGGGTTCCAGTGTA Probe: FAM – AAAATCCCTCAGACAGTCCT – MGB
UGT1A1	Forward: GAATCAACTGCCTTCACCAAAAT Reverse: AGAGAAAACCACAATTCCATGTTCT Probe: FAM – CTATCCCAGGAATTTGAA – MGB
UGT1A3	Forward: CAGAAGTATGGCAATGTTGAACAATA Reverse: GCCTCATTATGTAGTAGCTCCACACA Probe: FAM – TCTTTGGTCTATCATAGGTC – MGB
UGT1A4	Forward: TTTTTCTGCCCCTTATGCAAGT Reverse: ACAGCCACACGGATGCATAG Probe: FAM –TCAGAGAGAGGTGTCAGTGGTGGATCTTGT-TAMRA
UGT1A6	Forward: CTTCATTGGAGGTATCAACTGTAAGAA Reverse: AAGAGAAAACCACAATTCCATGTTC Probe: FAM-AGGAAAGACTTGTCTCAGGAATTTGAAGCC-TAMRA
UGT1A7	Forward: GAGGATCAGGACCGGGAGTT Reverse: GAAAATGCACTTCGCAATGGT Probe: VIC – TGGTTTTTGCCGATGCT – MGB
UGT1A9	Forward: AAACCCGTGATGCCCAAC Reverse: GGCTTCAAATTCCATAGGCAAC Probe: FAM – TGATCTTCATTGGTGGTATCAACTGCCATC-TAMRA
Human beta-actin	Forward: TGCCGACAGGATGCAGAAG Reverse: GCCGATCCACACGGAGTACT Probe: FAM-AGATCAAGATCATTGCTCCTCCTGAGCGC-TAMRA
Mouse beta-actin	Forward: ACGGCCAGGTCATCACTATTG Reverse: CAAGAAGGAAGGCTGGAAAAG Probe: FAM – CAACGAGCGGTTCCGATGCCC – MGB

2.1.7 Enzymes and dNTPs

Table 5. List of Enzymes Used in this Work.

Enzymes	Units (U)/µL	Supplied by
Restriction enzymes		
SnaBI	5	New England BioLabs
Collagenase		
Collagenase	280 U/mg	Biochrom AG
DNA Polymerases		
BioTherm™ *Taq* DNA Polymerase	5	Genecraft
SuperScript™ III RT	200	Invitrogen

Vent® DNA Polymerase	2	New England BioLabs
DNase		
DNase I, Amplification Grade	1	Invitrogen
Ligase		
T4-DNA-Ligase	400	New England BioLabs
Phosphatase		
Antarctic Phosphatase	5	New England BioLabs
dNTPs (dATP, dCTP, dGTP, dTTP)	10 mM	Genecraft

2.1.8 Antibodies

Table 6. List of Primary Antibodies Used in this Work.

Human Antigen	Description	Species	Company
UGT1A1	ab170858	Rabbit	Abcam
UGT1A3	M02	Mouse	Abnova
UGT1A4	ab192424	Rabbit	Abcam
UGT1A6	/	Rabbit	BD Gentest
UGT1A7	B01P	Mouse	Abnova
UGT1A9	ab88517	Mouse	Abcam
RXRα	sc-515929	Mouse	Santa Cruz Biotechnology
UGT1A	sc-271268	Rabbit	Santa Cruz Biotechnology
β-Actin	sc-47778	Mouse	Santa Cruz Biotechnology

Table 7. List of Secondary Antibodies Used in this Work.

Antibody	Description	Company
mouse monoclonal anti-rabbit IgG-HRP	sc-2357	Santa Cruz Biotechnology
m-IgGκ anti-mouse BP-HRP	sc-516102-CM	Santa Cruz Biotechnology

(Cruz Marker)

2.1.9 DNA and Protein-Markers

Table 8. List of DNA- and Protein Markers Used in this Work.

Name	Company
100 bp DNA Ladder	Genecraft
1 kb DNA Ladder	Genecraft
PageRuler Prestained Protein Ladder	Thermo Scientific
Precision Plus Protein™ Dual Color Standards	Bio-Rad
Low Range Prestained SDS-PAGE Standards	Bio-Rad
Protein Assay Reagent	Bio-Rad

2.1.10 Media and Reagents for Bacteria

Table 9. List of Media and Reagents Used for Bacteria in this Work.

Name	Composition
Ampicillin (1000 x)	100 mg/mL
LB-Agar	5 g/L Yeast, 10 g/L Peptone, 10 g/L NaCl, 15 g/L Agar
LB-Medium	5 g/L Yeast, 10 g/L Peptone, 10 g/L NaCl
Medium for generation of chemically competent *E. coli* JM109: LB-Medium + 20 mM $MgSO_4$	
SOC Medium	Thermo Fisher Scientific

2.1.11 Media and Reagents for Tissue Culture

Table 10. List of Cell Culture Media and Additives Used in this Work.

Component	Company
Collagen A	Biochrom AG
Dexamethasone	Sigma-Aldrich
Dulbecco's Modified Eagle Medium (DMEM) + GlutaMAX™	Gibco™, Thermo Fisher Scientific
Fetal Calf Serum	Gibco™, Thermo Fisher Scientific

Hank's Balanced Salt Solution (HBSS)	Gibco™, Thermo Fisher Scientific
Insulin-Transferrin-Selenium	Gibco™, Thermo Fisher Scientific
L-Glutamine	Gibco™, Thermo Fisher Scientific
Minimum Essential Medium (MEM) Non-Essential Amino Acids Solution (NEAA) (100 x)	Gibco™, Thermo Fisher Scientific
Opti-MEM®, Reduced Serum Medium	Gibco™, Thermo Fisher Scientific
Penicillin Streptomycin (Pen Strep)	Gibco™, Thermo Fisher Scientific
Phosphate Buffered Saline (PBS, pH 7.4, 10 x)	Gibco™, Thermo Fisher Scientific
Roswell Park Memorial Institute (RPMI) Medium 1640	Gibco™, Thermo Fisher Scientific
StemPro accutase®, Cell Dissociation Reagent	Gibco™, Thermo Fisher Scientific
Williams Medium E	Biochrom AG

2.1.12 Kits

Table 11. List of Kits Used in this Work.

Name	Company
Dual Luciferase Reporter Assay System	Promega
NucleoBond® PC 500 Plasmid Maxiprep	Macherey-Nagel
Nuclear Extraction Kit	Abcam
NucleoSpin® Gel and PCR Clean-up	Macherey-Nagel
NucleoSpin® Plasmid Mini-Prep	Macherey-Nagel
qPCR MasterMix Plus	Eurogentec
SuperScript™ III First-Strand Synthesis System for RT-PCR	Invitrogen
TGX Stain-Free FastCast Acrylamide (10 %) for SDS-PAGE	Bio-Rad
TaqMan™ MicroRNA Reverse Transcription	Thermo Fisher Scientific

2.1.13 Buffers and Utility Solutions

Table 12. List of Buffers and Utility Solutions Used in this Work.

Name	Composition
3 M Sodium acetate	4.1 g NaAc in 50 mL dH_2O
Loading Dye	50 % Glycerol, 0.2 % Orange-G, 1 x TAE
5 x Passive Lysis Buffer	Promega
PBS	137 mM NaCl, 2.7 mM KCl, 8 mM NaH_2PO_4, 2 mM KH_2PO_4
CutSmart® Buffer	50 mM Potassium Acetate, 20 mM Tris-acetate, 10 mM Magnesium Acetate, 100 µg/mL BSA, pH 7.9
Antarctic Phosphatase Buffer (NEB)	50 mM Bis Tris-propane, 1 mM $MgCl_2$, 0.1 mM $ZnCl_2$, pH 6.0
BioTherm *Taq* DNA Polymerase Buffer (Genecraft)	160 mM $(NH_4)_2SO_4$, 670 mM Tris-HCl pH 8.8 (at 25 ºC), 15 mM $MgCl_2$, 0.1 % Tween 20
DNase I Reaction Buffer	Invitrogen
ThermoPol® Reaction Buffer (for Vent DNA Polymerase)	20 mM Tris-HCl, 10 mM $(NH_4)_2SO_4$, 10 mM KCl, 2 mM $MgSO_4$, 0.1 % Triton® X-100, pH 8.8
T4-DNA-Ligase Buffer (NEB)	500 mM Tris-HCl, 100 mM $MgCl_2$, 100 mM DTT, 10 mM ATP, 250 µg/mL BSA
TAE-Buffer (50 x)	0.8 M Tris-base, 0.2 M Na-acetate, 20 mM EDTA, pH 7.8

2.1.14 Buffer for Generation of Chemically Competent *E. coli* JM109

- Buffer 1: 0.1 M $CaCl_2$ (in deionized water)
- Buffer 2: 0.1 M $CaCl_2$, 15 % Glycerol (in deionized water)

2.1.15 Buffer for Generation of Primary Hepatocytes from Mice

- EGTA solution (1/10 dilution of 10 x Collagenase solution with Aqua dest.): 800 mg/L NaCl, 400 mg/L KCl, 88.17 mg/L NaH_2PO_4 (H_2O), 124.45 mg/L Na_2HPO_4, 2380 mg/L HEPES, 350 mg/L $NaHCO_3$

- Collagenase solution (10 x): 80 g/L NaCl, 4 g/L KCl, 881.7 mg/L NaH_2PO_4 (H_2O), 1.2045 g/L Na_2HPO_4, 23.8 g/L HEPES, 3.5 g/L $NaHCO_3$ adjusted to pH 7.35-7.4 with 10 N NaOH
- Collagenase solution (1 x): recipe according to 10 x Collagenase solution with additional 560 mg/L $CaCl_2$ (2 H_2O) carefully added while stirring for 1 h

2.1.16 Buffer for Generation of Microsomes from Cell Lines

- UGT buffer: 0.5 M Tris, 0.1 M $MgCl_2$, pH 7.6

2.1.17 Buffers for Western Blot

Table 13. List of Buffers for Western Blot Used in this Work.

Name	Composition
Laemmli Buffer (2 x)	10 mL glycerol, 10 mL 10 % SDS, 12.5 mL Stacking Gel Buffer, 10 mL 0.5 M DTT, 7.5 mL Aqua dest., 0.5 – 1 g Bromophenol blue
PBS with Tween-20 (PBST)	137 mM NaCl, 2.7 mM KCl, 8 mM NaH_2PO_4, 2 mM KH_2PO_4, 0.1 % Tween-20
Resolving Gel Buffer (4 x)	181.7 g Tris, 40 mL 10 % SDS, ad 1000 mL with Aqua dest. and adjusted to pH 8.8
Running Buffer (10 x)	30 g Tris, 144 g Glycin, 100 mL 10 % SDS, ad 1000 mL with Aqua dest.
Stacking Gel Buffer (4 x)	60.6 g Tris, 12 mL 10 % SDS, ad 1000 mL with Aqua dest. and adjusted to pH 6.8
Transfer Buffer (1 x)	200 mL Trans-Blot Turbo 5 x Transfer buffer (Bio-Rad), 600 mL Aqua dest., 200 mL Ethanol absolute

2.1.18 Chemicals

Table 14. List of Chemicals Used in this Work.

Component	Company
Acetic acid	Carl Roth
Agarose	Carl Roth

Alamethicin	Sigma-Aldrich
Ammonium peroxydisulfate (APS)	Carl Roth
Aqua, distilled	Fresenius Kabi
Bio-Rad Protein Assay	Bio-Rad
Bromophenol blue	AppliChem
Calcium Chloride Dihydrate	Honeywell Fluka
Chloroform	J.T. Baker
Clarity Western Blotting ECL Substrate	Bio-Rad
DEPC-treated water	Ambion
Dithiothreitol (DTT)	Carl Roth
Dimethyl Sulfoxide (DMSO)	Sigma-Aldrich
Ethylene glycol-bis (β-aminoethyl ether)-N,N,N',N'-tetraacetic acid (EGTA)	Carl Roth
Ethanol 99.9 %	Carl Roth
Ethylenediaminetetraacetic acid (EDTA)	Merck
EZ-Vision In-Gel Solution (10,000 x)	VWR
Glycerol	Carl Roth
Glycine	Carl Roth
Hydrochloric acid (1 N HCl)	Carl Roth
Ketamine (10 %)	WDT
LB Agar	Invitrogen, Thermo Fisher Scientific
LB broth base	Invitrogen, Thermo Fisher Scientific
4 x Laemmli Sample Buffer	Bio-Rad
Lipofectamine™ 2000 Transfection Reagent	Invitrogen
Nuclease-free water	Ambion, Thermo Fisher Scientific
Powdered milk	Carl Roth
2-Propanol	AppliChem
Sodium dodecyl sulfate (SDS)	Bio-Rad
Tetramethylethylenediamine (TEMED)	AppliChem
Tris(hydroxymethyl)-aminomethane (Tris)	Carl Roth
TRIzol® Reagent	Invitrogen
Trypan blue	Carl Roth
Tween-20	Merck

Xylazine (2 %)	Ceva

2.1.19 Consumables

Table 15. List of Consumables Used in this Work.

Component	Company
100 µM cell strainer	Falcon
Falcon tubes (15 mL, 50 mL)	Sarstedt
Hard-Shell® PCR-plates 96-well	Bio-Rad
Overnight culture tube (14 mL)	Greiner Bio-One
Microplate 96-well	Greiner Bio-one
Parafilm M film	Bemis Packaging
PCR plates twin.tec 96	Eppendorf
Pipette tips (10 µL, 200 µL, 300 µL, 1000 µL)	Sarstedt
Pipette tips (10 µL, 200 µL, 300 µL, 1000 µL) with Filter	StarLab
Pipette tip Plastibrand (5 mL)	Merck
Plastic Petri dishes	Sarstedt
Polystyrene cuvettes for photometer	Sarstedt
Reaction tubes (0.5 mL, 1.5 mL)	Sarstedt
Reaction tubes (2 mL)	Eppendorf
Sealing tape	Thermo Scientific
Serological pipette (2 mL)	Sarstedt
Serological pipette (5 mL, 10 mL, 25 mL)	Corning Inc.
Serological pipette (50 mL)	Greiner Bio-One
8-Strip PCR caps	STARLAB
8-Strip PCR tubes	STARLAB
Tissue culture flask T75 (75 cm^2)	Sarstedt
Tissue culture flask T175 (175 cm^2)	Sarstedt
Trans-blot Turbo midi-size nitrocellulose membrane 0.45 µm	Bio-Rad
Trans-blot Turbo midi-size transfer stacks	Bio-Rad

Ultracentrifuge tubes (1.5 mL)	Beckman
6-Well cell culture plate	Greiner Bio-One
12-Well cell culture plate	Greiner Bio-One

2.1.20 Technical Devices

Table 16. List of Technical Devices Used in this Work.

Device	Company
Analytical balance	Sartorius
BioPhotometer plus	Eppendorf
Chemiluminescence Imaging Detection System (ChemiDoc™ MP Imaging System)	Bio-Rad
Compact Shaker KS 15	Edmund Bühler
Cooling Centrifuge Heraeus Multifuge X3 FR	Thermo Fisher Scientific
Cooling Centrifuge 5424 R	Eppendorf
Gel Electrophoresis Power Source (300 V)	VWR
Heracell 150i CO_2 Incubator	Thermo Fisher Scientific
HERAfreeze Ultra-Low Temperature Freezer HFU T Series (-80 °C)	Thermo Fisher Scientific
Incubator Hood TH 15	Edmund Bühler
Laboratory fume hood (Secuflow)	Waldner
Leica Inverted Microscope (IMC S40) DM IL LED	Leica Microsystems
Luminometer Lumat LB 9507	Berthold
Mars Class 2 Safety Cabinet	Scanlaf
Microwave	Severin
Mini-Centrifuge	IKA
Mini-PROTEAN Tetra Cell (for 1-D vertical gel electrophoresis)	Bio-Rad
Mini Rocking Shaker (see-saw)	Stuart
PCR thermocycler	Peqlab, VWR
Peri-Star Peristaltic Pump	World Precision Instruments

Pipette (10 µL, 200 µL, 1000 µL)	Eppendorf
Precision balance	Sartorius
Real-Time Thermal Cycler CFX 96 C1000 Touch	Bio-Rad
Refrigerator	Liebherr
Thermoblock	Eppendorf
TissueLyser LT	Qiagen
Trans-Blot Turbo Transfer System	Bio-Rad
Universal Oven UN55	Memmert
Vortex Genie 1 Touch Mixer	Scientific Industries
Water bath	Lauda

2.1.21 Annexes

Additional material was used in this work:

- Cuvette Rack (Merck)
- µCuvette G1.0 (Eppendorf)
- MIDI standard horizontal gel electrophoresis unit (Carl Roth)
- Neubauer counting chamber (Marienfeld)
- Potter-Elvehjem Homogenisator
- Repeater Pipette (Eppendorf)

2.2 Methods

2.2.1 Prediction of miRNA Binding Sites

The full-length UGT1A 3'-UTR (679 bp) was analyzed for MREs using the software tools RegRNA (v2.0) [143], PicTar [144], miRanda [145] and RNAhybrid [146], applying the default settings. The predicted energy of mRNA:miRNA duplex formation was denoted as Minimum Free Energy (MFE) in the unit kcal/mol. Predictions that stated MFE-values lower than -20 kcal/mol and a MRE seed match composed of 7-9 base pairs were considered for further investigation.

2.2.2 Amplification of Nucleotide Sequences by Polymerase Chain Reaction (PCR)

PCR reactions were performed according to good laboratory practice. In order to perform the amplification of specific DNA sequences by Polymerase Chain Reaction (PCR) the BioTherm™ *Taq* DNA Polymerase or high-fidelity Vent® DNA Polymerase (Table 5) were used.

Standard PCR reaction (50 µL total volume):

5 µL 10 x BioTherm™ *Taq* DNA Polymerase Buffer or 10 x ThermoPol® Reaction Buffer
2.5 µL 10 µM Forward Primer
2.5 µL 10 µM Reverse Primer
1.0 µL 10 mM dNTPs
0.5 µL 5 U/µL BioTherm™ *Taq* DNA Polymerase or 2 U/µL Vent® DNA Polymerase
1.0 µL DNA template (10-50 ng)
37.5 µL dH_2O

Standard PCR conditions:

95 °C 3 min
95 °C 30 s
50-60 °C 30 s
72 °C 1 min for 1 kb of the amplified nucleotide sequence } 25-40 cycles
72 °C 5 min

2.2.3 Mutagenesis of Nucleotide Sequences in the UGT1A 3'-UTR

In order to disrupt the predicted MRE for miR-214-5p and miR-486-3p in the UGT1A 3'-UTR two PCR reactions (1 and 2) were performed to generate two DNA fragments (Figure 5).

1) The PCR reaction to generate the first DNA fragment contained the UGT1A 3'-UTR forward amplification primer and the seed mutagenesis primer in reverse orientation. For the generation of the second DNA fragment, the seed mutagenesis primer in forward orientation and the UGT1A 3'-UTR reverse amplification primer were used (Table 2). The PCR reaction was performed according to standard conditions (section 2.2.2), and running a maximum of 25 cycles using high-fidelity Vent® DNA Polymerase, and 10-50 ng pGL3-UGT1A-3'-UTR as DNA template.

2) Both PCR products were separated by agarose gel electrophoresis. The DNA fragments were gel-purified, and 10-50 ng of each DNA template was included in the same PCR reaction. For the generation of the PCR product, the UGT1A 3'-UTR forward and reverse amplification primers were used. The Vent® DNA Polymerase was utilized and the PCR reaction was performed for 30 cycles. The cloning of the mutated insert generated the novel DNA plasmid pGL3-UGT1A-3'-UTR seed mutation with a mutated nucleotide sequence for the miRNA of interest.

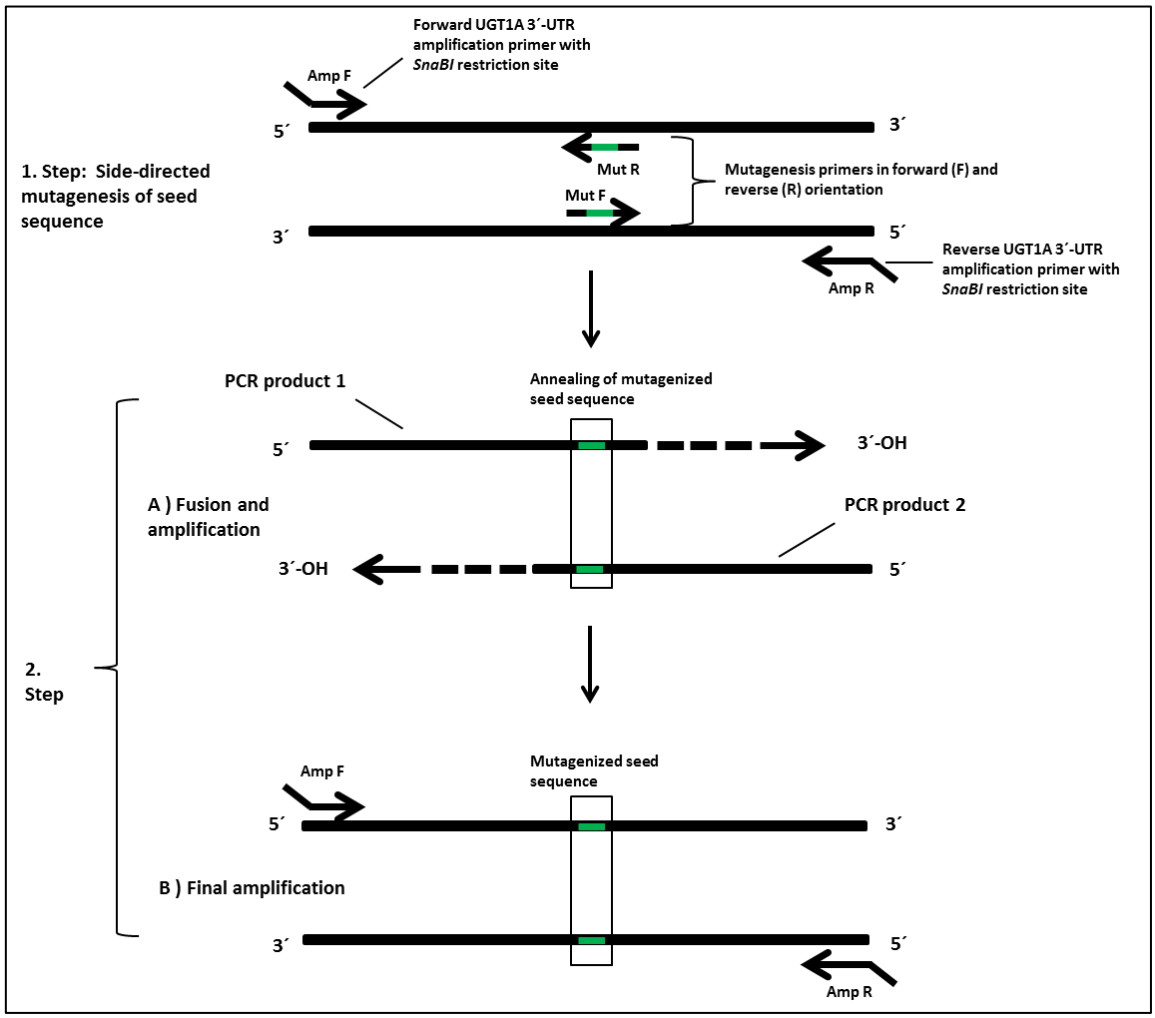

Figure 5. Site-Directed Mutagenesis of MRE Seed Sequence in the UGT1A 3'-UTR. In a two-step PCR reaction, the nucleotide sequence (termed as seed sequence) within the UGT1A 3'-UTR-located MRE responsible for high complementarity with the miRNA of interest 5'-end was disrupted using UGT1A 3'-UTR forward amplification (Amp F) and the seed mutagenesis primer in reverse orientation (Mut R), whereas the seed mutagenesis primer in forward orientation (Mut F) was included in the PCR reaction containing the UGT1A 3'-UTR reverse amplification primer (Amp R; step 1). Both PCR products were gel-purified, mixed in a molar ratio (step 2A) and the PCR was carried out containing UGT1A 3'-UTR forward and reverse amplification primers (step 2B). Thereby, the nucleotide sequences necessary for miR-214-5p and miR-486-3p seed region complementarity were mutated.

2.2.4 Agarose Gel Electrophoresis

Agarose gel electrophoresis was performed to identify, separate, test for the presence of DNA molecules (analytical gel) and for the purification of PCR products or restriction digested DNA (preparative gel).

Throughout the entire analysis, 2 % agarose gels were established. For this, 2 g agarose (Table 14) were mixed in 100 mL 1 x TAE Buffer (Table 12) and heated at 700 W for 3 min in the microwave. Then, 10 µL 10,000 x EZ-Vision® In-Gel Solution were added, this is a fluorescent DNA dye leading to DNA visualization upon UV exposure at 280 nm. The DNA samples were mixed with the correct amount of 6 x Loading Dye to reach the final concentration of 1 x Loading Dye, and subjected to gel electrophoresis at 120 V for 45 min. The detection and visualization of DNA molecules was carried out by using ChemiDoc™ Gel Imaging System and the respective Image Lab Software Version 5.2. For preparative purposes, DNA molecules of interest were excised from the agarose gel under brief UV exposure.

2.2.5 Clean-up of PCR Products

DNA molecules of interest were purified by silica gel columns using the NucleoSpin® Gel and PCR Clean-up Kit according to the manufacturer's protocol (Macherey-Nagel). In the final step DNA molecules were eluted from the column using 20-35 µL Aqua dest.

2.2.6 Enzymatic Reactions during the Process of DNA Cloning

A) Restriction Digestion

To ligate vector and insert DNA molecules containing the restriction sites, a restriction digestion was required. Therefore, ~ 3 µg purified DNA was mixed with 10 % CutSmart® buffer, 5 U *SnaBI*, and filled up with Aqua dest. to the final volume of 40 µL. The restriction digestion was incubated at 37 °C for 2 h and terminated by heating at 65 °C for 20 min. Agarose gel electrophoresis (section 2.2.4) was performed to confirm the correct restriction digestion.

B) Vector Dephosphorylation

In cloning, the dephosphorylation of 5'-ends of DNA phosphomonoesters prevents the recircularization of the linearized DNA plasmid during ligation, thereby promoting cloning efficiency. The purified DNA plasmid was mixed with 10 % Antarctic

Phosphatase Buffer and 1 U of Antarctic Phosphatase (Table 5) per 1 µg of DNA and diluted with Aqua dest. to the final volume of 40 µL. The reaction was incubated at 37 °C for 1 h, and terminated by heat inactivation at 80 °C for 2 min.

C) Ligation

The gel-purified plasmid and insert DNA molecules were combined by ligation in an insert : vector molar ratio of at least 3 : 1. The ligation reaction was composed of x µL DNA plasmid, x µL DNA insert, 400 U T4-DNA-Ligase (Table 5), 1 µL 10 x T4-DNA-Ligase Buffer, the solution was adjusted to the final volume of 10 µL with Aqua dest. The ligation reaction was carried out overnight at 16 °C and terminated by heating at 65 °C for 10 min.

2.2.7 Generation of Chemically Competent *E. coli* JM109

The entire procedure was performed on ice, all buffers were stored on ice and technical devices were pre-cooled at 4 °C. At first, the bacterial strain was restreaked on a LB-agar plate from a freezer stock under sterile conditions and according to good microbiological practice. The LB-agar plate was incubated overnight at 37 °C. Next, 5 mL LB-medium were inoculated with a single colony from this plate, and the liquid culture was incubated overnight shaking at 250 rpm and 37 °C. Then, 4 mL of the culture were used for the inoculation of 400 mL LB-medium. The culture was incubated shaking at 250 rpm and 37 °C until OD_{600} ~ 0.5, then split, and incubated on ice for 10 min. Post centrifugation at 3,000 rpm for 5 min, the supernatant was discarded, and the cell pellet was gently resuspended in 40 mL 0.1 M $CaCl_2$ buffer. After another centrifugation step at 2,700 rpm for 5 min, the supernatant was discarded, and the cell pellet was resuspended as described in the step before. Both cell suspensions were consolidated and incubated on ice for 1 h. The cell suspension was centrifuged at 2,700 rpm for 5 min, the supernatant was discarded, and the cell pellet was gently resuspended in 8 mL 0.1 M $CaCl_2$ buffer containing 15 % glycerol. The chemically competent cells were aliquoted and stored at -80 °C until use.

2.2.8 Heat-Shock Transformation

The chemically competent *E. coli* JM109 were carefully thawed on ice. Then, 5 µL ligation reaction was added to the cells and mixed by flicking the tube. The cells were incubated on

ice for 30 min, then at 42 °C for 45 s and on ice for another 2 min. Finally, 200 µL pre-warmed SOC medium was added to the cells followed by an incubation period of 1 h at 37 °C and shaking at 250 rpm. The entire cell suspension was spread on pre-warmed LB-agar plates containing ampicillin at a final concentration of 100 µg/mL. The LB-agar plates were incubated overnight at 37 °C, to promote the propagation of the plasmid-carrying transformants.

2.2.9 Colony Analysis

To test the bacterial colonies on LB-agar plates that carried DNA plasmid pGL3-UGT1A-3'UTR, a colony PCR analysis was performed. For this, a PCR master mix was set up as described in section 2.2.2. Additionally, a colony was picked, patched on another ampicillin containing LB-agar plate and resuspended in the PCR master mix. The PCR reaction contained pGL3 vorXbaF and pGL3 hinXbaR (Table 2) primers flanking the *SnaBI* restriction site. The PCR was performed for 25 cycles at the conditions described in section 2.2.2. Then, 10 µL of the PCR reaction were pipetted in an agarose gel electrophoresis as described in section 2.2.4 and DNA bands were detected. Next, the positive clone was picked and used to inoculate a 5 mL LB-medium with ampicillin overnight culture, in order to isolate the DNA plasmid in a Mini-Prep, and to analyze it by sequencing. At a correct sequence, 500 µL of the initial 5 mL overnight culture were used to inoculate 200 mL LB-medium and prepare a plasmid Maxi-Prep.

2.2.10 Plasmid Isolation

A) Isolation by Mini-Prep

Plasmids were isolated from bacterial colonies on LB-agar plates by picking a single colony with a pipette tip and inoculating it in 5 mL LB-medium overnight culture. Then, depending on the saturation of the *E. coli* LB culture 2-4 mL were centrifuged at 11,000 x g for 30 s, and the DNA plasmid was isolated according to manufacturer's instructions in the NucleoSpin® Plasmid Mini-Prep Kit (Macherey-Nagel). For the elution of the DNA plasmid were used 35-50 µL of Aqua dest.

B) Isolation by Maxi-Prep

For the isolation of higher DNA plasmid concentrations (necessary for downstream applications) a plasmid Maxi-Prep was performed. For this, 200 mL of an *E. coli* LB culture was grown overnight, and the bacterial cells were harvested at 6,000 x g, 4 °C for 15 min. To further proceed with the plasmid Maxi-Prep, the NucleoBond® PC 500 Plasmid Maxiprep Kit was used according to the manufacturer's instructions. The final elution of the DNA plasmid was performed using 100-300 µL of Aqua dest.

2.2.11 Determination of DNA Plasmid Concentrations

For the determination of DNA plasmid concentrations, the BioPhotometer plus (Eppendorf) and the respective µCuvette G1.0 were used. After an adequate dilution of the DNA plasmid in DNase-free water, 2 µL of DNA solution were pipetted on the marked area of the cuvette and DNA concentrations were measured at 260 nm using the spectrophotometer.

2.2.12 Cell Culture

Human HCC (HepG2), Caucasian colorectal adenocarcinoma (Caco-2), human esophageal squamous cell carcinoma (Kyse-70), and human embryonic kidney (Hek293) cell lines were used throughout all the experiments. HepG2 and Kyse-70 cells were maintained in RPMI 1640, whereas Caco-2 and Hek293 cells were maintained in DMEM GlutaMAX™. All media were supplemented with 10 % fetal calf serum and 1 % penicillin-streptomycin. The Caco-2 medium was additionally supplemented with 1% non-essential amino acids. All cells were cultivated in an incubator under a humidified atmosphere at 37 °C and 5 % CO_2.

The cell lines were grown to 80-90 % confluency and split twice a week. For this, the culture medium was removed, the cells were rinsed in 10 mL 1 x PBS, and the remaining solution was discarded. Additionally, 4 mL cell dissociation reagent (accutase®) were added and the cells were detached at 37 °C for 15 min. Then, 6 mL cell culture medium was used to resuspend the cells and 4 mL HepG2, 1 mL Hek293, 2 mL Caco-2, and 2 mL Kyse-70 were transferred into a new cell culture flask. The flask was filled with culture medium to the final volume of 25 mL for the purpose of cell culture continuation.

2.2.13 Transfection of Human Cell Lines or Mouse Primary Hepatocytes

Hek293 cells were used for luciferase reporter gene assays. The cells were transfected with a reporter gene construct (pGL3-based), the transfection control vector (pRL-TK), and a miRNA. The HepG2, Caco-2, and Kyse-70 cells were transfected with a miRNA for the determination of UGT1A mRNA and protein expression. In line with *in vitro* RNA/protein analysis (section 2.2.14 and 2.2.23), mouse primary hepatocytes were transfected with a miRNA followed by the isolation of microsomes for the quantification of UGT enzyme activity.

The assays listed below were performed in different setups:

- 12-well plate: luciferase assay, total volume per well: 1 mL
- 6-well plate: RNA/protein isolation, total volume per well: 2 mL
- T75 cell culture flask: hepatocyte cultivation and followed by microsome isolation, total volume: 12 mL

The transfection solution for each approach was prepared in two different tubes labeled A and B, which were fused at the end. The volume of the transfection solutions differed for the luciferase assay (0.5 mL), RNA/protein isolation (1 mL), hepatocyte cultivation (6 mL), and the required individual reagents (Table 17).

Table 17. Composition of Transfection Solutions in Cell Culture Experiments.

Volume per well or flask (according to the assay)	Luciferase assay	RNA/protein isolation	Hepatocyte isolation	
Opti-MEM®	50 µL	100 µL	600 µL	Solution A
Lipofectamine 2000	2 µL	2 µL	12 µL	
Opti-MEM®	440 µL	898 µL	5388 µL	Solution B
pGL3-based reporter construct	1 µg	/	/	
pRL-TK vector	3 ng	/	/	
miRNA (final concentration)	5 nM	5 nM	5 nM	

2.2.14 RNA Isolation

For RNA isolation, cells were seeded at different cell counts in 6-well plates:

- Kyse-70: 1.5 x 10^5 cells/well
- Caco-2: 1.2 x 10^5 cells/well
- HepG2: 3 x 10^5 cells/well

and transfected with 1 mL transfection solution as described in section 2.2.13. On the next day, cells were coated with 1 mL culture medium and incubated for another 48 h until RNA (or proteins) were isolated. Total RNA was isolated from human cells or mice livers by applying the TRIzol® Reagent (Table 14). For this, cells were washed with 1-2 mL 1 x PBS and detached by adding 0.5 mL accutase® per well, and incubated at 37 °C for 15 min. Then, 0.5 mL cell culture medium was added to each well, the cells were resuspended and centrifuged at 300 x g for 7 min. The pelleted cells were washed with 5 mL 1 x PBS, centrifuged (300 x g, 7 min, RT) and resuspended in 0.5 mL TRIzol® Reagent. The cells were incubated at RT for 5 min. For the RNA isolation from mice livers, 50 mg of liver tissue was homogenized using 0.5 mL TRIzol® Reagent and a metal bead at 300 rpm for 3 min in a tissue lyser, proceeding with the protocol applicable to both procedures:
100 µL chloroform were added to the TRIzol® Reagent and the tube was thoroughly vortexed for 10 s. The reaction was incubated at RT for 15 min followed by centrifugation at 12,000 x g, 4 °C for 15 min. The aqueous phase was completely removed. The RNA was precipitated by the addition of 250 µL isopropanol, the slight inversion of the tube and an incubation period for 10 min at RT. The tube was centrifuged at 12,000 x g, 4 °C for 10 min, and the RNA was washed with 0.5 mL 70 % ethanol. Finally, the tube was centrifuged at 7,500 x g, 4 °C for 5 min. The RNA pellet was dried and resuspended in 30-50 µL DEPC-treated water. The RNA concentration was measured after a 1:5 dilution (RNA from cells) or a 1:10 dilution (RNA from mice livers) as described in section 2.2.11.

2.2.15 Reverse Transcription Polymerase Chain Reaction (RT-PCR)

For reverse transcription of RNA or miRNA, the SuperScript™ III First-Strand Synthesis System or TaqMan™ MicroRNA Reverse Transcription Kit was used. The heat incubation and thermal cycling steps were performed using 8-Strip PCR tubes (Table 15) and a PCR thermocycler (Table 16). For cDNA synthesis, either 1 µg (cell-derived), 5 µg (liver tissue-derived), or 10 ng (human sera-derived) RNA were used as starting material. The steps for reverse transcription of RNA or miRNA are distinguished and outlined in table 18.

Table 18. Composition of Master Mixes and Processed Steps during Reverse Transcription

Reverse Transcription (for RNA)	**Reverse Transcription (for miRNA)**
<u>Dnase I denaturation Master Mix</u> x µL RNA (1 µg/5 µg) 1 µL Dnase I Reaction Buffer (10 x) 1 µL Dnase I (1 U/µL) adjusted to 10 µL with DEPC-treated water Incubation at RT for 15 min. The reaction was stopped by addition of 1 µL EDTA (25 mM) and incubation at 65 °C for 10 min. 1.5 µL were removed to check for Dnase I degradation efficiency.	<u>Reverse Transcription Master Mix (15 µL total volume)</u> 4.16 µL Nuclease-free water 1.50 µL Reverse Transcription Buffer (10 x) 0.19 µL RNase inhibitor (20 U/µL) 0.15 µL dNTP Mix (100 mM) 1.00 µL MultiScribe™ Reverse Transcriptase (50 U/µL) 3.00 µL RT primer premix (miRNA-specific, 5 x) 5.00 µL RNA sample (10 ng) <u>RT conditions</u> 16 °C 30 min 42 °C 30 min 85 °C 5 min
<u>Reverse transcription initiation Master mix</u> 9.5 µL RNA mix (from previous step) 1 µL Oligo(dT)$_{20}$ (50 µM) 1 µL dNTP Mix (10 mM) The reaction was incubated at 65 °C for 5 min and stored on ice for 1 min.	
<u>Final reverse transcription Master mix</u> 2 µL RT Buffer (10 x) 4 µL $MgCl_2$ (25 mM) 2 µL DTT (100 mM) 0.5 µL RNase OUT™ (40 U/µL) 0.5 µL SuperScript™ III RT (200 U/µL) 8.5 µL of this Master mix were added to adjust the final volume of 20 µL. The RT reaction was incubated at 50 °C for 50 min, and 85 °C for 5 min.	

2.2.16 TaqMan-qPCR

For relative quantification of *UGT1A* or the miRNA of interest, the TaqMan principle was applied during quantitative Real-Time PCR (TaqMan-qPCR) [147]. The TaqMan principle is characterized by 15-30 bp oligonucleotide probes with complementary sequences to the target gene. These TaqMan probes are composed of a covalently attached reporter fluorophore at the 5'-end and a quencher fluorophore at the 3'-end. Due to the spatial proximity of both fluorophores, the fluorescence signal is quenched via Foerster Resonance Energy Transfer (FRET). However, during PCR, the dual-labeled probe specifically hybridizes to the complementary target sequence through Watson-Crick DNA base pairing, which is followed by the probe hydrolysis based on the DNA polymerase 5'-3' exonuclease activity (Figure 6). The fluorescence signal increases as the PCR product accumulates during the exponential phase of the PCR.

For UGT1A-based TaqMan-qPCR, the qPCR MasterMix Plus-Kit (Table 11) was used containing the HotGoldStar-DNA Polymerase, respective primers and dual-labeled probes (Table 4). For relative miRNA quantification, the TaqMan® Universal PCR Master Mix II and the TaqMan® Small RNA Assay primer and probe premix were used. The 5'-fluorophore dyes were 6-carboxyfluorescein (FAM) or 2'-chloro-7'phenyl-1,4-dichloro-6-carboxy-fluorescein (VIC), and the 3'-fluorophore dyes were 5-carboxy-tetramethylrhodamine (TAMRA) and Minor Groove Binder (MGB). In order to quantify the amount of target gene in the *UGT1A* assay, the expression of the reference gene *ß-actin* was measured. The SV40-miRNA spike-in control was measured as the internal control during miRNA quantification from cirrhotic and healthy individuals. The snoRNA234 was used as reference gene for miRNA quantification from fibrotic mice livers.

The HotGoldStar-DNA Polymerase initiated the polymerization process by the 3'-OH end of the primer and displaced the oligonucleotide probe from the 5'-end by its 5'-3'exonuclease activity. The fluorescence signal was detected by cleavage of the 5'-fluorophore dye and hydrolysis of the probe.

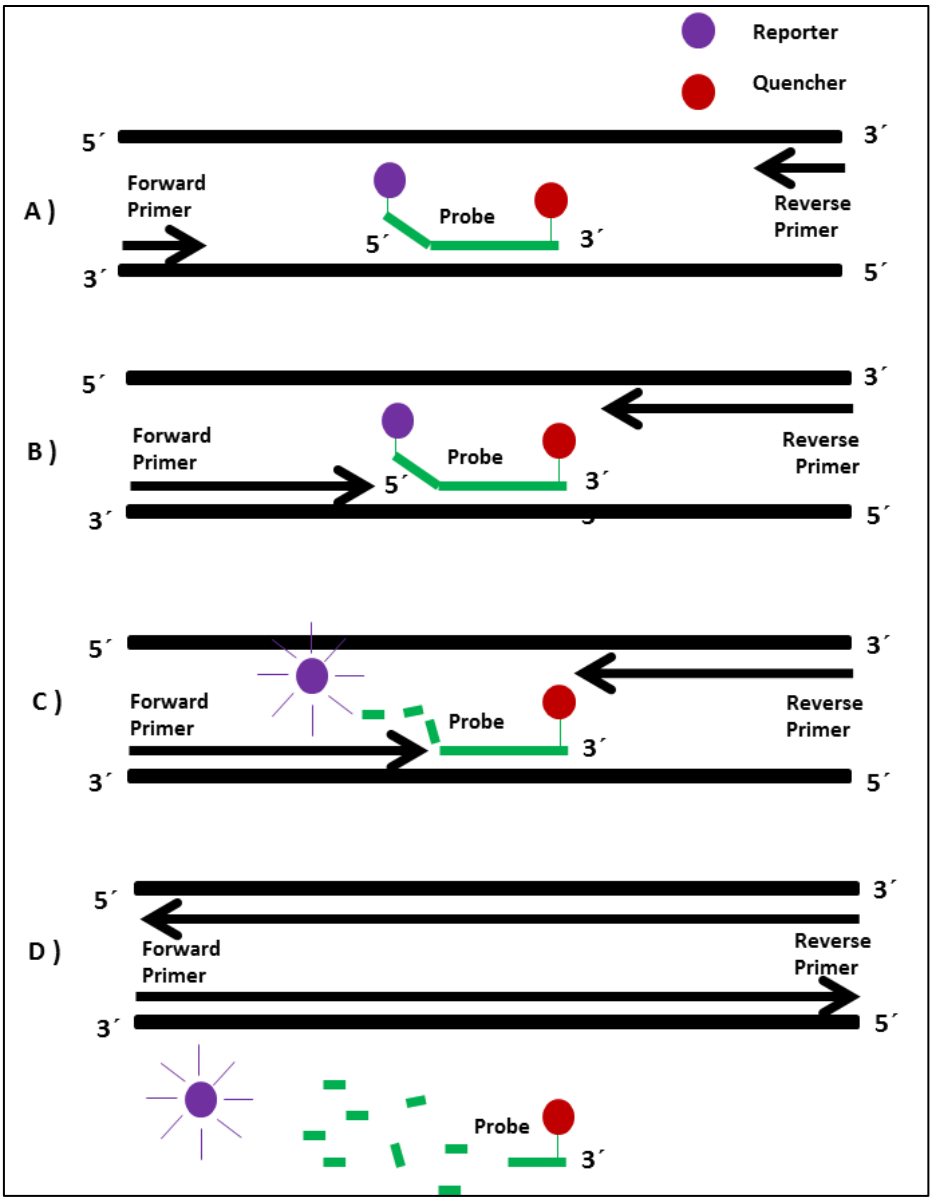

Figure 6. Schematic Representation of the TaqMan Principle. Dual-labeled oligonucleotide probes with a covalently attached fluorophore at the 5'-end (reporter) and a quencher fluorophore at the 3'-end (quencher) hybridize to the complementary target sequence during polymerization in the PCR (A). Yet, the fluorescence signal is quenched by the FRET effect as both molecules are in close spatial proximity. The DNA polymerase with its 5'-3'exonuclease activity displaces the strand (B) and cleaves the probe from the 5'-end releasing the fluorophore (C). The fluorescence signal is fully detected after the oligonucleotide probe is hydrolyzed and the polymerization is completed (D).

Standard TaqMan-qPCR reaction mix for *UGT1A* expression analysis (25 µL reaction):

Master Mix (Eurogentec)	12.5 µL
100 nM Probe	0.25 µL
600 nM Primer Forward	1.5 µL
600 nM Primer Reverse	1.5 µL
cDNA (diluted)	1 µL
ddH_2O ad 25 µL	8.25 µL

Standard TaqMan-qPCR reaction mix for *β-actin* expression analysis (25 µL reaction):

Master Mix (Eurogentec)	12.5 µL
200 nM Actin Probe	0.5 µL
300 nM Primer Forward	0.75 µL
300 nM Primer Reverse	0.75 µL
cDNA (diluted)	1 µL
ddH_2O ad 25 µL	9.5 µL

Standard TaqMan-qPCR reaction mix for analysis of circulating miRNA expression (10 µL reaction):

TaqMan® Small RNA Assay (20x)	0.50 µL
Product from RT reaction	1.33 µL
TaqMan® Universal PCR	
Master Mix II (2x), no UNG	5.00 µL
Nuclease-free water	3.17 µL

The TaqMan-qPCR reactions were performed in triplicates. The Master Mix contained the enzyme premix, oligonucleotide primers and the probe, and was diluted in ultra-pure water to the total volume of 24 µL. The *UGT1A* isoform-specific Master Mix was distributed on the 96-well plate by an automatic repeater pipette, and 1 µL of cDNA was manually pipetted. The Master Mix for the expression analysis of circulating miRNA contained the enzyme, primer and probe premix, 1.33 µL cDNA and was set up to the final volume of 10 µL with nuclease-free water. Then, the 96-well PCR plate was covered with a plastic tape and analyzed using the Thermal Cycler CFX 96 C1000 Touch and corresponding software CFX Manager (Bio-Rad).

Standard TaqMan-qPCR reaction conditions for *UGT1A* and miRNA expression analysis:

50 °C 2 min
95 °C 10 min
95 °C 15 s
60 °C 1 min
} 40 cycles

2.2.17 Luciferase Reporter Gene Assay

In order to analyze the effect of a miRNA of interest on the UGT1A 3'-UTR, luciferase reporter gene assays were carried out. Therefore, the luciferase-encoding reporter plasmid pGL-Basic was used as the recipient plasmid for cloning of 679 bp UGT1A 3'-UTR between the luciferase open reading frame (ORF) and the SV 40 poly A signal. This resulted in DNA plasmid pGL3-UGT1A-3'-UTR. Thereby, the activity of pGL3-UGT1A-3'-UTR-encoded luciferase after miRNA transfection would shed light on the effect of a miRNA with the UGT1A 3'-UTR. Additional mutation in the UGT1A 3'-UTR led to the generation of DNA plasmid pGL3-UGT1A-3'-UTR seed mutation as explained before (chapter 2.2.3).

For the luciferase reporter gene assay, the Dual-Luciferase® Reporter Assay System (Promega) was used. For this, the human embryonic kidney cell line (Hek293) was transfected with the following molecules:

- pGL3-based reporter vector encoding Firefly luciferase *Photinus pyralis*
- pRL-TK vector encoding luciferase *Renilla reniformis*
- miRNA of interest

On the first day, Hek293 cells were detached as described before in section 2.2.12, counted in a Neubauer counting chamber, and in a 12-well plate layout, 50,000 cells were seeded in each well.

On the second day, the cells were transfected as described in section 2.2.13. Briefly, a solution labeled as A was prepared and incubated in the dark for 5 min. Meanwhile a solution labeled as B was prepared containing Opti-MEM®, 1 µg pGL3-based reporter plasmid, the transfection control vector pRL-TK and a miRNA. Both solutions A and B were consolidated and incubated in the dark for 20 min, in order to allow DNA plasmid-miRNA-liposome complexes to form. The Hek293 cells were gently washed with 1 x PBS,

0.5 mL transfection solution was applied to each well in triplicate, and the cells were incubated at 37 °C.

On the third day, 0.5 mL growth medium was added to each well and the cells were incubated for 48 h at 37 °C.

On the fifth day, the cells were washed with 1 x PBS, lysed with 1 x Passive Lysis Buffer (Promega), and agitated at 350 rpm for 15 min, in order to release the luciferases and measure their activities. To measure the bioluminescence at the luminometer, 2 different reactions were performed after the addition of 10 µL cell suspension to each well of a 96-well plate:

- 50 µL Luciferase Assay Reagent II were added by the luminometer to create a stabilized luminescent signal and quantify the Firefly luminescence. The luciferase activity corresponded to the Relative Light Units (RLU) measured for 10 s.
- 50 µL Stop & Glo® Reagent were added and the Firefly luminescence was quenched and the pRL-TK encoded *Renilla* luciferase reporter was simultaneously measured that corresponded to the internal transfection control signal measured for 10 s.

In order to analyze the effect of a miRNA, a ratio of Firefly and *Renilla* luminescence was calculated and resulted in an RLU quotient. Every quotient was divided by the miR-control quotient to establish a fold-change. Besides DNA plasmid pGL3-UGT1A-3'-UTR, the empty vector pGL3 was transfected to account for the potential miRNA off-target interactions with the pGL3-backbone. The results were analyzed by Microsoft Excel 2010 and determined the relative luciferase fold-changes at the miRNA-UGT1A 3'-UTR interaction. Data values are represented as means of each treatment. The error values are expressed as the standard error of each treatment after at least three independent replicates.

2.2.18 Preparation of Nuclear Extracts

Nuclear extracts were prepared to study the effect of miRNAs on the expression of TFs involved in the transcriptional regulation of *UGT1A* genes [48]. Nuclear extracts were prepared from HepG2 cells in a 6-well plate layout, seeded at 2.5 x 10^6 cells per well, and following the transfection protocol and cell culture steps outlined in section 2.2.14. The preparation of nuclear extracts was performed according to the manufacturer's instructions in the Nuclear Extraction Kit (Abcam). In a first step, the cell pellet from the adherent cells was prepared. To achieve this, the growth medium was removed, and the cells were washed twice with 5 mL 1 x PBS. The cells were dissociated with 0.5 mL accutase®, resuspended in 0.5 mL growth medium, and centrifuged at 1,000 rpm for 5 min. The supernatant was removed and the cells were resuspended in 100 µL 1 x Pre-Extraction buffer per 10^6 cells. The cell suspension was transferred to 1.5 mL tubes, incubated on ice for 10 min, vigorously vortexed

for 10 s and centrifuged at 12,000 rpm for 1 min. The supernatant was discarded, and 2 volumes of Extraction buffer supplemented with 1:1000 diluted DTT solution and protease inhibitor cocktail were added to the nuclear pellet, which was incubated on ice for 15 min with occasional vortexing. The suspension was centrifuged at 14,000 rpm, 4 °C for 10 min, and the supernatant containing the nuclear extract was measured by Bradford assay described in section 2.2.22.

2.2.19 Isolation of Mouse Primary Hepatocytes

The isolation of mouse primary hepatocytes was pursued to create an *ex vivo* model for the study of *UGT1A* expression after miRNA transfection. For this, the laboratory-available *htgUGT1A*-WT mouse model was used to isolate primary hepatocytes and study the non-coding RNA-based knockdown of hepatic drug-metabolizing enzymes [148]. Thereby, results obtained from this experiment can be transferred to the *in vivo* situation in the mouse itself.

For the experiment, all the solutions (EGTA solution, 1 x Collagenase solution, and Williams medium E) were preheated to 37 °C. The Williams medium E, 1 x Collagenase solution and material were prepared as follows:

1) 500 mL of Williams medium E were supplemented with 5 mL Pen/Strep, 10 mL L-glutamine and 50 mL FCS.

2) 50 mL of this Williams medium E were supplemented with 500 µL 100 x Insulin-Transferrin-Selenium mix and 5 µL 0.39 mg/mL dexamethasone dissolved in DMSO. This modified Williams medium E was used throughout all steps.

3) 500 mL of HBSS solution were supplemented with 10 % FCS.

4) 100 mL of 1 x Collagenase solution were supplemented with 42 mg Collagenase.

5) 5 mL of collagen A was diluted in a 1:2 proportion with 5 mL Aqua dest. and the solution was added to a T75 cell culture flask, incubated at 37 °C for 30 min. The collagen A solution was removed, the flask was washed with 5 mL 1 x PBS and was ready to be used.

A male *htgUGT1A*-WT mouse was narcotized with 0.4-0.5 mL Ketamine/Xylazine (12.15 mL NaCl added with 0.9 mL Ketamine (10%) and 0.45 mL Xylazine (2%)) by intraperitoneal injection. The abdomen was opened, and the liver was perfused with EGTA solution at 5.6 mL/min for 5 min using a peristaltic pump. Then, the liver was perfused with 1 x Collagenase solution at 5.6 mL/min for 10 min. The liver was covered with warm 1 x Collagenase solution, transferred to a Petri plate and homogenized with tweezers under the laminar flow cabinet. A 25 mL pipette was used to filtrate the homogenous suspension through a 100 µM

cell strainer into a 50 mL Falcon tube. The Petri dish was washed with chilled HBSS solution, the suspension was transferred to the 50 mL Falcon tube, and the maximum volume was adjusted with HBSS. The Falcon tube was centrifuged at 50 x g, 4 °C for 3 min, and the supernatant was discarded. The cell pellet was gently resuspended with 5 mL HBSS and the maximum volume of 50 mL was adjusted with HBSS. The Falcon tube was centrifuged at 50 x g, 4 °C for 3 min and the washing step was repeated one more time. Then, the supernatant was discarded and 5 mL preheated Williams medium E were used to gently resuspend the cell pellet. The primary hepatocytes were counted in a Neubauer counting chamber by preparing a 1:5 dilution with trypan blue. Approximately 1 x 10^7 hepatocytes were transferred to the T75 cell culture flask and incubated at 37 °C for 2 h. The Williams medium E was removed, the cells were gently washed with 5 mL 1 x PBS, and 10 mL preheated Williams medium E was added. The hepatocytes were cultivated overnight at 37 °C, transfected with miR-control or miR-486-3p, coated with preheated Williams medium E, incubated for another 24 h, until microsomes were isolated on the fourth day.

2.2.20 Isolation of Microsomes

Microsomes were isolated from mouse primary hepatocytes, as these vesicles of hepatocyte ER contain phase I and II enzymes, including UGTs [149]. After the removal of Williams medium E from the cell culture flask, hepatocytes were washed with 5 mL 1 x PBS and dissociated with 2 mL accutase®. The hepatocytes were resuspended in 3 mL Williams medium E (as prepared in section 2.2.19) and centrifuged at 1,000 x g, 4 °C for 5 min. The supernatant was removed.

All the subsequent steps were performed on ice, so that the technical devices required to be pre-chilled to 4 °C. The pellet was resuspended in 1-2 mL UGT buffer and mechanically homogenized ten-times at 300 rpm using Potter-Elvehjem tissue grinders. The homogenous suspension was transferred to 1.5 mL tubes and centrifuged at 2,000 x g for 10 min. The supernatant was transferred to new 1.5 mL tubes and centrifuged at 10,000 x g for 10 min. The supernatant was collected in ultracentrifugation tubes, the pellet was resuspended in 1 mL UGT buffer, and centrifuged at 10,000 x g for 10 min. This supernatant was collected in the ultracentrifugation tubes and centrifuged at 100,000 x g for 1 h. Then, the pellet was resuspended in 100-200 µL UGT buffer and the protein concentration was determined by Bradford assay.

2.2.21 Activity Assay

For the determination of UGT enzyme activity, the UGT-Glo™ Assay (Promega) was performed in 96-well plates according to the manufacturer's instructions. The capacity of UGT enzymes to glucuronidate a proluciferin substrate was measured using the previously isolated microsomes.

Two reactions labeled as A and B were performed in parallel. A) In wells without uridine 5'-diphosphoglucuronic acid (UDPGA) cofactor, 10 µL Aqua dest. were added. B) In the parallel wells, UDPGA was pipetted at a final concentration of 4 mM diluted in Aqua dest. The general UGT reaction mixture contained 1 x UGT buffer (supplemented with 1:160 diluted alamethicin), 50 µM proluciferin substrate, 0.5 µg microsomes, and diluted with Aqua dest. to the final volume of 20 µL. A non-UGT control was prepared without microsomes.

The 96-well plate was stored in a plastic bag and incubated at 37 °C for 90 min. Next, 20 µL of Luciferin detection reagent (supplemented with 1:100 diluted D-cysteine) were added to each well with a multichannel pipette, the plate was vigorously agitated and incubated at RT for 20 min. The luminescence was determined using a luminometer.

2.2.22 Measurement of Protein Concentration

The protein concentration was measured by Bradford assay according to the principles described by Bradford [150]. Briefly, the protein assay reagent (Bio-Rad) was diluted at a ratio of 1:5 in distilled water, and 990 µL of the final solution were transferred to polystyrene cuvettes. The protein samples were diluted at a ratio of 1:5 or 1:10, and 10 µL of the corresponding dilution were added to the cuvette. The cuvette was sealed with Parafilm, mixed by inversion, and incubated at RT for 5 min. The protein concentration was measured spectrophotometrically at 595 nm using the BioPhotometer plus (Eppendorf).

2.2.23 Western Blot

Western Blot analysis was performed for the qualitative as well as semi-quantitative analysis of UGT1A proteins after miRNA transfection [151]. For protein isolation, Caco-2, HepG2 and Kyse-70 cells were seeded in 6-well plates as described in section 2.2.14. Each well was washed with 1-2 mL 1 x PBS, and the cells were detached using 0.5 mL accutase®. Then, the cells were resuspended in 0.5 mL cell culture medium, centrifuged (300 x g, RT, 7 min), and washed with 5 mL 1 x PBS. After centrifugation (300 x g, RT, 7 min), the cells were

resuspended in 100-200 µL 1 x PBS, and subjected to three freeze (-80 °C) thaw (37 °C) cycles, in order to lyse cells and release the proteins. The protein concentration was determined as explained in section 2.2.22. For the separation of proteins by Sodium Dodecyl Sulfate-Polyacrylamide Gel Electrophoresis (SDS-PAGE), 20 µg protein was mixed with 2 x Laemmli Buffer and diluted with 1 x PBS to the final volume of 20 µL. The proteins were denatured at 95 °C for 5 min, stored on ice for 2 min, and then pipetted to a denaturing polyacrylamide gel that was prepared according to the TGX Stain-Free™ FastCast™ Acrylamide Kit (Bio-Rad).

Composition of the denaturing polyacrylamide gel:

Stacking gel (5-10 %)
1.5 mL Stacker A solution (Bio-Rad)
1.5 mL Stacker B solution (Bio-Rad)
15 µL 10 % APS
3 µL TEMED

Resolving gel (10-20 %)
4 mL Resolver A solution (Bio-Rad)
4 mL Resolver B solution (Bio-Rad)
40 µL 10 % APS
4 µL TEMED

The gel electrophoresis was performed at 150 V for 50 min in 1 x SDS running buffer using the Mini-PROTEAN Tetra Cell (Bio-Rad). The separated proteins were transferred from the gel to a nitrocellulose membrane by blotting. In order to mask the protein-free surface of the membrane, the membrane was blocked by using 5-10 mL of a 5 % powdered milk-PBST solution, shaking at RT for 1 h. Then, the primary antibody was diluted in a range between 1:500 to 1:3000 in 5 % powdered milk-PBST solution and dispensed on the membrane. The membrane was incubated overnight shaking at 4 °C. On the next day, the membrane was washed with PBST three times (15 min each) to remove the nonspecifically bound primary antibody. The horseradish peroxidase (HRP)-coupled secondary antibody was diluted at 1:2000 in PBST and applied to the membrane. The membrane was incubated at RT shaking for 1 h. Finally, the membrane was washed with PBST three times, and the proteins were

detected. To visualize the protein bands the Clarity™ Western ECL substrate was used. The substrate was composed of the luminol/enhancer solution and the peroxide solution mixed in a 1:1 ratio, and dispensed on the membrane. The membrane was incubated at RT shaking for 5 min, placed in a ChemiDoc™ MP Imaging System (Bio-Rad), and the protein bands were visualized using Image Lab software 5.2.

2.2.24 Statistical Analysis

Statistical analysis was performed using GraphPad Prism version 8 (GraphPad Software). The data values are represented as the mean of the group (or treatment) under investigation. Additionally, the error values are expressed as the standard error of the mean (SEM) for each group using at least three independent replicates. The Student's t-test (two-tailed) was applied to compare the experimental groups to the control group. To compare miRNA expression levels in cirrhotic patients and healthy controls, a Welch's t-test was performed. This analysis accounts for the different sample sizes in the compared groups. The differences were considered significant when *p*-values were below 0.05.

3 Results

3.1 Identification of Novel UGT1A-Regulating miRNAs

Despite the progress in the miRNA research area, still limited data focussing on the implication of post-transcriptional regulation of drug-metabolizing *UGT1A* expression and liver disease development exists. Therefore, this study aimed to identify novel UGT1A-downregulating miRNAs and connect their potential overexpression to the development of severe liver diseases (e.g. liver fibrosis and cirrhosis) due to an impaired UGT1A-mediated detoxification of endo- and xenobiotics, as well as other reactive metabolites. Accordingly, an array of 30 miRNAs previously identified to be dysregulated in HCC was selected for this experimental analysis [135].

3.2 Regulation of UGT1A 3'-UTR Luciferase Activity by miRNAs

Mammalian miRNAs were described to silence target gene expression by partial hybridization to MREs in the 3'-UTR of the target mRNA which can result in mRNA decay or translational inhibition [86]. In order to investigate the effect of 30 miRNAs on the common UGT1A 3'-UTR, a luciferase reporter gene assay was performed with the goal of identifying miRNAs that reduce the luciferase activity. To perform this assay, the luciferase DNA plasmid construct that contains the genetic element of interest was generated. Therefore, the UGT1A 3'-UTR was cloned into the pGL3-Basic vector chosen as the DNA plasmid, based on the presence of the desired restriction sites in a polylinker. For the UGT1A 3'-UTR insertion, the entire 679 bp of the common UGT1A 3'-UTR were cloned between the Firefly luciferase ORF and the SV40 poly A signal (Figure 7).

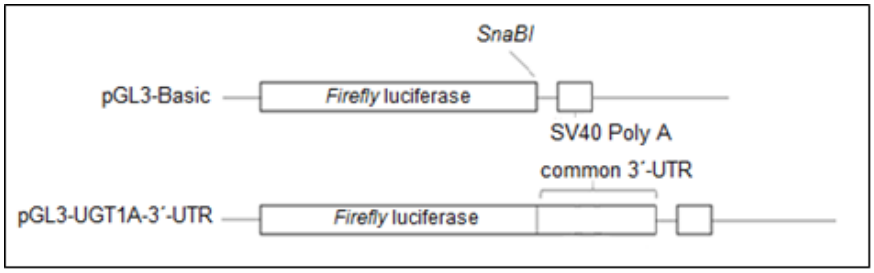

Figure 7. Insertion of the Shared UGT1A 3'-UTR into pGL3-Basic Reporter Vector. The restriction site *SnaBI* was introduced into the pGL3-Basic vector, and then 679 bp of the common UGT1A 3'-UTR were cloned between the Firefly luciferase ORF and the SV40 poly A signal. The corresponding DNA plasmid was termed pGL3-UGT1A-3'-UTR and used as a luciferase reporter construct during luciferase assays.

The generated DNA plasmid was designated pGL3-UGT1A-3'-UTR and used as a luciferase reporter construct during luciferase assays performed in Hek293 cells. Hek293 cells were chosen for luciferase assays, because they express low UGT1A mRNA levels [59]. A reduced, near-absent expression of endogenous UGT1A mRNA levels in Hek293 would, therefore, eliminate the potential bias of a miRNA for endogenously expressed UGT1A mRNAs containing the common 3'-UTR. To consider the possibility for a miRNA-mediated unspecific plasmid backbone interaction, miRNAs were co-transfected with pGL3-Basic. The transfection of DNA plasmids (pGL3-Basic constructs and transfection control plasmid pRL-TK) and a miRNA into Hek293 cells was performed using a cationic liposome-based transfection protocol described to provide high transfection efficiency throughout established cell lines [152]. Thereby, the underlying transfection principle is termed lipofection which harnesses the entrapment of nucleic acids in liposomes, followed by their fusion with the plasma membrane of cultured cells [153]. For lipofection, Lipofectamine 2000® was used which is a transfection reagent that contains cationic lipid components and a neutral helper lipid able to form liposomes in an aqueous environment [154]. By the formation of DNA-miRNA-liposome complexes, the negative charge of the nucleic acids is masked which allows to overcome the plasma membrane's electrostatic repulsion [152]. Therefore, the nucleic acid-containing liposome is positively charged on the surface which enables the fusion of the liposome with the negatively charged plasma membrane. The fusion is further mediated by the neutral helper lipid. In that way, the nucleic acids are released into the cytoplasm of the recipient cells where they can enter the nucleus for gene transcription (i.e., pGL3-based plasmids), or remain in the cytoplasm for the formation of the RISC complex (i.e., miRNA). After cultivation and lysis of Hek293 cells, the luminescent reporter activities of the pGL3-encoded Firefly luciferase and pRL-TK-encoded *Renilla* luciferase were determined. Therefore, this dual luciferase assay system was used for the reporter quantification in the mammalian cells (Hek293). Among the bioluminescent reporters, the *Renilla* luciferase reporter was used as internal control to which measurement of the Firefly luciferase reporter was normalized. Two individual substrate solutions were prepared and used in the bioluminometer. Thereby, the Firefly luciferase emits photons via oxidation of beetle luciferin, forming the product molecule oxyluciferin. In contrast, the *Renilla* luciferase catalyzes the oxidation of coelenterazine to coelenteramide and light [155]. In this way, a ratio of both luciferase Relative Light Unit (RLU) signals was calculated. Then, results were compared to the miR-control group, in order to generate fold-changes of the luciferase

activity. Since DNA plasmids pGL3-Basic or pGL3-UGT1A-3'-UTR were transfected, the difference between both groups resulted in the interaction of the miRNA with the UGT1A 3'-UTR (as explained in section 2.2.17).

Figure 8 displays the interaction of the investigated miRNAs with the common UGT1A 3'-UTR. A slightly induced relative luciferase activity was observed in miRNA transfected Hek293 cells compared to miR-control transfection. In detail, a statistically significant induction of luciferase activity was detected after miR-16a (1.23-fold), miR-34a (1.35-fold), and miR-200b (1.25-fold) transfection. Comparable results were observed for miR-25 (1.20-fold), miR-106b (1.20-fold), miR-199a-5p (1.25-fold), miR-221 (1.20-fold), and miR-224 (1.25-fold), although these results are not statistically significant. A slight, statistically insignificant induction of the relative luciferase activity was observed for miR-15a (1.10-fold), miR-17 (1.19-fold), miR-18a (1.18-fold), miR-20a (1.13-fold), miR-21 (1.15-fold), miR-29a (1.09-fold), miR-93 (1.03-fold), miR-122 (1.15-fold), miR-148a (1.07-fold), miR-151-5p (1.13-fold), miR-155 (1.15-fold), miR-181a-5p (1.10-fold), miR-183-5p (1.05-fold), miR-199a-3p (1.09-fold), miR-216a (1.10-fold), miR-222 (1.07-fold), miR-330 (1.07-fold), miR-4321 (1.13-fold), and miR-519d (1.10-fold). On the contrary, the luciferase activity was statistically significantly reduced by miR-214-5p (0.44-fold) and miR-486-3p (0.42-fold) compared to miR-control. A weak, statistically insignificant reduction of the luciferase activity was observed after miR-214-3p (0.02-fold) transfection.

This data indicates that the investigated miRNAs are capable to elicit an inductive or inhibitory effect on luciferase activity after hybridization to the common UGT1A 3'-UTR. Particularly noteworthy is the fact that among the thirty selected miRNAs miR-214-5p and miR-486-3p exhibited a substantial reduction of the UGT1A 3'-UTR luciferase activity.

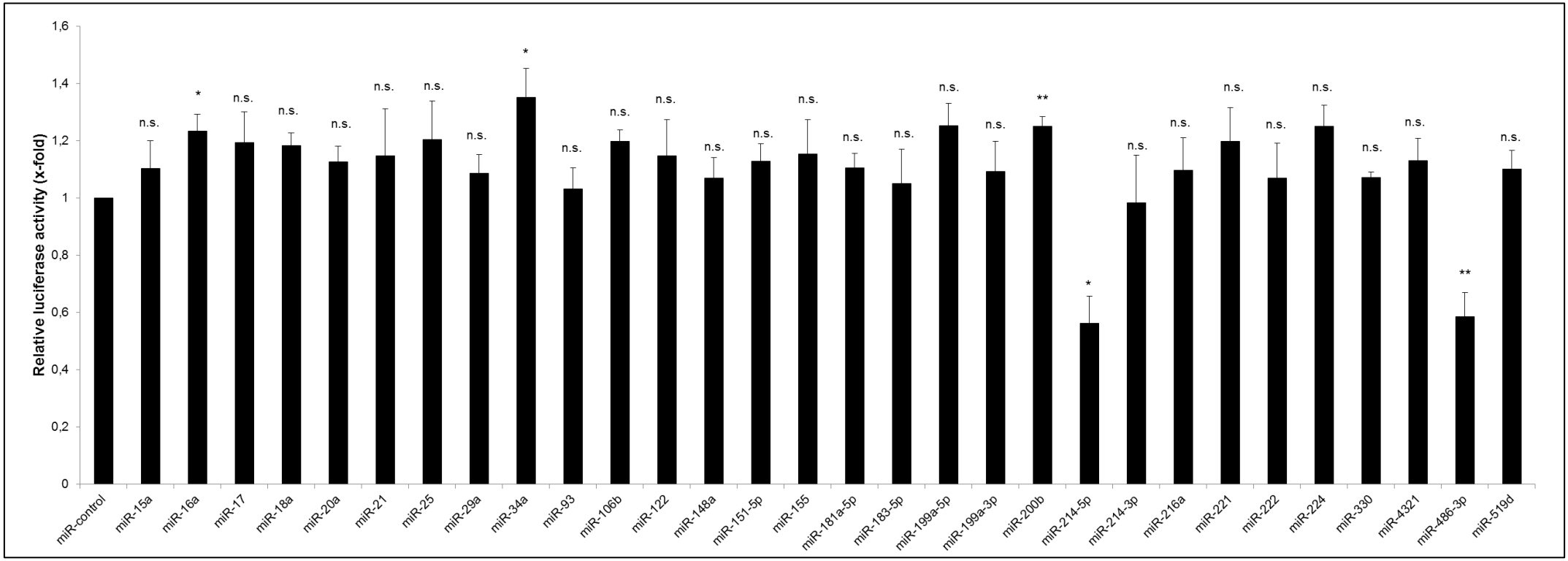

Figure 8. Effect of miRNAs on UGT1A 3'-Untranslated Region (UTR) in Luciferase Reporter Gene Assays. The post-transcriptional effect of thirty miRNAs dysregulated in HCC was studied in a luciferase reporter gene assay. Hek293 cells were, therefore, transfected with reporter plasmid pGL3-UGT1A-3'-UTR, transfection control vector pRL-TK, and a miRNA. Of note, miR-16a, miR-34a, and miR-200b significantly induced the relative luciferase activity, whereas the relative luciferase activity was significantly reduced after miR-214-5p and miR-486-3p transfection. The plasmids pGL3-Basic, pRL-TK, and a miRNA were transfected to consider potential miRNA off-target interactions with the reporter construct. The columns represent the fold-changes of the relative luciferase activity in a miRNA-UGT1A 3'-UTR interaction. The data represents the means and the Standard Error of the Mean (SEM) of three independent replicates. Significance was calculated relative to the pGL3-Basic. *: $p < 0.05$; **: $p < 0.01$; n.s.: not significant.

3.3 Regulation of UGT1A mRNA Levels by miRNAs in HepG2 Cells

MiRNAs regulate gene expression by binding to complementary sequences in the 3'-UTR of the target mRNA leading to mRNA degradation. The aim of this analysis was to test whether the investigated miRNAs were able to reduce isoform-specific UGT1A mRNA levels in liver cells. So far, fresh human liver samples are scarce and human hepatocytes are known to underlie *in vitro* phenotypic instability [156]. Therefore, human cell lines were utilized. Liver-derived cells or tissues were selected, because the liver is the major organ involved in drug metabolism in the human body. Moreover, it also expresses the majority of *UGT1A* genes. Thus, the human hepatoma cell line HepG2 was used for *UGT1A* expression analysis [157]. HepG2 cells are derived from liver biopsies of a 15-year-old Caucasian male's HCC [158]. Moreover, these cells are epithelial-like, nontumorigenic and higly proliferative with a stable phenotype and a near unlimited life span. However, the major drawback of adherent HepG2 cells is the relatively low expression of drug-metabolizing enzymes, including UGT1As, compared to the human liver or primary cultured human hepatocytes [159]. This ultimately requires sensitive detecting techniques for gene expression analysis [157].

To determine *UGT1A* gene expression, the combination of RT-PCR and Real-Time PCR was performed. This method requires the total RNA isolation from HepG2 cells and the use of oligo(dT)-based reverse transcription in a first step. In the second step, the relative quantification of UGT1A mRNA expression was performed using Real-Time PCR with isoform-specific primers and probes (Table 4) (section 2.2.16). Real-Time PCR has been described as a highly sensitive technique that can detect as little as a single copy of a specific transcript [160]. The UGT1A mRNA expression was quantified relative to *β-actin* expression. This reference gene was expressed throughout different treatments across various cell lines, including HepG2 (data not shown).

The results of UGT1A mRNA expression after miRNA transfection are shown in figures 9-14. In the following sections, the results are separately listed for each UGT1A isoform. Furthermore, the UGT1A mRNA expression is compared to the miR-control transfected HepG2 cells.

UGT1A1

UGT1A1 mRNA expression was significantly induced by miR-34a (2.25-fold), miR-122 (2.90-fold), miR-181a-5p (1.77-fold), miR-199a-5p (1.69-fold), miR-200b (1.19-fold), miR-

221 (1.35-fold), and miR-222 (1.88-fold). Likewise, miR-93 (1.12-fold), miR-106b (1.08-fold), and miR-224 (1.58-fold) slightly but insignificantly induced UGT1A1 mRNA expression. On the contrary, the UGT1A1 mRNA expression was significantly reduced by miR-16a (0.39-fold), miR-18a (0.27-fold), miR-25 (0.49-fold), miR-29a (0.41-fold), miR-151-5p (0.49-fold), miR-183-5p (0.75-fold), miR-199a-3p (0.27-fold), miR-214-5p (0.39-fold), miR-216a (0.25-fold), miR-4321 (0.41-fold), miR-486-3p (0.60-fold), and miR-519d (0.27-fold). In addition, an insignificant reduction of UGT1A1 mRNA expression was observed after miR-15a (0.04-fold), miR-17 (0.04-fold), miR-20a (0.16-fold), miR-21 (0.27-fold), miR-148a (0.12-fold), miR-214-3p (0.18-fold), and miR-330 (0.46-fold) transfection. No post-transcriptional effect was observed after miR-155 transfection (Figure 9).

UGT1A3

A highly significant upregulation of the UGT1A3 mRNA expression was detected after miR-34a (2.52-fold) and miR-122 (1.97-fold), followed by miR-222 (1.31-fold), miR-199a-5p (1.24-fold), and miR-106b (1.21-fold) transfection. No significant induction was determined when HepG2 cells were transfected with miR-20a (1.09-fold), miR-21 (1.07-fold), miR-200b (1.26-fold), miR-221 (1.19-fold), and miR-224 (1.16-fold). A significant downregulation of the UGT1A3 mRNA expression resulted after miR-17 (0.35-fold), miR-18a (0.54-fold), miR-25 (0.32-fold), miR-29a (0.47-fold), miR-151-5p (0.26-fold), miR-183-5p (0.59-fold), miR-199a-3p (0.32-fold), miR-214-5p (0.32-fold), miR-214-3p (0.42-fold), miR-330 (0.61-fold), miR-486-3p (0.57-fold), and miR-519d (0.26-fold) transfection. Furthermore, miR-16a (0.09-fold), miR-93 (0.13-fold), miR-148a (0.05-fold), miR-155 (0.20-fold), miR-181a-5p (0.05-fold), miR-216a (0.20-fold), and miR-4321 (0.20-fold) insignificantly reduced UGT1A3 mRNA expression. No effect on UGT1A3 mRNA expression resulted after miR-15a transfection (Figure 10).

UGT1A4

UGT1A4 mRNA expression was significantly repressed after miR-16a (0.60-fold), miR-18a (0.44-fold), miR-20a (0.53-fold), miR-29a (0.55-fold), miR-34a (0.55-fold), miR-106b (0.53-fold), miR-181a-5p (0.62-fold), miR-199a-5p (0.66-fold), miR-199a-3p (0.50-fold), miR-221 (0.50-fold), and miR-519d (0.53-fold) transfection. An insignificant reduction of UGT1A4 transcription was detected after miR-15a (0.07-fold), miR-17 (0.41-fold), miR-122 (0.25-fold), miR-148a (0.64-fold), miR-151-5p (0.55-fold), miR-155 (0.61-fold), miR-183-5p (0.07-

fold), miR-214-5p (0.28-fold), miR-214-3p (0.12-fold), miR-216a (0.16-fold), miR-222 (0.05-fold), miR-330 (0.37-fold), miR-4321 (0.07-fold), and miR-486-3p (0.37-fold) transfection. A slight, insignificant induction of UGT1A4 mRNA levels was observed after overexpression of miR-25 (1.07-fold), miR-93 (1.04-fold), and miR-200b (1.07-fold). No post-transcriptional effect was observed after miR-21 and miR-224 transfection (Figure 11).

UGT1A6

Similarly to the UGT1A4 mRNA expression, UGT1A6 mRNA levels were significantly reduced following transfection with miR-15a (0.38-fold), miR-16a (0.53-fold), miR-18a (0.62-fold), miR-25 (0.62-fold), miR-29a (0.47-fold), miR-155 (0.42-fold), miR-199a-3p (0.48-fold), miR-221 (0.42-fold), miR-486-3p (0.57-fold), and miR-519d (0.38-fold). An insignificant reduction of UGT1A6 mRNA levels was detected after miR-17 (0.21-fold), miR-20a (0.29-fold), miR-21 (0.35-fold), miR-34a (0.19-fold), miR-93 (0.35-fold), miR-106b (0.14-fold), miR-122 (0.26-fold), miR-148a (0.37-fold), miR-151-5p (0.21-fold), miR-183-5p (0.12-fold), miR-200b (0.04-fold), miR-214-5p (0.35-fold), miR-214-3p (0.22-fold), miR-216a (0.39-fold), miR-222 (0.34-fold), miR-330 (0.21-fold), and miR-4321 (0.39-fold) transfection. Only miR-199a-5p (1.19-fold) and miR-224 (1.02-fold) induced UGT1A6 mRNA levels, however the results were not statistically significant. In case of miR-181a-5p, no post-transcriptional effect was determined (Figure 12).

UGT1A7

UGT1A7 mRNA expression was significantly upregulated after miR-15a (2.36-fold), miR-18a (2.36-fold), miR-20a (3.21-fold), miR-21 (3.36-fold), miR-106b (1.61-fold), miR-122 (2.32-fold), miR-148a (3.36-fold), miR-151-5p (3.11-fold), miR-155 (4.14-fold), miR-181a-5p (2.93-fold), miR-199a-5p (3.03-fold), miR-199a-3p (3.39-fold), miR-200b (3.25-fold), miR-221 (2.21-fold), miR-222 (1.78-fold), and miR-224 (2.75-fold) transfection. An insignificant induction of UGT1A7 mRNA levels resulted after miR-16a (1.43-fold), miR-17 (3.14-fold), miR-25 (1.50-fold), miR-29a (1.61-fold), miR-93 (1.21-fold), miR-216a (1.21-fold), miR-330 (1.14-fold), miR-486-3p (1.14-fold), and miR-519d (1.21-fold) transfection. Only miR-4321 (0.86-fold) significantly repressed UGT1A7 mRNA expression. A comparable repression was observed after miR-214-5p (0.79-fold) and miR-183-5p (0.61-fold) overexpression, though these results were not significant. An insignificant, slight

reduction was detected after miR-214-3p (0.25-fold) transfection. After miR-34a transfection, no post-transcriptional effect was detected (Figure 13).

UGT1A9

UGT1A9 mRNA expression was significantly induced after miR-122 (1.56-fold), miR-148a (2.28-fold), miR-155 (2.09-fold), miR-181a-5p (2.47-fold), miR-199a-5p (4.25-fold), miR-200b (3.75-fold), miR-221 (2.59-fold), and miR-222 (3.03-fold) transfection. Other miRNAs such as miR-16a (1.44-fold), miR-20a (1.25-fold), miR-21 (1.19-fold), miR-34a (1.25-fold), miR-93 (1.19-fold), miR-151-5p (1.31-fold), miR-199a-3p (1.25-fold), miR-214-3p (1.53-fold), miR-216a (1.13-fold), miR-224 (1.69-fold), miR-486-3p (1.06-fold), and miR-519d (1.41-fold) were also able to induce UGT1A9 mRNA levels, but these results were not statistically significant. Among the 30 investigated miRNAs, only miR-25 (0.56-fold) and miR-214-5p (0.47-fold) significantly reduced *UGT1A9* gene transcription. A reduction of UGT1A9 mRNA expression was calculated for miR-15a (0.03-fold), miR-106b (0.06-fold), miR-183-5p (0.13-fold), and miR-4321 (0.44-fold). However, these results were not statistically significant. Compared to miR-control treatment, no significantly altered UGT1A9 mRNA expression was observed after miR-17, miR-18a, miR-29a, and miR-330 transfection (Figure 14).

Taken together, this data indicates the variable effects of a miRNA in different UGT1A isoforms. Interestingly, differential effects of miRNAs on different UGT1A isoforms were observed revealing that a miRNA can induce the expression of one UGT1A isoform, but reduce the expression of another. This finding is of particular interest, as all UGT1A isoforms share the common UGT1A 3'-UTR. Since miRNAs usually mediate inhibitory effects, it is worth mentioning that some of the investigated miRNAs exhibited an inductive effect on UGT1A mRNA expression, indicating additional miRNA-mediated regulatory mechanisms. Noteworthy, miR-214-5p, miR-486-3p, and miR-519d showed the highest consistency in their inhibitory effect across all UGT1A isoforms.

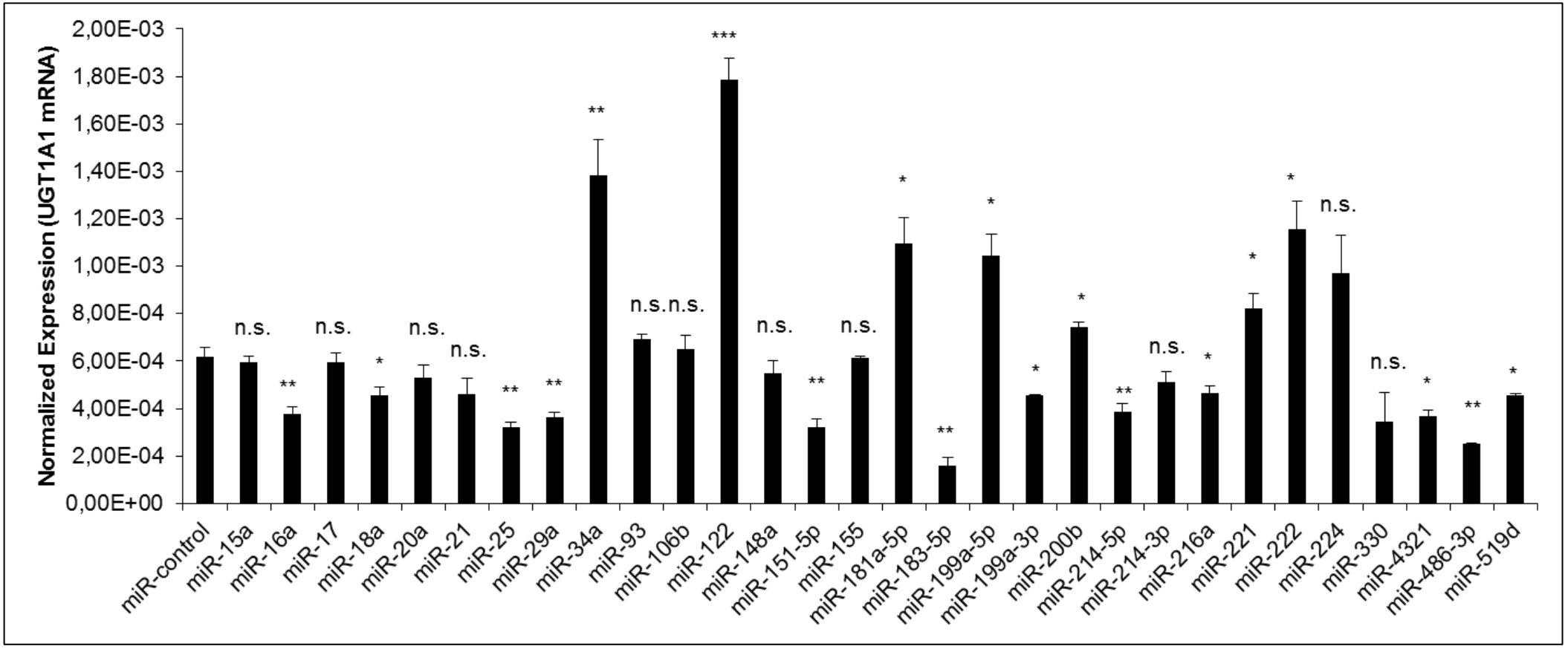

Figure 9. Expression of UGT1A1 mRNA after miRNA Transfection into HepG2 Cells. An array of 30 microRNAs was overexpressed in HepG2 cells and the UGT1A1 mRNA expression was determined by TaqMan-qPCR. The columns display the mRNA expression of the *UGT1A1* gene relative to β-actin. The transfection of miR-34a, miR-122, miR-181a-5p, miR-199a-5p, and miR-222 significantly induced the mRNA expression. Whereas miR-25, miR-29a, miR-151-5p, miR-183-5p, and miR-486-3p transfection led to the most pronounced, significant reduction of UGT1A1 mRNA levels compared to the miR-control treatment. The columns represent the mean ± SEM of three independent replicates. Significance was calculated relative to the miR-control treatment. SEM: Standard Error of the Mean; *: $p < 0.05$; **: $p < 0.01$; ***: $p < 0.001$; n.s.: not significant.

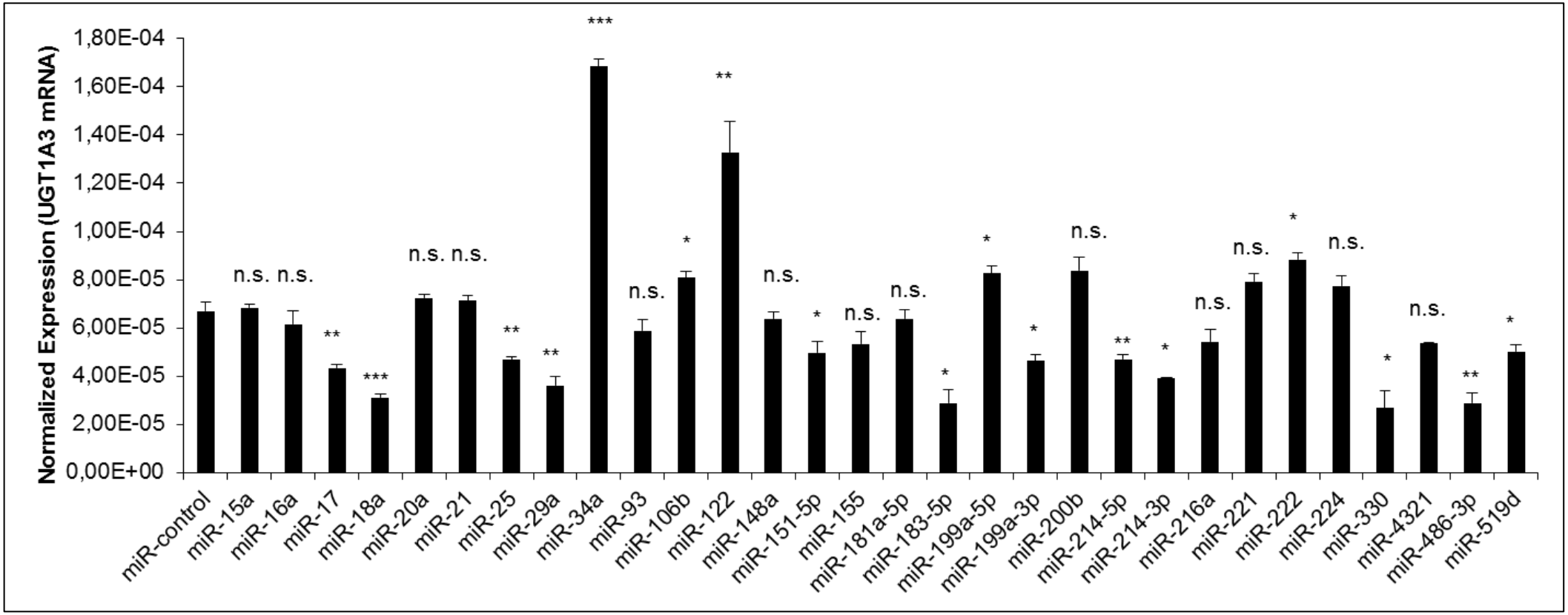

Figure 10. Expression of UGT1A3 mRNA after miRNA Transfection into HepG2 Cells. An array of 30 microRNAs was overexpressed in HepG2 cells and the UGT1A3 mRNA expression was determined by TaqMan-qPCR. The columns display the mRNA expression of the *UGT1A3* gene relative to β-actin. The transfection of miR-34a, miR-122, miR-199a-5p, and miR-222 significantly induced the mRNA expression. Whereas miR-18a, miR-29a, miR-183-5p, miR-330, and miR-486-3p transfection led to the most pronounced, significant reduction of UGT1A3 mRNA levels compared to the miR-control treatment. The columns represent the mean ± SEM of three independent replicates. Significance was calculated relative to the miR-control treatment. SEM: Standard Error of the Mean; *: $p < 0.05$; **: $p < 0.01$; ***: $p < 0.001$; n.s.: not significant.

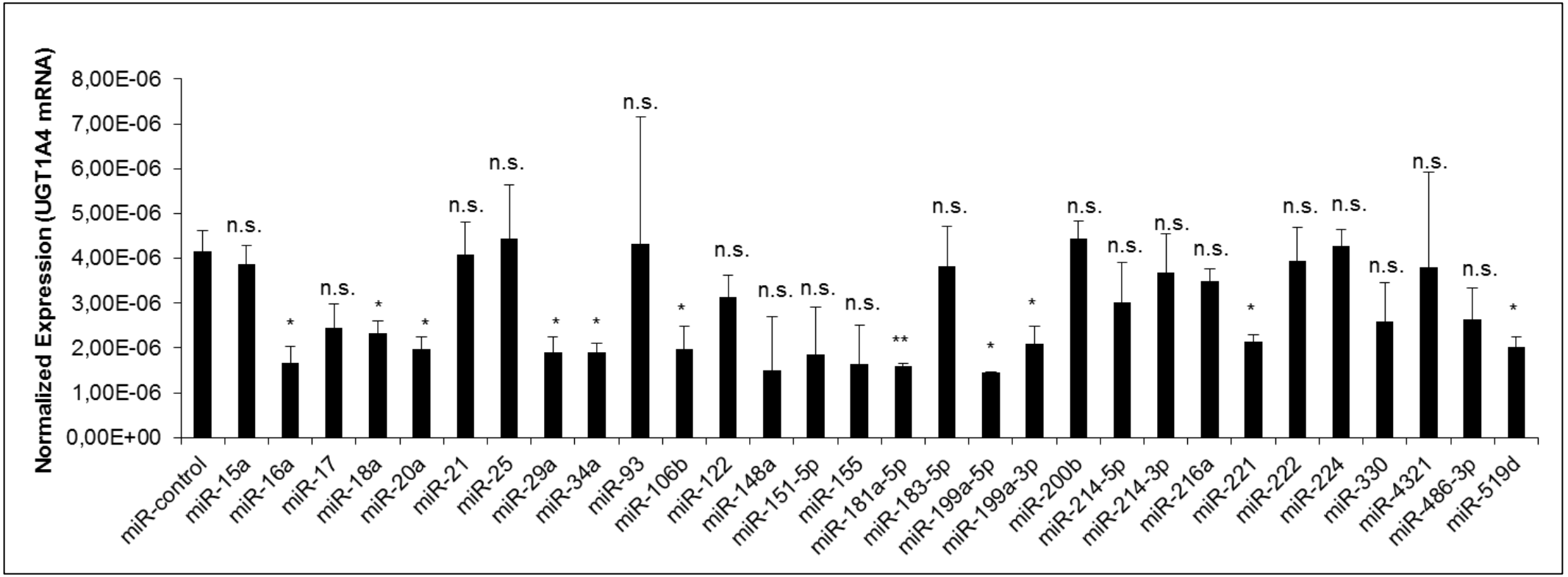

Figure 11. Expression of UGT1A4 mRNA after miRNA Transfection into HepG2 Cells. An array of 30 microRNAs was overexpressed in HepG2 cells and the UGT1A4 mRNA expression was determined by TaqMan-qPCR. The columns display the mRNA expression of the *UGT1A4* gene relative to β-actin. The transfection of miR-16a, miR-181a-5p, and miR-199a-5p led to the most pronounced, significant reduction of UGT1A4 mRNA levels compared to the miR-control treatment. The columns represent the mean ± SEM of three independent replicates. Significance was calculated relative to the miR-control treatment. SEM: Standard Error of the Mean; *: $p < 0.05$; **: $p < 0.01$; n.s.: not significant.

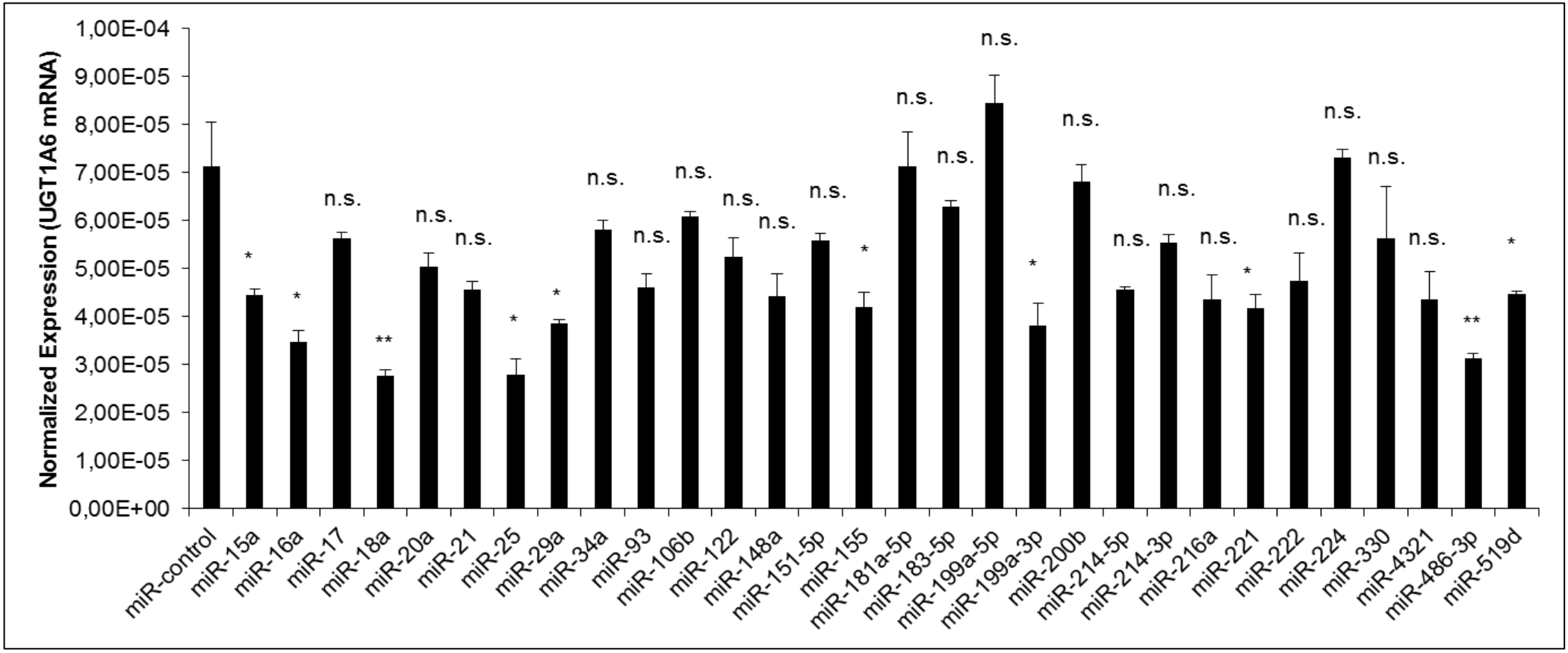

Figure 12. Expression of UGT1A6 mRNA after miRNA Transfection into HepG2 Cells. An array of 30 microRNAs was overexpressed in HepG2 cells and the UGT1A6 mRNA expression was determined by TaqMan-qPCR. The columns display the mRNA expression of the *UGT1A6* gene relative to β-actin. The transfection of miR-18a, miR-25, and miR-486-3p led to the most pronounced, significant reduction of UGT1A6 mRNA levels compared to the miR-control treatment. The columns represent the mean ± SEM of three independent replicates. Significance was calculated relative to the miR-control treatment. SEM: Standard Error of the Mean; *: $p < 0.05$; **: $p < 0.01$; n.s.: not significant.

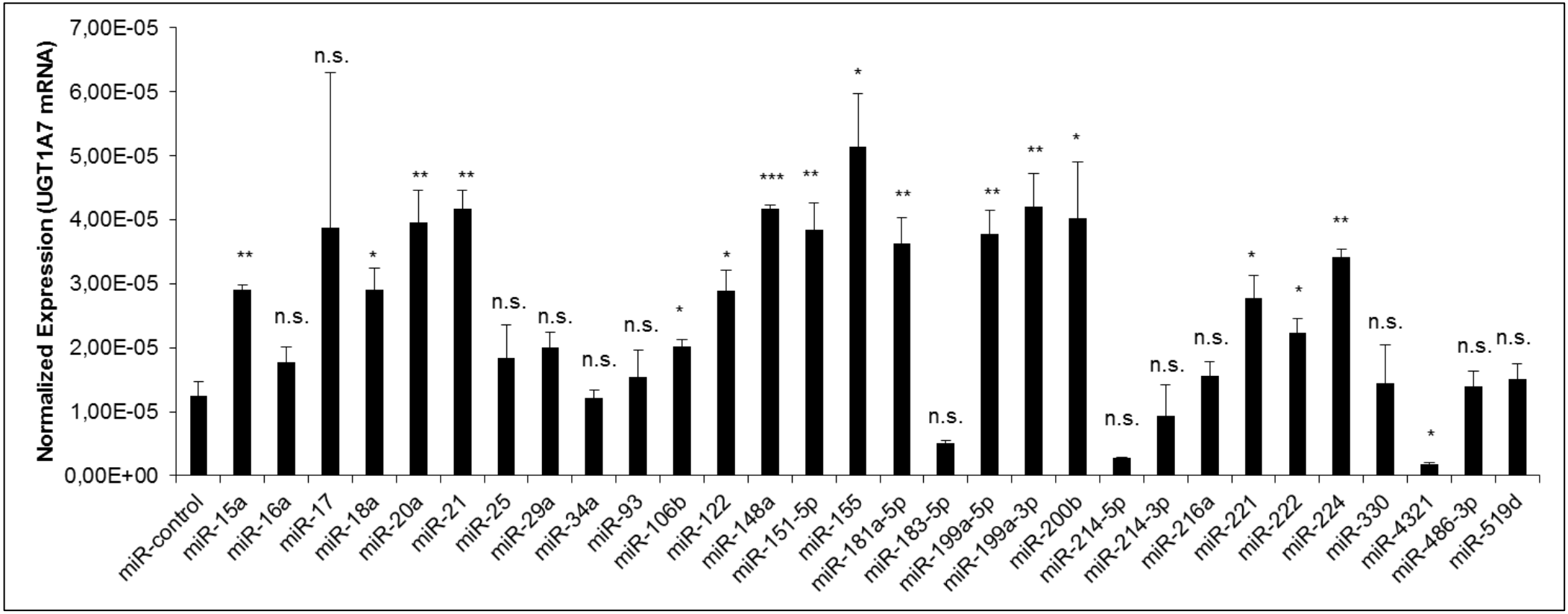

Figure 13. Expression of UGT1A7 mRNA after miRNA Transfection into HepG2 Cells. An array of 30 microRNAs was overexpressed in HepG2 cells and the UGT1A7 mRNA expression was determined by TaqMan-qPCR. The columns display the mRNA expression of the *UGT1A7* gene relative to β-actin. The overexpression of miR-20a, miR-21, miR-148a, miR-151-5p, miR-155, miR-181a-5p, miR-199a-5p, miR-199a-3p, miR-200b, and miR-224 significantly induced the mRNA levels to the highest extent. Whereas miR-4321 transfection led to the most pronounced, significant reduction of UGT1A7 mRNA levels compared to the miR-control treatment. The columns represent the mean ± SEM of three independent replicates. Significance was calculated relative to the miR-control treatment. SEM: Standard Error of the Mean; *: $p < 0.05$; **: $p < 0.01$; ***: $p < 0.001$; n.s.: not significant.

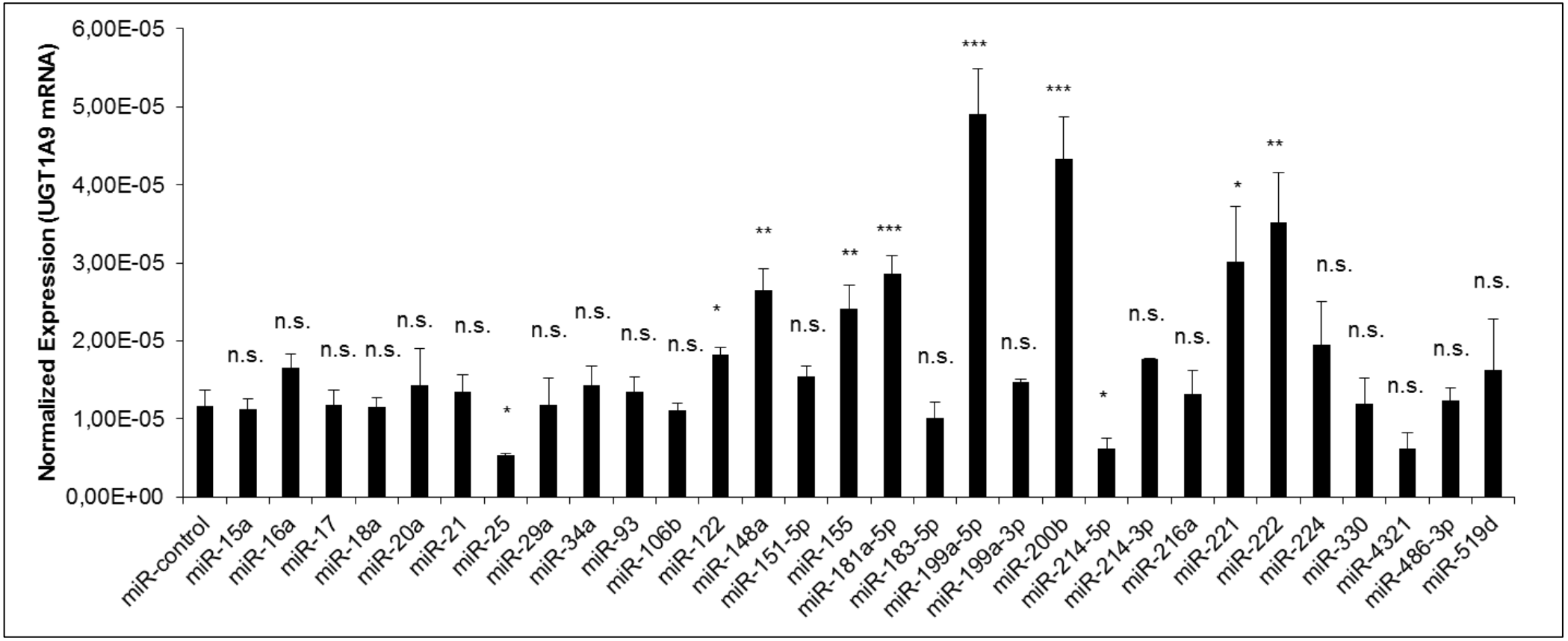

Figure 14. Expression of UGT1A9 mRNA after miRNA Transfection into HepG2 Cells. An array of 30 microRNAs was overexpressed in HepG2 cells and the UGT1A9 mRNA expression was determined by TaqMan-qPCR. The columns display the mRNA expression of the *UGT1A9* gene relative to β-actin. The transfection of miR-148a, miR-155, miR-181a-5p, miR-199a-5p, miR-200b, miR-221, and miR-222 significantly induced the mRNA expression to the greatest extent. Whereas miR-25 and miR-214-5p transfection led to the most pronounced, significant reduction of UGT1A9 mRNA levels compared to the miR-control treatment. The columns represent the mean ± SEM of three independent replicates. Significance was calculated relative to the miR-control treatment. SEM: Standard Error of the Mean; *: $p < 0.05$; **: $p < 0.01$; ***: $p < 0.001$; n.s.: not significant.

3.4 Regulation of UGT1A Protein Levels by miRNAs in HepG2 Cells

MiRNAs have been described to regulate a target gene by translational inhibition, depending on the sequence complementarity between a miRNA and the mRNA 3'-UTR [110]. Based on the previous results from the UGT1A isoform-specific mRNA expression analysis, a potential miRNA-mediated translational inhibition of the several UGT1A mRNA isoforms was examined. In order to perform this analysis, the 30 investigated miRNAs were transfected into HepG2 cells, and posteriorly the isolated protein mixture was analyzed using Western blot.

Initially, the HepG2 cells were lysed by three freeze-thaw-cycles, this means, the cell suspension is placed in a freezer (-80 °C) and then thawed (37 °C). The traditional freeze-thaw protocol is based on ice crystals that form during the freezing process, and ultimately contract during thawing which causes cells to swell and disintegrate. The freeze-thaw-cycle cell lysis was performed in this work, because it was previously described that scraping, and freeze-thaw-cycling is a simple, yet efficient method for harvesting and lysing of adherent mammalian cells [161]. The isolated protein mixture was applied to a denaturing Sodium Dodecyl Sulfate-Polyacrylamide Gel Electrophoresis (SDS-PAGE). SDS is an anionic detergent that denatures secondary and tertiary structures of protein molecules and coats them with a negative charge so that all proteins migrate towards the positive pole during PAGE. Since the protein negative charge is proportional to its size, the protein's molecular weight can be estimated by comparison to protein bands of known molecular weight [151]. The Laemmli SDS-PAGE system applied in this work was a discontinuous gel that contained an upper stacking and lower resolving gel that had different polyacrylamide concentrations. This resulted in a high resolution with well-defined protein band definition. Hence, the upper stacking gel is a lower percentage polyacrylamide gel where proteins move through rapidly and "stack" into a tight band before the higher percentage polyacrylamide or "resolving" gel which promotes the final separation [162]. The gel-separated protein bands were transferred and immobilized on a nitrocellulose membrane. For this, an electric charge was applied to the blotting chamber that enabled the negatively charged protein bands to travel from the gel onto the membrane available for later immunoprobing with an antibody. Nitrocellulose membranes were used for blotting, because they yield lower background staining compared to the high-affinity PVDF membranes [163]. Two sets of antibodies were subjected to the immunoprobing experiment: 1) The primary antibody that is directed against the target protein, i.e. the UGT1A isoenzyme. 2) A secondary antibody conjugated to horseradish peroxidase (HRP) that binds to the primary

antibody. Based on the principle of chemiluminescence, the HRP-coupled secondary antibody binds to the primary antibody, then the HRP catalyzes the oxidation of the substrate luminol (in the presence of peroxide) to a peroxy intermediate which is turned to the 3-aminophthalate dianion that leads to the light generation detected by a digital imager (as described in section 2.2.23) [151]. In doing so, the effect of the investigated miRNAs on the UGT1A protein expression was determined. Figures 15-20 illustrate the post-transcriptional effects of miRNAs on UGT1A protein expression. The effect of the investigated miRNAs on UGT1A protein expression was then compared with the miR-control transfection.

In the following sections, the results of the Western blot are listed for each UGT1A protein:

UGT1A1

Among the 30 investigated miRNAs, miR-106b and miR-122 markedly induced UGT1A1 protein expression. This effect was less pronounced after the transfection of miR-15a, miR-16a, miR-17, miR-18a, miR-20a, miR-21, miR-25, miR-29a, miR-93, miR-155, miR-181a-5p, miR-199a-5p, miR-200b, and miR-222. In contrast to the induction, miRNAs that slightly reduced UGT1A1 protein expression compared to the miR-control treatment were miR-34a, miR-148a, miR-151-5p, miR-183-5p, miR-199a-3p, miR-214-5p, miR-214-3p, miR-216a, miR-221, miR-224, miR-330, miR-4321, miR-486-3p, and miR-519d (Figure 15).

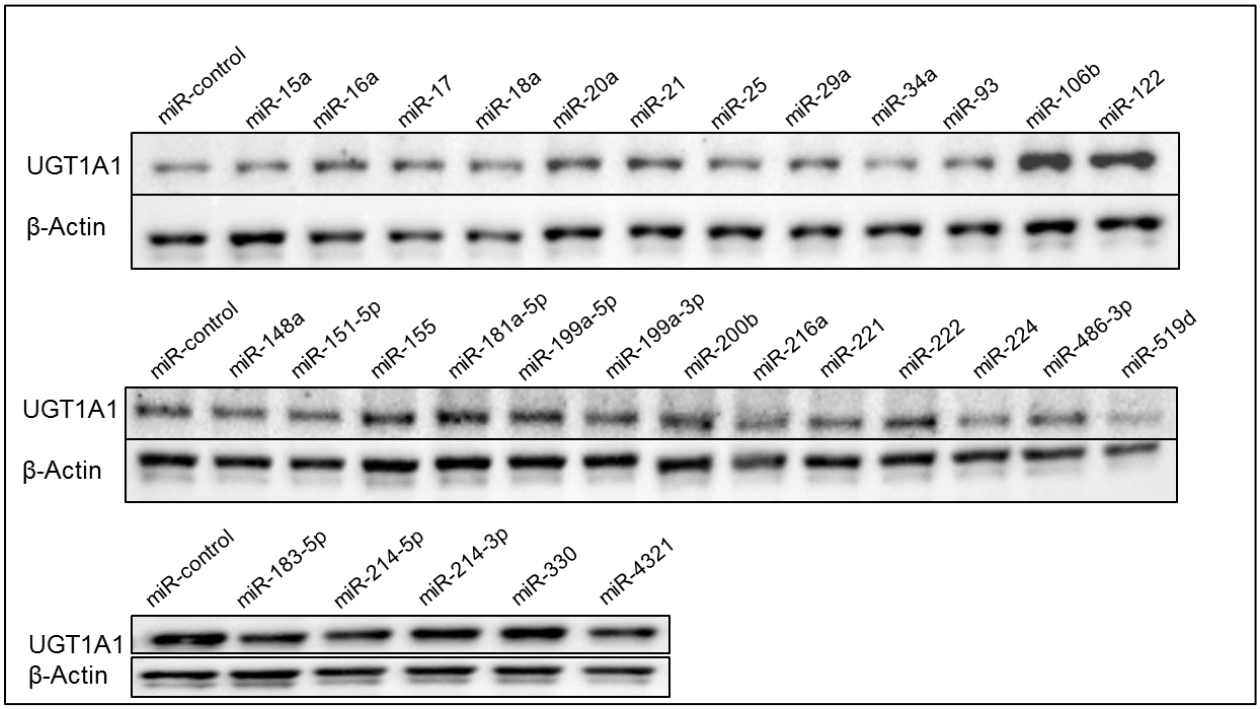

Figure 15. UGT1A1 Western Blot of miRNA Transfected HepG2 Cells. An array of 30 miRNAs was overexpressed in HepG2 cells and UGT1A1 protein levels were determined by Western blot. Of note, the strongest induction of protein expression was revealed after miR-106b and miR-122 transfection, whereas miR-34a, miR-214-5p, miR-224, miR-4321, and miR-519d considerably reduced UGT1A1 protein levels compared to the miR-control treatment. β-actin was used as a loading control.

UGT1A3

The UGT1A3 protein expression was predominantly induced by miR-106b and miR-122 compared to the miR-control treatment. The induction of protein expression was less pronounced after the transfection of miR-15a, miR-16a, miR-17, miR-18a, miR-20a, miR-21, miR-25, miR-29a, miR-93, miR-148a, miR-151-5p, miR-155, miR-181a-5p, miR-199a-5p, miR-200b, miR-214-5p, miR-214-3p, miR-216a, miR-222, miR-330, miR-4321, and miR-486-3p. In contrast to the induction of UGT1A3 protein expression, the reduction of UGT1A3 protein expression was detected after miR-34a and miR-199a-3p transfection. No visible changes in UGT1A3 protein expression were observed after transfection of miR-183-5p, miR-221, miR-224, and miR-519d (Figure 16).

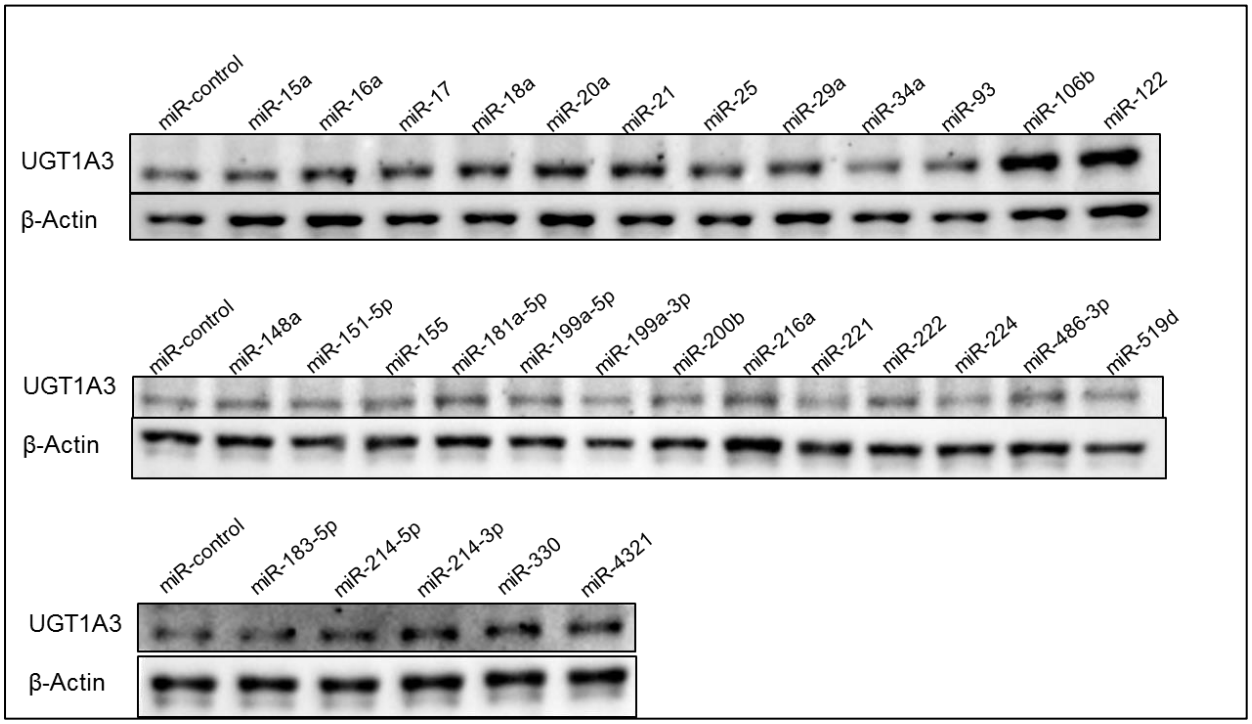

Figure 16. UGT1A3 Western Blot of miRNA Transfected HepG2 Cells. An array of 30 miRNAs was overexpressed in HepG2 cells and UGT1A3 protein levels were determined by Western blot. The most pronounced induction of protein expression was observed after miR-106b and miR-122 transfection. On the contrary, UGT1A3 protein levels were markedly reduced after miR-34a and miR-199a-3p transfection compared to the miR-control treatment. β-actin was used as a loading control.

UGT1A4

The UGT1A4 protein expression was markedly induced by miR-20a, miR-106b, miR-122, miR-148a, miR-155, miR-181a-5p, miR-199a-3p, miR-200b, miR-216a, miR-221, miR-224, and miR-486-3p. However, the induction of UGT1A4 protein expression was less pronounced after miR-15a, miR-16a, miR-17, miR-21, miR-151-5p, miR-199a-5p, miR-214-5p, miR-214-3p, miR-222, miR-330, and miR-519d transfection. On the other hand, the UGT1A4 protein expression was reduced by miR-18a, miR-29a, miR-34a, and miR-4321. Of note, the UGT1A4 protein levels were unaffected after miR-25, miR-93, and miR-183-5p transfection compared to the miR-control treatment (Figure 17).

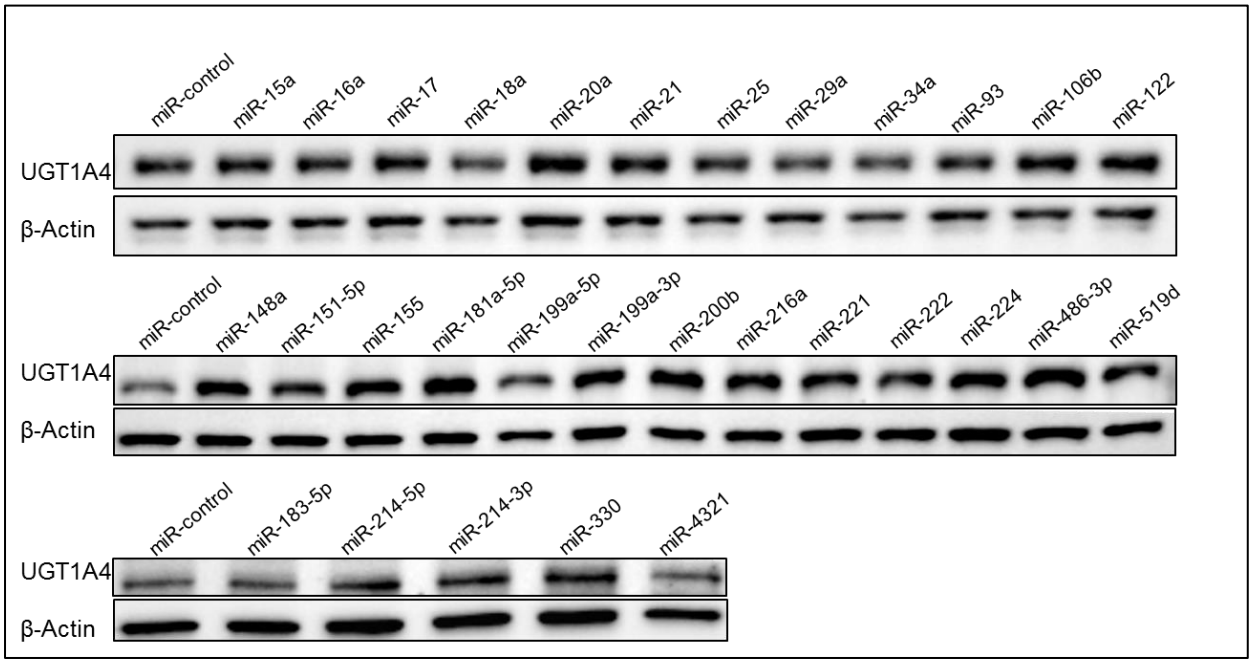

Figure 17. UGT1A4 Western Blot of miRNA Transfected HepG2 Cells. An array of 30 miRNAs was overexpressed in HepG2 cells and UGT1A4 protein levels were determined by Western blot. Of note, a pronounced induction of protein expression was detected after miR-20a, miR-148a, miR-181a-5p, miR-200b, and miR-486-3p transfection. An inhibition of UGT1A4 protein levels was observed after miR-18a, miR-29a, and miR-34a transfection compared to the miR-control treatment. β-actin was used as a loading control.

UGT1A6

The UGT1A6 protein expression was markedly induced by miR-183-5p, miR-214-5p, miR-214-3p, miR-330, and miR-4321 compared to miR-control treatment. Other miRNAs led to a less pronounced induction of UGT1A6 protein levels. Among these miRNAs were miR-16a, miR-20a, miR-93, miR-106b, miR-122, and miR-216a. In contrast to the induction, the UGT1A6 protein expression was slightly reduced by miR-18a, miR-25, miR-34a, miR-151-5p, miR-155, miR-181a-5p, miR-199a-5p, miR-199a-3p, miR-200b, miR-221, miR-222, miR-224, miR-486-3p, and miR-519d. Of note, no differences in UGT1A6 protein expression were observed after the transfection of miR-15a, miR-17, miR-21, miR-29a, and miR-148a (Figure 18).

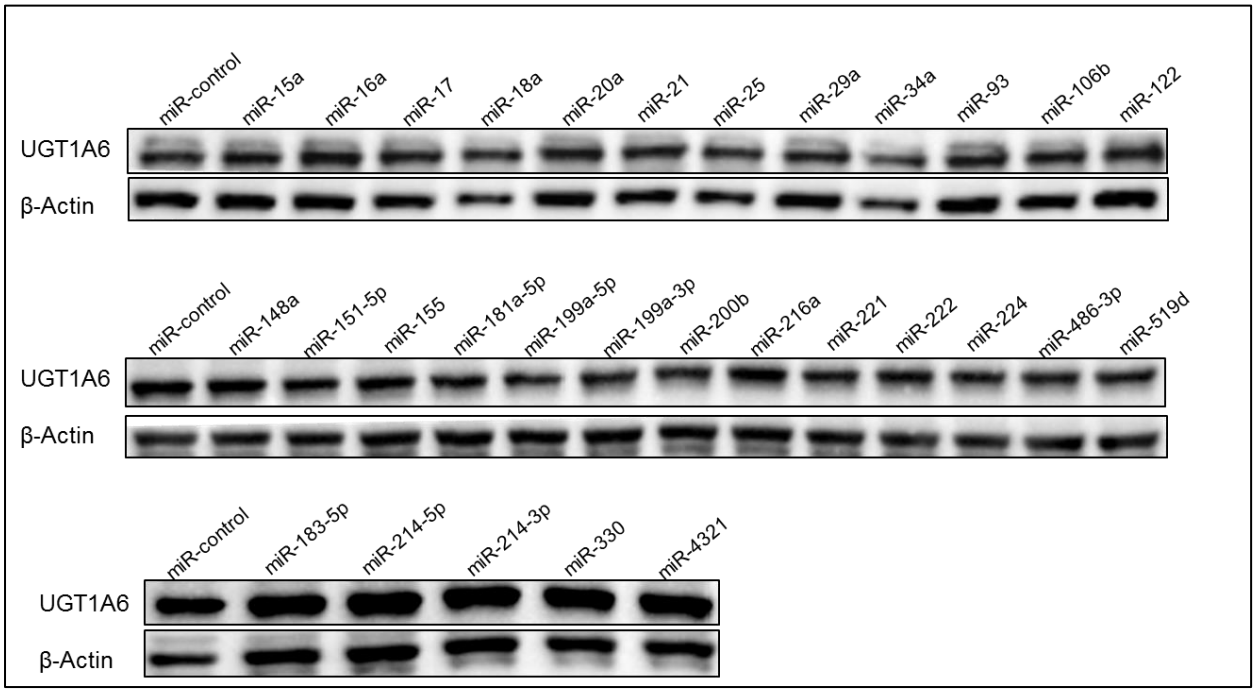

Figure 18. UGT1A6 Western Blot of miRNA Transfected HepG2 Cells. An array of 30 miRNAs was overexpressed in HepG2 cells and UGT1A6 protein levels were determined by Western blot. The transfection of miR-183-5p, miR-214-5p, miR-214-3p, miR-330, and miR-4321 markedly induced UGT1A6 protein expression. In contrast, the overexpression of miR-18a, miR-34a, miR-151-5p, miR-199a-5p, miR-224, miR-486-3p, and miR-519d resulted in a reduction of protein levels compared to the miR-control treatment. β-actin was used as a loading control.

UGT1A7

The UGT1A7 protein expression was markedly induced by miR-15a, miR-16a, miR-20a, miR-21, miR-122, miR-155, miR-183-5p, and miR-199a-5p. The inductive effect was less pronounced after transfection of miR-17, miR-18a, miR-25, miR-29a, miR-34a, miR-93, miR-106b, miR-148a, miR-151-5p, miR-181a-5p, miR-199a-3p, miR-200b, miR-214-5p, miR-214-3p, miR-216a, miR-221, miR-222, miR-224, miR-330, miR-486-3p, and miR-519d. The weakest induction of UGT1A7 protein expression was observed after the overexpression of miR-4321. Of note, a miRNA-mediated reduction of the UGT1A7 protein expression could not be observed (Figure 19).

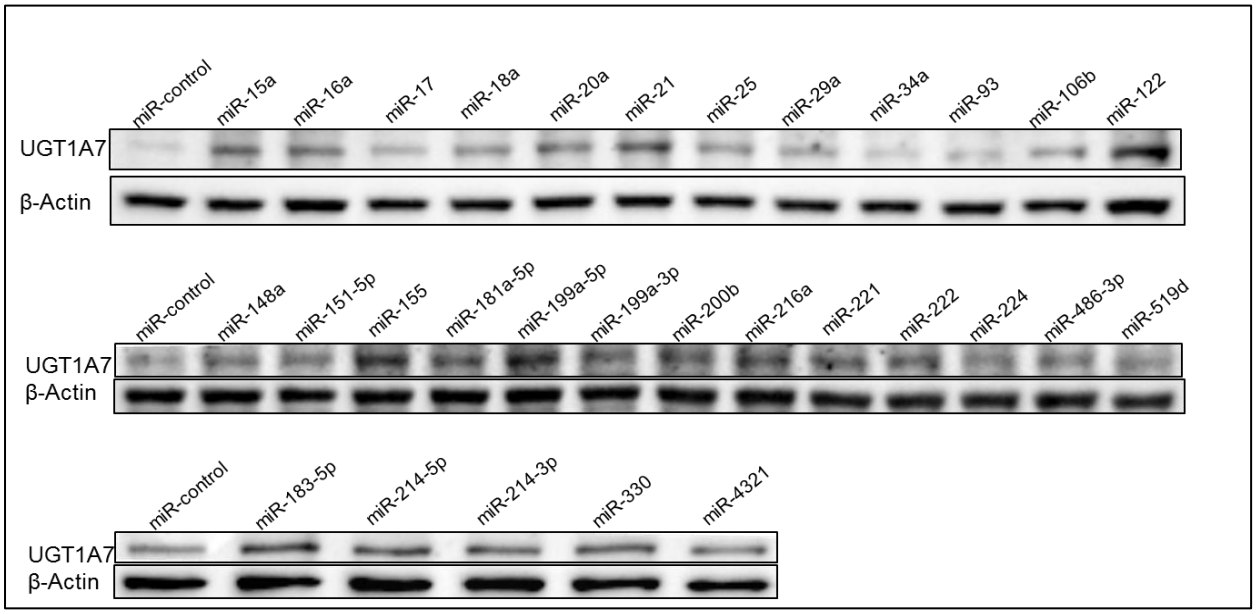

Figure 19. UGT1A7 Western Blot of miRNA Transfected HepG2 Cells. An array of 30 miRNAs was overexpressed in HepG2 cells and UGT1A7 protein levels were determined by Western blot. Of note, a considerable induction of protein expression was detected after miR-122, miR-155, and miR-199a-5p transfection. No considerable inhibition of UGT1A7 protein levels was observed compared to the miR-control treatment. β-actin was used as a loading control.

UGT1A9

The UGT1A9 protein expression was markedly induced after miR-106b, miR-122, miR-155, miR-181a-5p, miR-216a, miR-221, miR-222, miR-330, miR-4321, and miR-486-3p transfection. However, miR-15a, miR-16a, miR-17, miR-18a, miR-20a, miR-21, miR-25, miR-29a, miR-34a, miR-93, miR-151-5p, miR-199a-5p, miR-199a-3p, miR-200b, miR-214-3p, miR-224, and miR-519d transfection resulted in a less pronounced induction of the UGT1A9 protein levels compared to the miR-control treatment. In contrast to the inductive effect, miR-148a, miR-183-5p, and miR-214-5p exerted a slightly inhibitory effect on UGT1A9 protein expression compared to the miR-control treatment (Figure 20).

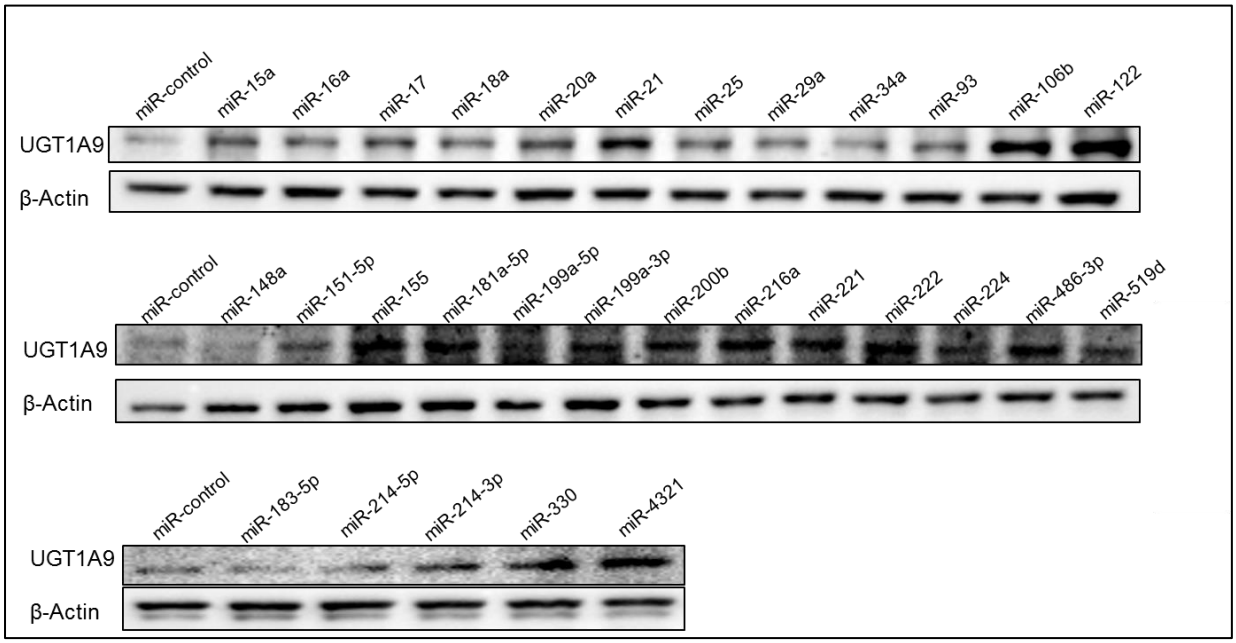

Figure 20. UGT1A9 Western Blot of miRNA Transfected HepG2 Cells. An array of 30 miRNAs was overexpressed in HepG2 cells and UGT1A9 protein levels were determined by Western blot. UGT1A9 protein expression was markedly induced among others after miR-21, miR-106b, miR-122, miR-155, miR-181a-5p, miR-199a-3p, miR-216a, miR-221, and miR-222 compared to the miR-control treatment. A slight reduction of protein levels was observed after miR-148a, miR-183-5p, and miR-214-5p transfection. β-actin was used as a loading control.

Collectively, this data indicates that several miRNAs are capable of inducing or reducing the UGT1A protein expression. Furthermore, the modulatory effect was shown to occur in an isoform-specific manner, with the same miRNA being able to cause an inhibitory or inductive effect in different UGT1A isoforms. Of note, miR-122 consistently induced protein expression of all UGT1A isoforms. This is of particular importance, because miR-122 was reported to be upregulated in healthy livers suggesting a hepatoprotective effect [164].

3.5 Post-Transcriptional Regulation of miRNAs in Extrahepatic Cell Lines

Among the 30 investigated miRNAs, the candidate miRNAs that led to the highest consistency in the reduction of *UGT1A* expression across the different previous experiments (chapters 3.1-3.4) were selected for further analysis in extrahepatic cell lines, in order to extrapolate from the potential disturbance of *UGT1A* expression in these cells to extrahepatic tissues and their associated damage through the UGT1A-impaired accumulation of potentially harmful compounds. Among the miRNAs, miR-214-5p, miR-486-3p, and miR-519d were selected for further investigation, as they led to the highest consistency in the downregulation of the hepatic *UGT1A* expression. Moreover, miR-214-5p and miR-486-3p repressed UGT1A 3'-UTR

luciferase activity which is why they were considered as interesting candidates for further analysis. The cell line analyses were performed in non-liver (extrahepatic) cells, specifically esophagus and colon carcinoma. The esophagus and tissues of the gastrointestinal tract are the first to be in contact with xenobiotics such as drugs or nutrients. For this reason, a functional UGT1A-mediated glucuronidation in these tissues is crucial for the elimination of potentially harmful compounds before they enter the systemic circulation [165]. As representative cells of the aerodigestive tract (i.e., entry site of xenobiotics), the esophageal squamous carcinoma (Kyse-70) cells were used to study the effects of local *UGT1A* post-transcriptional regulation. As depictive cells of the gastrointestinal tract, the colon carcinoma cell line (Caco-2) was utilized based on their considerable *UGT1A* expression. The three selected miRNAs were overexpressed in the Kyse-70 and Caco-2 cells, then the total RNA and proteins were isolated and UGT1A isoform-specific mRNA and protein expression were determined by TaqMan-qPCR and Western blot, respectively.

The results of UGT1A mRNA expression in extrahepatic cell lines (Kyse-70 and Caco-2) are separately shown below:

Kyse-70 cells

The effect of post-transcriptional miR-214-5p, miR-486-3p, and miR-519d regulation on UGT1A mRNA expression in Kyse-70 cells is outlined in figure 21. The result after miRNA transfection is compared to miR-control transfected Kyse-70 cells. In detail, miR-486-3p (0.28-fold) significantly reduced UGT1A1 mRNA expression, whereas an insignificant effect of UGT1A1 mRNA expression was observed after miR-214-5p transfection. UGT1A1 mRNA levels were insignificantly reduced by 0.05-fold after miR-519d transfection.

UGT1A3 mRNA expression was reduced after miR-486-3p (0.09-fold) transfection, though this result was insignificant. A slight, insignificant induction of UGT1A3 mRNA levels was detected after miR-214-5p (1.04-fold) and miR-519d (1.13-fold) transfection.

UGT1A4 mRNA expression was slightly reduced by miR-214-5p (0.06-fold) and miR-486-3p (0.23-fold), whereby these results failed to be statistically significant. An insignificant induction of UGT1A4 mRNA levels was observed after miR-519d (1.12-fold) transfection.

Similar to UGT1A4, UGT1A6 mRNA expression was reduced after miR-214-5p (0.08-fold) and miR-486-3p (0.11-fold) transfection. A minor induction of UGT1A6 mRNA levels was observed after miR-519d (1.11-fold) transfection. However, these results were not statistically significant.

UGT1A7 mRNA levels were reduced after transfection of miR-214-5p (0.31-fold) and miR-486-3p (0.35-fold). A slight, insignificant induction of UGT1A7 mRNA expression was detected after the transfection of miR-519d (1.04-fold).

UGT1A9 mRNA expression was reduced after miR-214-5p (0.35-fold) transfection, whereas an induction was observed after the overexpression of miR-519d (1.12-fold). No effect on UGT1A9 mRNA expression resulted by miR-486-3p. Taken together, the results for UGT1A7 and UGT1A9 mRNA expression were not statistically significant.

Caco-2 cells

The post-transcriptional effect of miR-214-5p, miR-486-3p, and miR-519d on UGT1A mRNA expression in Caco-2 cells is outlined in figure 22. The result after miRNA transfection is compared to miR-control transfected cells.

UGT1A1 mRNA expression was significantly reduced after miR-214-5p (0.40-fold), miR-486-3p (0.49-fold), and miR-519d (0.40-fold) transfection. In addition, UGT1A3 mRNA expression was significantly repressed after the transfection of miR-214-5p (0.35-fold), miR-486-3p (0.45-fold), and miR-519d (0.61-fold). A considerable, significant reduction of the UGT1A4 mRNA expression was observed when Caco-2 cells were transfected with miR-214-5p (0.54-fold) and miR-519d (0.54-fold). However, the reduction was less pronounced after miR-486-3p (0.33-fold) transfection. UGT1A6 mRNA expression was significantly reduced after miR-214-5p (0.29-fold), miR-486-3p (0.37-fold), and miR-519d (0.40-fold) transfection. The UGT1A7 mRNA expression was statistically significant reduced by the overexpression of miR-486-3p (0.46-fold). On the contrary, the reduction of UGT1A7 mRNA levels after miR-214-5p (0.59-fold) and miR-519d (0.59-fold) transfection failed to be significant. UGT1A9 mRNA expression was significantly reduced when cells were transfected with miR-214-5p (0.56-fold), miR-486-3p (0.49-fold), and miR-519d (0.54-fold).

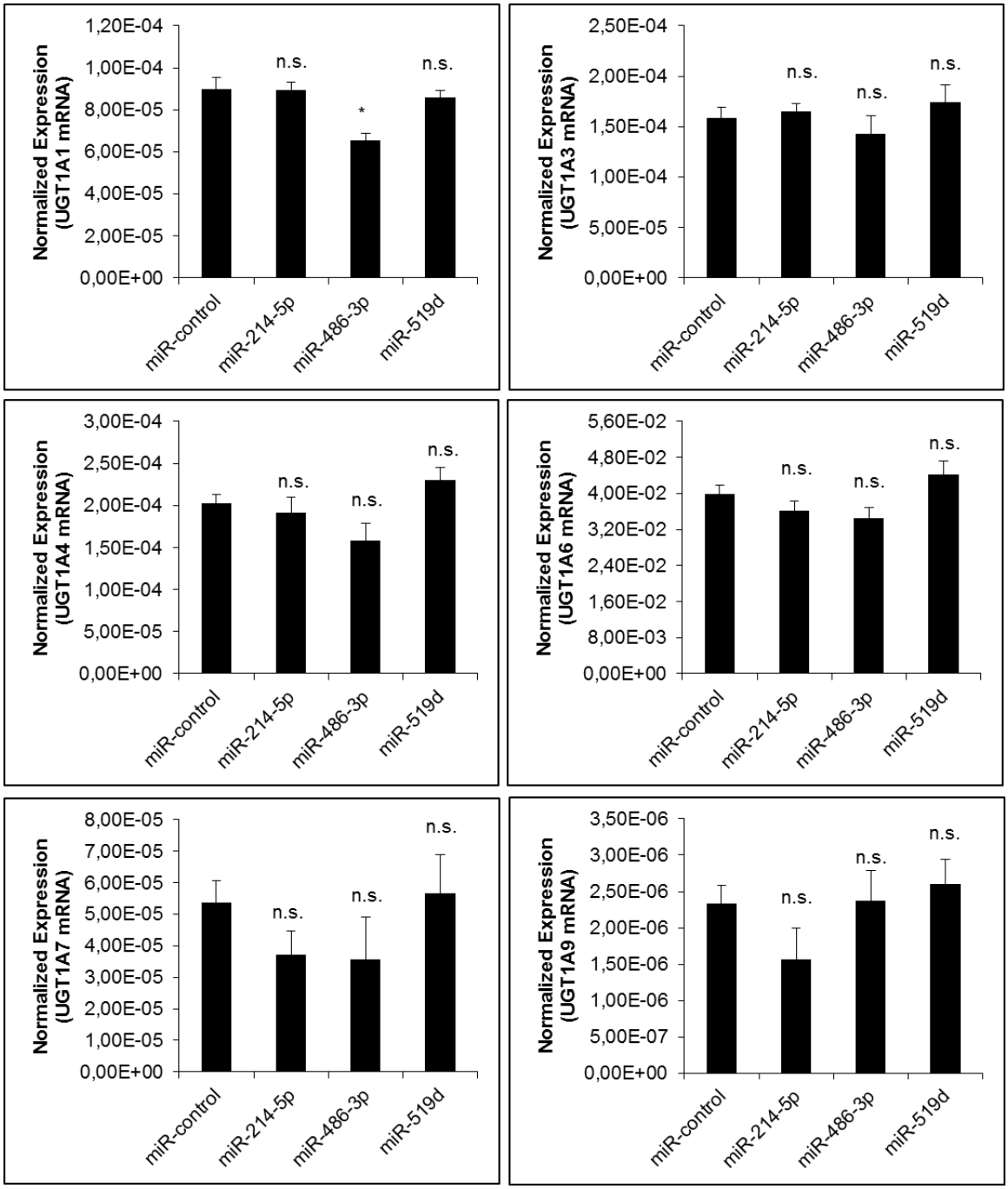

Figure 21. UGT1A mRNA Levels after Transfection of miRNAs into Kyse-70 Cells. The candidate miRNAs (miR-214-5p, miR-486-3p, and miR-519d) were overexpressed in Kyse-70 cells and the UGT1A mRNA expression was determined by TaqMan-qPCR. A statistically significant reduction of UGT1A1 mRNA expression was detected after miR-486-3p transfection compared to the miR-control treatment. The columns represent the mean ± SEM of three independent replicates. Significance was calculated relative to miR-control treatment. SEM: Standard Error of the Mean; *: $p < 0.05$; n.s.: not significant.

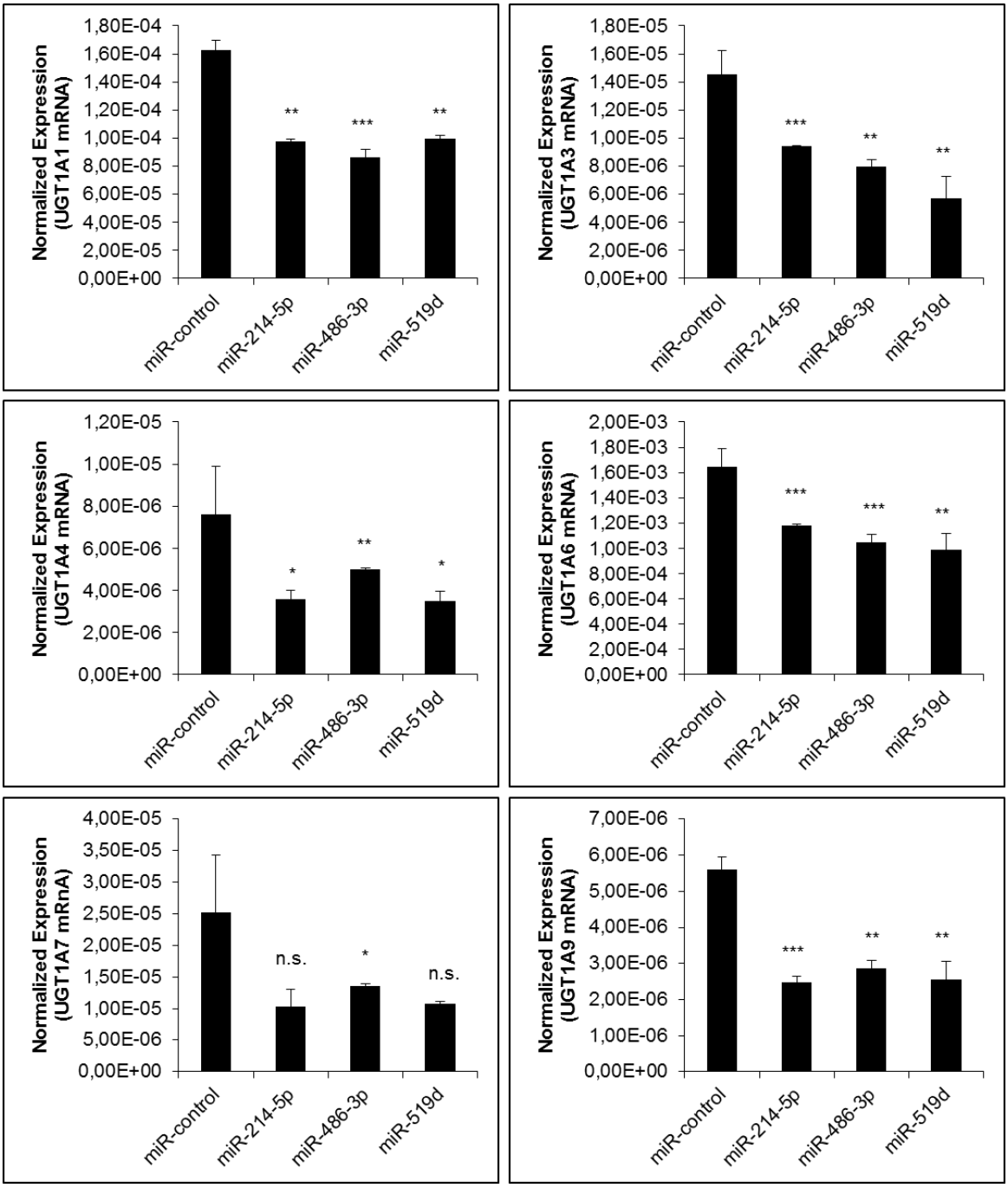

Figure 22. UGT1A mRNA Levels after Transfection of miRNAs into Caco-2 Cells. The candidate miRNAs (miR-214-5p, miR-486-3p, and miR-519d) were overexpressed in Caco-2 cells and the UGT1A mRNA expression was determined by TaqMan-qPCR analysis. A significant reduction of UGT1A1, UGT1A3, UGT1A4, UGT1A6, and UGT1A9 mRNA expression was observed after the transfection of the investigated miRNAs. The UGT1A7 mRNA levels were only significantly repressed by miR-486-3p compared to the miR-control treatment. The columns represent the mean ± SEM of three independent replicates. Significance was calculated relative to miR-control. SEM: Standard Error of the Mean; *: $p < 0.05$; **: $p < 0.01$; ***: $p < 0.001$; n.s.: not significant.

To investigate a potential translational inhibition of UGT1A enzymes in these two celltypes, the three miRNAs (miR-214-5p, miR-486-3p, and miR-519d) were overexpressed in Kyse-70 and Caco-2 cells and the UGT1A protein expression was determined. In terms of the

extrahepatic UGT1A protein expression, the transfection of miR-214-5p, miR-486-3p, and miR-519d into Kyse-70 cells resulted only in a reduction of UGT1A4 protein expression mediated by miR-214-5p and miR-486-3p. In contrast, miR-519d induced the UGT1A4 protein expression compared to the miR-control treatment (Figure 23).

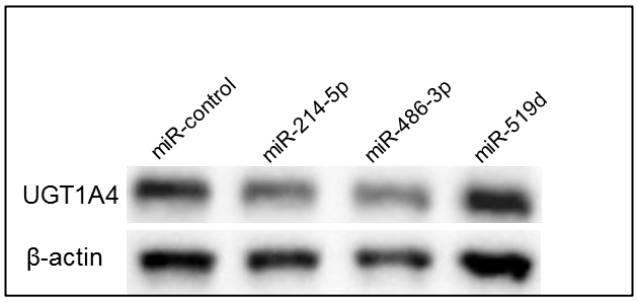

Figure 23. UGT1A4 Protein Expression after Transfection of miRNAs into Kyse-70 Cells. The three candidate miRNAs were overexpressed in Kyse-70 cells and a Western blot analysis was performed. The figure depicts the reduction of UGT1A4 protein levels after transfection of miR-214-5p and miR-486-3p. β-actin was used as a loading control.

Dissimilarly, the overexpression of miR-214-5p, miR-486-3p, and miR-519d in Caco-2 cells led to the reduction of UGT1A4, UGT1A7, and UGT1A9 protein levels compared to miR-control transfected cells (Figure 24).

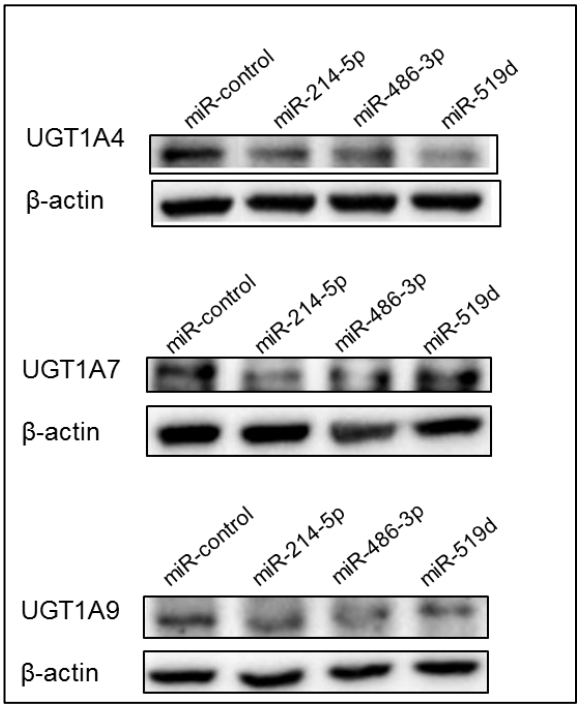

Figure 24. UGT1A Protein Expression after Transfection of miRNAs into Caco-2 Cells. The candidate miRNAs (miR-214-5p, miR-486-3p, and miR-519d) were overexpressed in Caco-2 cells and a Western blot analysis was carried out to detect a potential reduction of UGT1A protein expression. The miRNAs markedly repressed UGT1A4, UGT1A7, and UGT1A9 protein levels compared to the miR-control treatment. Of note, UGT1A7 protein expression was only slightly reduced after the transfection of miR-519d. β-actin was used as a loading control.

For UGT1A7, miR-519d only slightly reduced the protein expression compared to miR-control transfected Caco-2 cells. Collectively, this data demonstrates a celltype-specific effect exhibited by the three candidate miRNAs. Of note, the post-transcriptional effect exhibited by the miRNAs demonstrated higher consistency across UGT1A mRNA and protein expression in Caco-2 cells.

3.6 Bioinformatic Search for miRNA Recognition Elements

A bioinformatic predictive approach aimed to identify the potential MREs of the candidate miRNAs (miR-214-5p, miR-486-3p, and miR-519d) within the UGT1A 3'-UTR. The *in silico* analysis facilitated the understanding of the possible molecular mechanism exhibited by the miRNAs of interest. For the bioinformatic analysis, the web-based software tools RegRNA (v2.0), PicTar, miRanda, and RNAhybrid were used, applying the default settings. RegRNA 2.0 is an integrated web server application that examines a random RNA sequence on functional RNA motifs and sites, including miRNA target sites [143]. In order to confirm the RegRNA-predicted interactions between the miRNA and the UGT1A 3'-UTR, the following mRNA:miRNA prediction tools were used: PicTar, miRanda, and RNAhybrid. These tools search for miRNA binding sites within a given target gene or sequence. Furthermore, RNAhybrid was applied for the graphical visualization of the RNA hybrid formation. Since a perfect complementarity between the miRNA seed region (5'-end nucleotides 2 to 8) and the mRNA 3'-UTR is sufficient for mRNA degradation [110], the chosen software tools focus on perfect sequence complementarity at the miRNA 5'-terminal end. The hybridization between a miRNA and the target mRNA is based on thermodynamic principles and displayed by Minimum Free Energy (MFE)-values, expressed in kcal/mol units. Hence, the lower the predicted MFE-value, the more energetically optimal is the hybridization of a miRNA to its target [146]. The *in silico* analysis resulted in a consistent prediction of two putative MREs, including the formation of an 8 nt sequence complementarity at the miRNA 5'-end for miR-214-5p and miR-486-3p (Figure 25). As a result of the predictive mRNA:miRNA duplex formation, the calculated MFE-values were -27.0 kcal/mol (miR-214-5p) and -26.8 kcal/mol (miR-486-3p). This indicated an energetically optimal RNA hybrid formation. A computational analysis regarding miR-519d failed to predict a MRE with perfect complementarity at the miRNA 5'-end in the UGT1A 3'-UTR, whereby miR-519d was not included in the subsequent mutagenesis procedure.

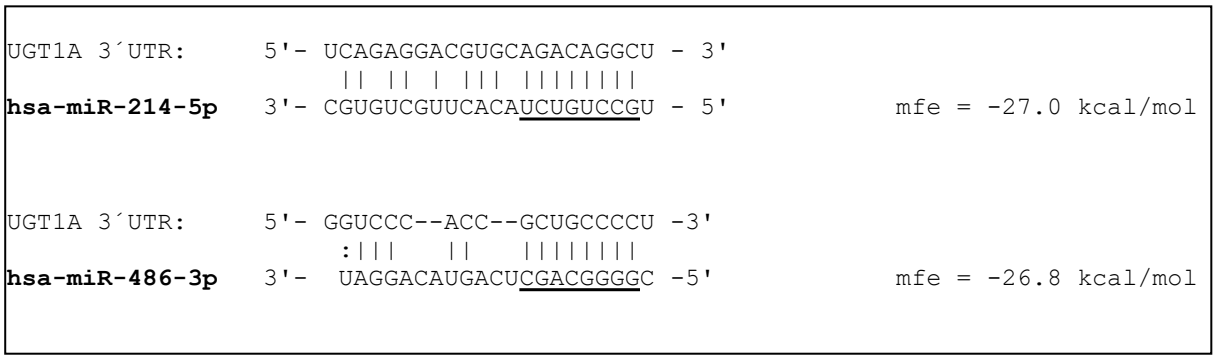

Figure 25. MicroRNA Recognition Elements with Corresponding Seed Match of miR-214-5p and -486-3p. The figure illustrates the 8 nucleotide sequence complementarity formed between the miRNA 5'-end (nucleotides 2 to 9) and the UGT1A 3'-UTR. The respective nucleotide sequence is underlined. The hybridization of miR-214-5p and miR-486-3p to the UGT1A 3'-UTR MRE is displayed by considerable minimum free energy (mfe) values. RNAhybrid was used to visualize and calculate the mfe-values.

To study the involvement of the predicted MREs in the regulation of UGT1A 3'-UTR luciferase activity, the 8 nt sequence (underlined in Figure 25), involved in miR-214-5p and miR-486-3p binding, were mutated using pGL3-UGT1A-3'-UTR as a DNA template. The 8 nt sequences were mutated by applying a site-directed mutagenesis approach. For this, PCR mutagenesis primers (~ 30 bp) were designed that had high complementarity up- and downstream the 8 nt target sequence. However, the target sequence was mutated by insertion of A and T nucleotides which disrupted the original sequence in the UGT1A 3'-UTR (Figure 25). In a two-step PCR: firstly, the mutation was incorporated forming two PCR fragments, applying an amplification and a mutagenesis primer (Table 2), and secondly, both PCR fragments were fused and amplified using UGT1A 3'-UTR amplification primers. The newly generated DNA fragment was inserted into the pGL3-Basic vector to generate a plasmid construct termed "pGL3-UGT1A-3'-UTR seed mutation" which contained the mutation in the MRE of miR-214-5p or miR-486-3p (Figure 26).

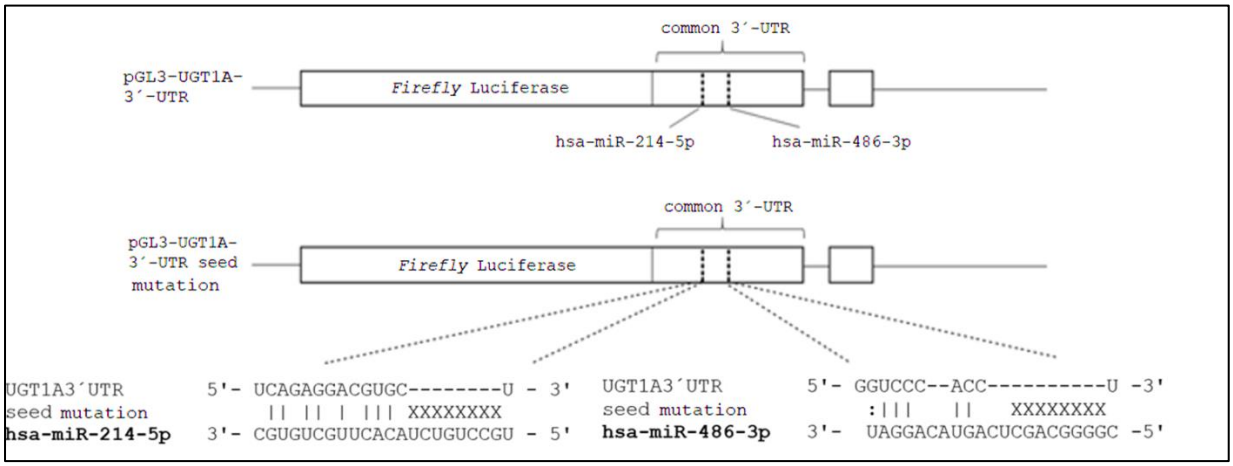

Figure 26. Mutagenesis of miR-214-5p and -486-3p MRE Nucleotide Sequence. The luciferase reporter construct pGL3-UGT1A-3'-UTR was used to mutate 8 nucleotides in the MRE involved in perfect complementarity with the 5'-end of miR-214-5p and miR-486-3p. The mutation was performed by insertion of A and T nucleotides which mutated the corresponding nucleotide sequence responsible for the seed match. The resulting DNA plasmid was termed pGL3-UGT1A-3'-UTR seed mutation and used as a reporter construct for the subsequent luciferase assay.

Then, the pGL3-UGT1A-3'-UTR seed mutation was transfected together with miR-214-5p or miR-486-3p into Hek293 cells. Next, the luciferase reporter gene assay was carried out. As a result of the mutagenesis, the relative luciferase activity was significantly recovered by 0.68-fold (miR-214-5p) and 0.27-fold (miR-486-3p) compared to the non-mutated plasmid (Figure 27).

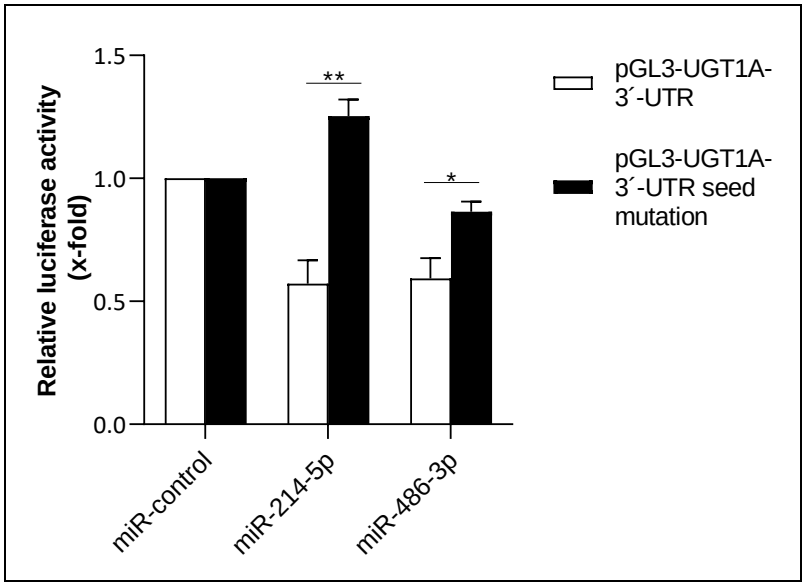

Figure 27. Luciferase Reporter Gene Assay after miR-214-5p and -486-3p MRE Mutation. The figure illustrates the relative luciferase activity with or without the eight nucleotides in the UGT1A 3'-UTR necessary for the perfect complementarity of miR-214-5p or miR-486-3p 5'-end nucleotides 2 to 9. The transfection of the non-mutated plasmid pGL3-UGT1A-3'-UTR and miR-214-5p or miR-486-3p into Hek293 cells decreased the relative luciferase activity, whereas luciferase activity significantly recovered after the mutation using pGL3-UGT1A-3'-UTR seed mutation. The columns represent fold means ± SEM of three independent replicates. Significance was calculated relative to the non-mutated plasmid. SEM: Standard Error of the Mean; *: $p < 0.05$; **: $p < 0.01$.

The results suggested that miR-214-5p and miR-486-3p regulate *UGT1A* expression by binding to the identified target sites in the common UGT1A 3'-UTR. After the site-directed mutagenesis of miRNA target sites in the UGT1A 3'-UTR, it was further questioned whether the application of antisense oligonucleotides (antimiRs) may repress miRNA functionality in a similar manner. AntimiRs are synthetically manufactured oligodeoxyribonucleotides that are antisense to the miRNA of interest. By targeting a miRNA, antimiRs are able to efficiently and irreversibly silence miRNAs [166]. For this reason, miR-214-5p or miR-486-3p and a sequence-specific antimiR (termed as "inhibitor (Inh)" in Figure 28) were co-transfected with pGL3-UGT1A-3'-UTR, then the luciferase activity was determined. This "loss-of-function" approach resulted in a statistically significant recovery of luciferase activity by 0.27-fold (miR-214-5p) and by 0.19-fold (miR-486-3p) compared to the inhibitor-free transfected Hek293 cells. The results indicate a miR-214-5p and -486-3p-mediated reduction of the luciferase activity associated with a specific hybridization to the target sites in the UGT1A 3'-UTR.

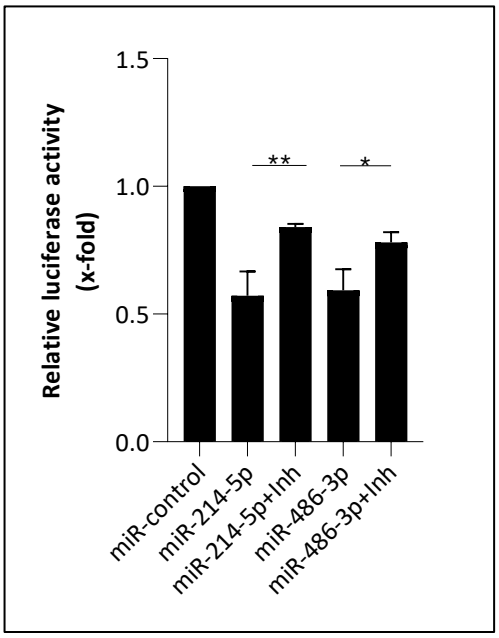

Figure 28. Luciferase Reporter Gene Assay after Co-Transfection of a Sequence-Specific Inhibitor. A sequence-specific inhibitor (Inh) was co-transfected with the luciferase reporter construct pGL3-UGT1A-3'-UTR and miR-214-5p or miR-486-3p into Hek293 cells, which was followed by the luciferase assay. The figure shows a repression of the relative luciferase activity after miR-214-5p or miR-486-3p transfection. However, this repression was significantly eliminated when a miR-214-5p or miR-486-3p sequence-specific inhibitor was co-transfected. The columns represent fold means ± SEM of three independent replicates. Significance was calculated relative to the inhibitor-free group. SEM: Standard Error of the Mean; *: $p < 0.05$; **: $p < 0.01$.

3.7 Indirect Regulation of *UGT1A* Expression by miRNAs

Apart from the post-transcriptional regulation of *UGT1A* expression, the study aimed to investigate whether the three candidate miRNAs (miR-214-5p, miR-486-3p, and miR-519d) were able to regulate *UGT1A* expression through the interaction with various TFs involved in *UGT1A* gene regulation. Recently, the downregulation of a TF by a miRNA was reported to repress the gene expression of a drug-metabolizing enzyme [123]. To pursue the hypothesis of miRNA-mediated inhibition of TFs, the bioinformatic tools PicTar and miRanda were utilized to predict common *UGT1A*-inducing TFs as potential targets of miR-214-5p, miR-486-3p, and miR-519d. PicTar and miRanda were able to evaluate the potential miRNA target based on thermodynamic features and sequence complementarity. The bioinformatic analysis predicted hybridization sites of the investigated miRNAs to the 3'-UTR of RXRα mRNA, whereas no binding sites were predicted for other TFs. RXRα is a nuclear receptor, as well as a TF that dimerizes with itself or other nuclear receptors to form heterodimers, which bind to promoter sequences driving the transcription of the target genes [52]. Therefore, several TFs rely on RXRα as heterodimer partner to promote the binding at responsive elements in *UGT1A* gene promoters [48].

According to the mRNA:miRNA binding prediction, RNAhybrid was used to calculate the corresponding MFE-values. The MFE-values were most pronounced for miR-214-5p (-31.3 kcal/mol), followed by the MFE-value for miR-486-3p (-29.9 kcal/mol), and miR-519d (-26.9 kcal/mol) (Figure 29). In an attempt to verify the bioinformatically predicted mRNA:miRNA interaction, miR-214-5p, miR-486-3p, and miR-519d were overexpressed in HepG2 cells, followed by the *RXRα* expression analysis. For the *RXRα* expression analysis HepG2 cells were used as the literature describes that *RXRα* expression is measurable in HepG2 cells, although the expression in respective cells is usually less than 25 % compared to the human liver level [167].

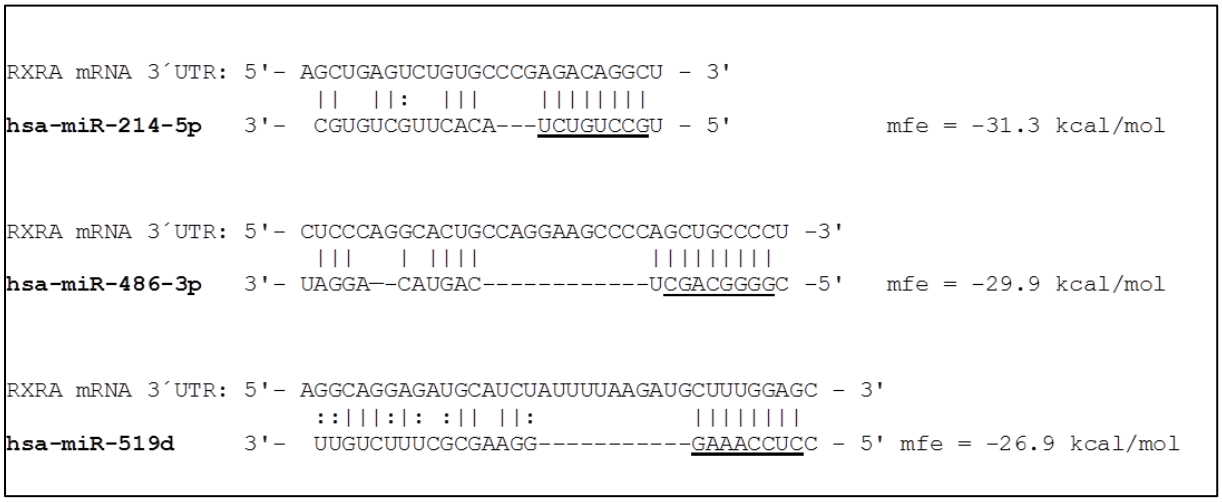

Figure 29. Bioinformatic Analysis of miRNA Target Sites in the 3'-UTR of RXRα mRNA. Web-based prediction tools such as PicTar and miRanda predicted MREs for miR-214-5p, miR-486-3p, and miR-519d in the 3'-UTR of RXRα mRNA. The corresponding perfect complementarity at the miRNA 5'-end from nucleotides 2 to 9 or 10 resulted in the formation of a seed match. The respective nucleotide sequence is underlined. RNAhybrid was used to calculate the mfe-values and visualize the hybridization sites.

To validate the predicted interaction, miR-214-5p, miR-486-3p, and miR-519d were overexpressed in HepG2 cells, total RNA was isolated, reverse transcribed and the expression of the RXRα mRNA was determined by TaqMan-qPCR. Equivalent to the bioinformatic analysis, the reduction of the RXRα mRNA levels was most pronounced after miR-214-5p (0.30-fold), followed by miR-486-3p (0.22-fold), and miR-519d (0.17-fold) transfection (Figure 30). However, the results did not show statistically significant differences while comparing them using t-test. The comparison was made using the control versus treatment (miR-specific), individually. As reduction of the RXRα mRNA expression was measured, the effect of the candidate miRNAs on the RXRα protein level using HepG2 cells was investigated. In order to achieve this goal, the 3 miRNAs (miR-214-5p, miR-486-3p, and miR-519d) were overexpressed in HepG2 cells. Then, the nuclear extracts were generated from the cells, because the RXRα protein has been reported to be localized in the nucleoplasm of human mammary epithelial cells [168].

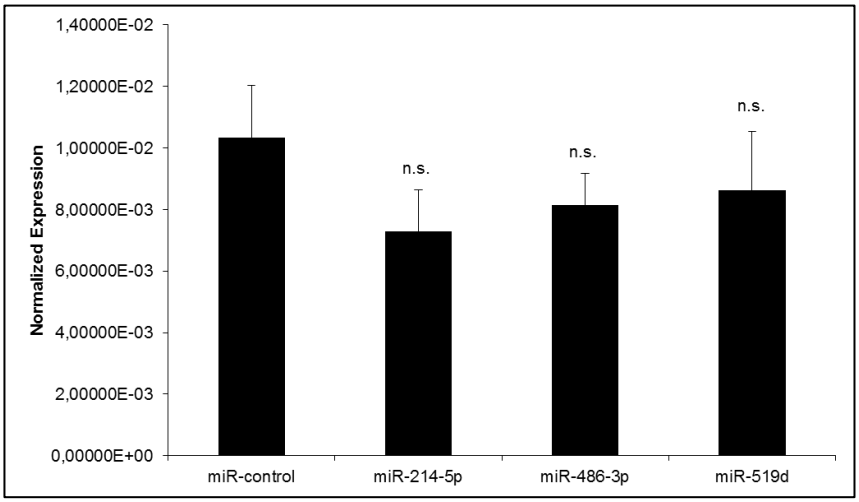

Figure 30. RXRα mRNA Levels after miRNA Transfection into HepG2 Cells. The three candidate miRNAs (miR-214-5p, miR-486-3p, and miR-519d) were overexpressed in HepG2 cells and the RXRα mRNA expression was determined by TaqMan-qPCR. The figure displays the expression of the *RXRα* gene relative to β-actin. Of note, the three miRNAs insignificantly reduced the mRNA expression compared to the miR-control treatment. The columns represent the mean ± SEM of three independent replicates. Significance was calculated relative to the miR-control treatment. SEM: Standard Error of the Mean; n.s.: not significant.

After the preparation of nuclear extracts, the isolated protein was separated by SDS-PAGE and the protein bands were transferred to a nitrocellulose membrane as described in section 2.2.23. The immunoprobing was performed using a RXRα antibody. The membrane imaging analysis revealed a slight induction of RXRα protein expression after miR-214-5p, miR-486-3p, and miR-519d transfection into HepG2 cells compared to the miR-control treatment (Figure 31). Hence, the lack of translational inhibition of the RXRα protein by the investigated miRNAs questioned their potential impact on the regulation of *UGT1A* gene transcription.

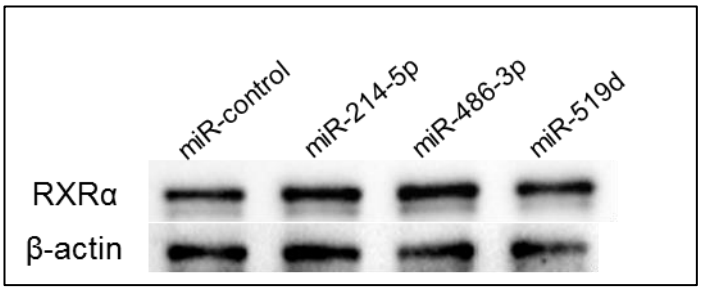

Figure 31. RXRα Protein Levels after miRNA Transfection into HepG2 Cells. The three candidate miRNAs were overexpressed in HepG2 cells, nuclear extracts were isolated and the RXRα protein levels were detected using Western blot analysis. The figure displays a slight inductive effect of miR-214-5p, miR-486-3p, and miR-519d on RXRα protein expression compared to the miR-control treatment. β-actin was used as a loading control.

3.8 Upregulation of miR-486-3p in Patients with Liver Cirrhosis

Our previous experimental findings underscored the negative regulation of *UGT1A* expression by miR-214-5p, miR-486-3p, and miR-519d (chapters 3.1-3.7). Thereby, the miRNA-mediated reduction of UGT1A-catalyzed glucuronidation is likely associated with an accumulation of potentially hazardous substances in hepatic and non-hepatic tissues possibly leading to the damage of various tissues, including the liver [120]. It is well-known that the xenobiotic metabolism can produce polar, nontoxic metabolites that can readily be excreted from the body. Furthermore, it can also create highly reactive metabolites like epoxides or quinones, which might exert detrimental effects to vital intracellular macromolecules [169]. Reactive metabolites can be classified as electrophiles (i.e., electron-deficient molecules) that can react with electron-rich species (i.e., nucleophiles) by covalent bond formation. These nucleophiles are common components of macromolecules such as proteins, lipids, and nucleic acids. The electrophiles can interact with these nucleophiles by attacking the lone electron pairs in the sulfur, nitrogen, and oxygen atoms which are constituents of the macromolecules, forming a stable covalent bond. Therefore, covalent bond formation between an electrophile and a protein can affect protein folding and structure. On the other hand, changes in the DNA can result in mutagenicity or carcinogenicity [169]. UGT1A enzymes are considered as potent antioxidants that can eliminate reactive metabolites by glucuronidation. Against this background, the miRNA-mediated reduction of *UGT1A* expression in the liver was hypothesized to impair the elimination of reactive metabolites. Thus, this can result in the progressive injury of hepatocytes associated with the onset of severe liver diseases (Figure 1). To further address the impact of the respective miRNAs in the development of liver disease, their expression was examined in the serum of cirrhotic patients aiming to relate them to the development or progression of liver cirrhosis. In order to investigate this hypothesis, blood samples were collected from human livers. The blood samples were collected from the liver vein of 60 liver cirrhosis patients, as well as peripheral blood from 42 healthy individuals (serving as a control). Following the blood processing, total RNA was isolated from the serum of all samples. In order to compare miR-214-5p, miR-486-3p, and miR-519d expression to an endogenous control, the SV-40 miRNA was spiked in the samples before RNA isolation, as SV-40 miRNA is a common endogenous control described before [137]. This procedure enabled the relative comparison and quantification of the studied miRNAs. After the circulating miRNA isolation from the serum, reverse transcription (RT) was carried out by using a stem-loop RT primer, which partially bound to the 3’-end of the investigated miRNA. Then, the RT product was

amplified by using a miRNA-specific forward primer and a universal reverse primer in an end-point PCR. Therefore, the universal reverse primer was complementary to the 3'-end stem loop sequence incorporated in the initial RT reaction [170]. The generated RT product was then used as the cDNA template for the final TaqMan-qPCR analysis. In TaqMan-qPCR, a fluorescently-labeled probe complementary to the miRNA of interest was applied. In this way, the relative expression of candidate miRNAs (miR-214-5p, miR-486-3p, and miR-519d) was determined. The analysis revealed a significant upregulation of miR-486-3p (1.60-fold) in cirrhotic patients compared to the control subjects (Figure 32). In contrary, miR-214-5p expression was only detected in the cirrhotic patients, whereas miR-519d could not be detected in any of the two groups of the study (data not shown).

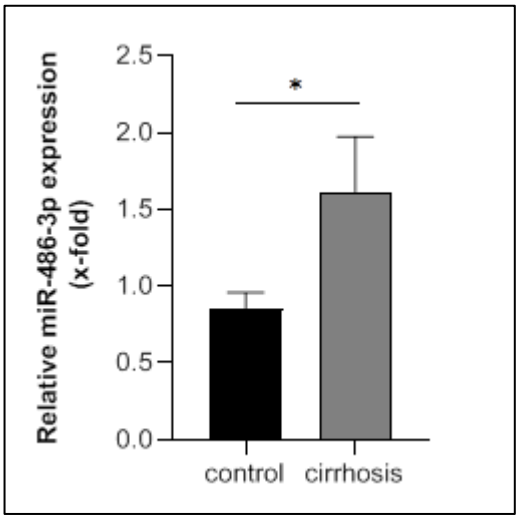

Figure 32. miR-486-3p Expression Levels in Cirrhotic and Control Subjects. The circulating miRNAs were isolated from the serum of cirrhotic patients and healthy individuals. The figure illustrates the relative miR-486-3p expression in cirrhotic patients and control subjects detected by TaqMan-qPCR analysis. miR-486-3p was observed to be 1.60-fold upregulated in cirrhotic individuals compared to healthy control subjects. SV-40 miRNA was spiked in before miRNA isolation and used as endogenous control. The columns represent fold means ± SEM of three technical replicates. Significance was calculated relative to the control group by t-test. SEM: Standard Error of the Mean; *: $p < 0.05$.

Taken together, the result indicates a potential impact of miR-486-3p in the development or progression of liver cirrhosis, which might be mediated through its capability to modulate *UGT1A* expression potentially affecting glucuronidation-based cytoprotection.

3.9 Upregulation of miR-486-3p in a Mouse Model of Alcoholic Liver Fibrosis and its Effects on *UGT1A* Expression

Since the etiology of roughly 75 % of the patients suffering from liver cirrhosis (section 3.8) was caused by alcohol abuse, this approach intended to translate the previous experiment to an animal model imitating ALD pathogenesis. To determine a potential upregulation of miR-486-3p in the early stage of fibrogenesis, a humanized transgenic (*htg*) *UGT1A* wildtype (wt) mouse model containing the entire human *UGT1A* gene locus except for *UGT1A8*, *UGT1A10* and pseudogenes (*UGT1A11* and *UGT1A12*) [139] (Figure 3) was used. As ethanol-drinking mice only develop steatosis and little or no inflammation a second stimulus, or "second hit", was required to induce fibrosis. Thus, *htgUGT1A*-WT mice were simultaneously treated with carbon tetrachloride (CCl_4) and ethanol. In detail, *htgUGT1A*-WT mice were fed with 5 % (v/v) ethanol over a total experimental period of 8 weeks, whereby 5 % (v/v) CCl_4 was intraperitoneally injected twice a week within the last 4 weeks. This procedure (ethanol-CCl_4) is supposed to evoke perisinusoidal and portal fibrosis, and bridging fibrosis [144]. At the end of the experiment, *htgUGT1A*-WT mice were sacrificed, and livers were isolated.

Following total RNA isolation, miR-486-3p was reverse transcribed using the miR-486-3p specific stem-loop RT primer to generate the first RT product. Mature miRNAs do not contain the poly A-tail which is representative for mRNA transcripts. This is the reason why miRNA reverse transcription utilizes a stem-loop RT primer which is partially complementary to the nucleotide sequence of the investigated miRNA (i.e., miR-486-3p). In that, the stem-loop harbors an additional nucleotide sequence that functions as the template in the second reaction. In the second RT reaction, this generated RT product is amplified using a miRNA-specific (i.e., miR-486-3p) forward primer and a universal reverse primer complementary to the stem-loop nucleotide sequence. In 2005, this principle was described by Chen *et al*. [171]. In this way, the cDNA template was synthesized and eventually included in the TaqMan-qPCR analysis for the relative quantification of miR-486-3p. The normalization of miR-486-3p gene expression levels was performed to endogenous control snoRNA234, which expression was shown to be stable across 12 normal mouse tissues, including the liver (data not shown). The miRNA expression analysis in ethanol-CCl_4 treated mice revealed a significant miR-486-3p upregulation by 1.34-fold in male mice compared to their water-drinking control counterparts (Figure 33). In order to examine a potential relation between the upregulated miR-486-3p and the *UGT1A* expression in fibrotic *htgUGT1A*-WT mice, the isolated RNA from the liver was again reverse transcribed. The resulting cDNA was used for the TaqMan-qPCR analysis to determine the UGT1A mRNA

expression. This analysis revealed a considerable reduction of UGT1A mRNA expression (Figure 34). Thereby, the UGT1A3 mRNA expression was significantly reduced by 218-fold, additionally, a significant reduction of UGT1A4 mRNA expression was observed (252-fold).

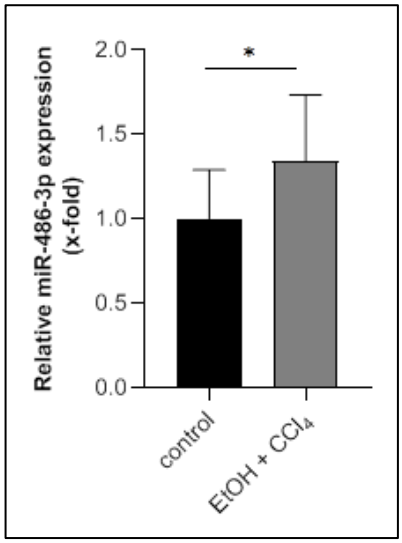

Figure 33. miR-486-3p Expression in a Mouse Model of Alcoholic Liver Fibrosis. Male *htgUGT1A*-WT mice were treated with ethanol (EtOH) and carbon tetrachloride (CCl_4) to generate a mouse model of alcoholic liver fibrosis. Mice were sacrificed, livers were isolated and the hepatic miR-486-3p expression was determined using TaqMan-qPCR analysis. The figure shows the relative expression of miR-486-3p after the experimental period of 8 weeks. Of note, miR-486-3p expression was significantly induced in ethanol-CCl_4 treated mice (EtOH + CCl_4) compared to the untreated, water-drinking counterparts (control). miR-486-3p expression levels were determined relative to endogenous control snoRNA234. The columns represent fold means ± SEM of three independent replicates. Significance was calculated relative to the control group by t-test. SEM: Standard Error of the Mean; *: $p < 0.05$.

In addition, the UGT1A7 and UGT1A9 mRNA levels were decreased by 2.40-fold and 4-fold, respectively compared to water-drinking control mice. These results suggested a possible relation between the upregulated miR-486-3p and the reduction of UGT1A mRNA expression in male *htgUGT1A*-WT mice with alcoholic liver fibrosis. This finding suggests a possible translation of the results from the animal model to the human situation, essentially implying that the upregulation of miR-486-3p in progressive liver diseases is associated with the reduced *UGT1A* expression further promoting liver injury by the accumulation of potentially hazardous substances and reactive metabolites.

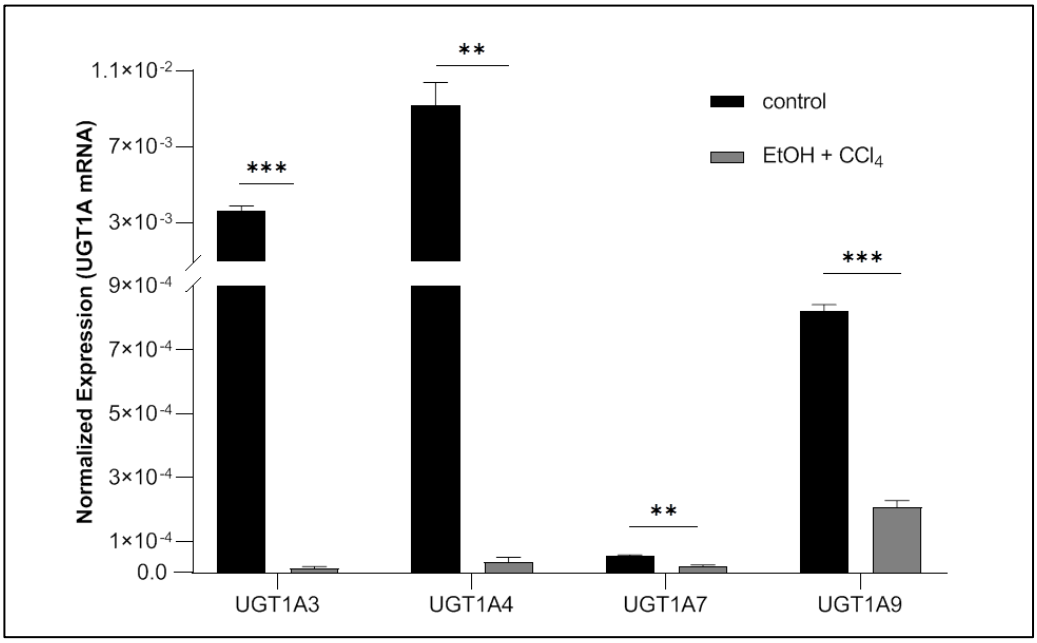

Figure 34. UGT1A mRNA Expression in a Mouse Model of Alcoholic Liver Fibrosis. Male *htgUGT1A*-WT mice were treated with ethanol (EtOH) and carbon tetrachloride (CCl_4) to generate alcoholic liver fibrosis. After the experiment ended, mice livers were isolated and the UGT1A mRNA expression was determined using TaqMan-qPCR analysis. The columns display mRNA expression of *UGT1A* genes relative to β-actin. The figure shows that the UGT1A3, UGT1A4, UGT1A7, and UGT1A9 mRNA expression was significantly reduced in the ethanol-CCl_4 treated mice (EtOH + CCl_4) compared to the untreated, water-drinking counterparts (control). Differences in expression levels were addressed by a broken y-axis. The columns represent the mean ± SEM of three independent replicates. Significance was calculated relative to the control group. SEM: Standard Error of the Mean; **: $p < 0.01$; ***: $p < 0.001$.

In an attempt to investigate the role of miR-486-3p upon UGT enzyme activity, the transgenic mouse model was utilized to examine the potential implication of miR-486-3p with xenobiotic metabolism *in vivo*. In doing so, the post-transcriptional effect of miR-486-3p could be translated to the level of catalytic activity highlighting miR-486-3p as a potential negative regulator of UGT1A-glucuronidation, whereby miR-486-3p could be linked to drug-induced toxicities associated with liver injury. To perform the procedure in mice, the first planned approach was to insert miR-486-3p into the mouse blood stream. However, unmodified exogenous miRNAs are prone to nucleolytic degradation [172]. Moreover, miRNA mimic delivery into a host can be potentially toxic and/or might require additional RNA modifications to increase its stability [172, 173]. Therefore, an *ex vivo* experiment was established where primary hepatocytes from male *htgUGT1A*-WT mice were isolated, transfected with miR-486-3p and subsequently used to measure UGT enzyme activity. The hepatocyte isolation protocol started with abdominal opening of male *htgUGT1A*-WT mice followed by mice liver perfusion with Ethylene Glycol Tetraacetic Acid (EGTA) solution. EGTA dissociates cells by chelating calcium, this results in the disruption of cell adhesion to the underlying matrix [174]. Then, a

collagenase solution was utilized leading to the degradation of ECM proteins including collagens. The liver was completely homogenized, washed and seeded in a cell culture flask coated with collagen A for optimal attachment. Following this, the primary hepatocytes were transfected with miR-486-3p and incubated for 48 hours for subsequent isolation of microsomes by ultracentrifugation. Microsomes are heterogenous, vesicle-like structures composed of endoplasmic reticulum containing proteins such as phase II enzymes, among them the UGTs [149]. The determination of UGT enzyme activity is a two-step reaction in a bioluminescent assay system. In this enzyme activity assay, the UGTs convert the added proluciferin substrate into a glucuronide. By the addition of a luciferin detection reagent, the unconjugated substrate is converted to light producing luciferins. As the glucuronide remains unconverted, no light signal is generated. Therefore, a higher UGT activity leads to a decline in the bioluminometer light output measurement. The output signal is measured as Relative Light Units (RLU). Then, the percentage proportion of the consumed substrate is calculated, hence representing the catalytic activity of UGT enzymes in the respective sample. Figure 35 shows the result of this *ex vivo* experiment. The data supports the previously generated results of an inhibitory effect of miR-486-3p on *UGT1A* expression. In detail, the overexpression of miR-486-3p in the isolated mouse hepatocytes reduced UGT enzyme activity by 11 % compared to the miR-control transfected sample.

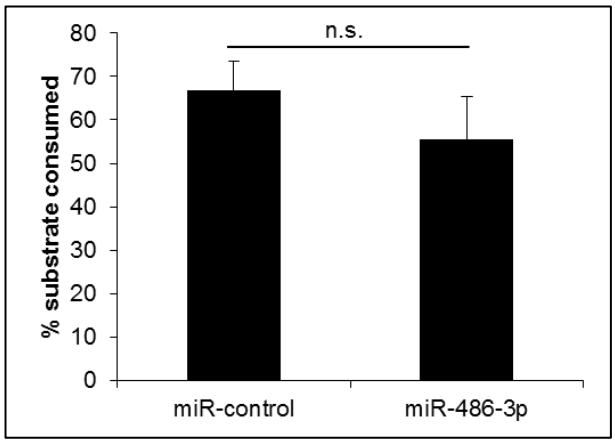

Figure 35. UGT Activity in Primary Hepatocytes of *htgUGT1A*-WT Mice after miR-486-3p Transfection. Primary hepatocytes were isolated from male *htgUGT1A*-WT mice and transfected with miR-486-3p. Later, UGT enzyme-residing microsomes were isolated which were used to perform the UGT enzyme activity assay. During the bioluminescent assay, the light output was measured as Relative Light Units (RLU) and used to calculate the percent (%) proportion of consumed substrate. The figure shows an insignificant reduction of the % proportion of the consumed substrate after miR-486-3p transfection compared to the miR-control treatment. The columns represent the mean ± SEM of three independent replicates. Significance was calculated relative to the miR-control treatment. SEM: Standard Error of the Mean; n.s.: not significant.

Although these results were not statistically significant, they further emphasize the negative *UGT1A* gene regulatory activity of miR-486-3p observed in various cell lines, as well as fibrotic mice livers. Moreover, this data provides direct evidence that miR-486-3p is not only capable to affect UGT1A enzymes on a transcriptional and translational level but also the catalytic activity, which is of crucial importance for the elimination of potentially harmful molecules and/or reactive metabolites probably arising during the progression of liver diseases.

4 Discussion

4.1 MicroRNA-Mediated Downregulation of Hepatic *UGT1A* Expression

In 2016, Chen *et al.* reviewed the role of non-coding miRNAs in hepatic detoxification [93]. The authors found that miRNAs regulate the biotransformation across all three enzyme-linked steps: I) functionalization, II) conjugation, and III) transport of the processed compounds. Thereby, an impaired UGT1A-mediated xenobiotic metabolism is likely to result in the accumulation of xenobiotics or reactive metabolites, essentially disturbing the antioxidative capacity of the organism. In the liver, this may result in the more severe progression of liver diseases supporting the conditions for fibrosis or cirrhosis development. Hence, the detection of *UGT1A*-downregulating miRNAs is crucial to unravel the molecular factors likely responsible for the development of these OS-induced liver damages. In this study, 30 miRNAs dysregulated in HCC were studied for such negative UGT1A-regulating features. The significant effects of each *UGT1A*-downregulating miRNA are discussed separately for each UGT1A isoform in the following chapters (4.1.1-4.1.5).

4.1.1 UGT1A1

So far, UGT1A1 belongs to the best-studied isoforms among the *UGT1A* gene locus, as it is the only physiological enzyme capable to glucuronidate the yellow bile pigment bilirubin [175]. Moreover, UGT1A1 detoxifies various therapeutic drugs (e.g. simvastatin, gemfibrozil, buprenorphine, and irinotecan metabolites) and mutagenic xenobiotics such as benzo(α)pyrenes and N-hydroxy-2-amino-1-methyl-6-phenylimidazol[4,5-*β*]pyridine (N-hydroxy-PhIP) [62], highlighting the crucial importance of this isoform in the elimination of potentially harmful compounds. Thus, reduced UGT1A1 activity is considered to be a risk factor for the development of diseases associated with an increased exposure of toxic environmental compounds (e.g. in HCC) or with altered drug metabolism leading to drug-caused toxicity and tissue damage [176].

In this study, a variety of miRNAs significantly reduced UGT1A1 mRNA levels such as miR-16a, miR-18a, miR-25, miR-29a, miR-151-5p, miR-183-5p, miR-199a-3p, miR-214-5p, miR-216a, miR-4321, miR-486-3p, and miR-519d (Figure 9). In agreement with the repressed UGT1A1 mRNA level, miR-151-5p, miR-183-5p, miR-199a-3p, miR-214-5p, miR-216a, miR-4321, miR-486-3p, and miR-519d also led to the reduction of UGT1A1 protein levels *in*

vitro (Figure 15). These results identify miRNAs capable to repress *UGT1A1* expression. In turn, the reduced *UGT1A1* expression can lead to elevated levels of metabolites, which may increase OS and promote ROS-induced tissue damage and disease development. The reduction of *UGT1A1* transcriptional activation has been extensively described before. In 2010, Strassburg has shown that SNPs in the *UGT1A1* promoter or coding sequence affect *UGT1A1* transcription, enzyme activity, or both [62]. It is suggested that *UGT1A1*-silencing miRNAs can lead to comparable outcomes, i.e. drug-induced toxicities [120], which is why the role of SNPs in the *UGT1A1* gene is further considered. To date, 113 genetic variants of the *UGT1A1* gene (*UGT1A1*1* to *UGT1A1*113*) were identified [62], including the prominent *UGT1A1*28* variant that is associated with Gilbert's syndrome. The *UGT1A1*28* variant is characterized by an additional insertion of a thymine-adenine (TA) repeat in the TATAA box element of the *UGT1A1* promoter ($A(TA)_6TAA$, wildtype variant) leading to $A(TA)_7TAA$, which decreases *UGT1A1* transcription by 70 % [177]. Wasserman *et al*. were the first to provide clinical evidence that the *UGT1A1*28* genetic variant is coupled to severe irinotecan-related toxicities such as diarrhea and neutropenia [178]. The miRNA-mediated downregulation of *UGT1A1* expression shown in this study, therefore, provides experimental evidence for a general mechanism possibly leading to compromised drug-glucuronidation or impaired antioxidative balance in other diseases. The first experimental proof of miRNA-mediated impaired drug metabolism by UGT1A1 was provided recently. In the research work by Dluzen *et al.*, a significantly reduced UGT1A1-mediated glucuronide formation was demonstrated when Huh-7 cells were transfected with miR-491-3p [120]. As a substrate for UGT1A1, the authors used the chemotherapeutic agent raloxifene which was reported to be specifically metabolized by glucuronidation. The study now provides evidence for the inhibition of UGT1A1 activity mediated by miR-486-3p indicating that the upregulation of miR-486-3p might affect the therapeutical treatment with drugs eliminated by UGT1A1, which possibly leads to drug-related toxicities or other side effects. This hypothesis is further supported by the results obtained in the UGT enzyme activity assay, where UGT(1A1) enzyme activity was reduced in mouse primary hepatocytes transfected with miR-486-3p. This is in line with the results described by Dluzen *et al*. for miR-491-3p and corroborates that miR-486-3p acts as a negative regulator of UGT(1A1)-mediated substrate metabolism *in vivo* (Figure 35).

4.1.2 UGT1A3 and UGT1A4

The human UGT1A3 and UGT1A4 share about 93 % identity in their amino acid sequences, whereby both enzymes glucuronidate partially the same substrate classes [43]. However, UGT1A3 represents a physiological enzyme able to glucuronidate bile acids [179]. Among the diverse etiologies, liver fibrosis can develop from cholestatic liver disease [180]. This pathological condition is characterized by an impaired bile flow from the liver to the duodenum resulting in the hepatic accumulation of cytotoxic bile acids. Due to their amphiphilic properties, bile acids can exhibit their detergent action upon hepatic lipids potentially leading to cell membrane disruption and hepatocyte apoptosis and the generation of ROS [181]. In this work, the UGT1A3 mRNA levels were significantly reduced by miR-17, miR-18a, miR-25, miR-29a, miR-151-5p, miR-183-5p, miR-199a-3p, miR-214-5p, miR-214-3p, miR-330, miR-486-3p, and miR-519d (Figure 10). Ogawa *et al.* reported that miR-199a-3p was upregulated in human livers with advanced fibrosis [182]. Among the *UGT1A3*-downregulating miRNAs examined in this study, miR-199a-3p was also identified to reduce UGT1A3 protein levels in HepG2 cells (Figure 16). Consequently, this study provides experimental evidence for a miR-199a-3p-mediated reduction of *UGT1A3* expression, which may lead to the accumulation of toxic bile acids in the liver hence stimulating the progression of fibrogenesis, because of impaired UGT1A3-mediated bile acid glucuronidation. As increased levels of detergent bile acids in cholestatic livers are associated with hepatocyte death and an elevated ROS production, the downregulation of UGT1A3 might increase hepatic OS, a well-known driver for fibrosis in cholestasis-related liver diseases [183]. Moreover, the miR-199a-3p-mediated reduction of UGT1A3 may also lead to the impaired glucuronidation of drugs or other endo- and xenobiotics, which are used to treat various disease conditions in human tissues that may augment the possibility of drug-related side effects.

The UGT1A4 enzyme shows maximal specific activity towards aliphatic alcohols, C_{19} steroids, and sapogenins which was absent for UGT1A3 [43]. In view of the generated results obtained for *UGT1A4* expression, numerous miRNAs significantly repressed UGT1A4 mRNA levels (Figure 11). These miRNAs were miR-16a, miR-18a, miR-20a, miR-29a, miR-34a, miR-106b, miR-181a-5p, miR-199a-5p, miR-199a-3p, miR-221, and miR-519d. In line with the reduced mRNA levels, the UGT1A4 protein levels decreased after transfection of miR-18a, miR-29a, and miR-34a (Figure 17). Interestingly, an upregulated miR-34a expression was reported in ALD and in liver fibrosis [184, 185]. Based on the results of the

present study, this suggests that the UGT1A4-catalyzed endo- and xenobiotic glucuronidation may consequently be impaired in individuals with ALD through the overexpression of miR-34a. The deficient antioxidative capacity in ALD and liver fibrosis triggered by miR-34a may, therefore, promote the progression from ALD to more severe liver fibrosis/cirrhosis. Hong *et al*. reported that in three mouse models of CCl_4-induced fibrosis, members of the miR-34 family were upregulated (Figure 36, panel 3) [186]. In line with Hong *et al*., the negative regulation of *UGT1A* expression by upregulated miR-34a expression is likely to be also transferable to our murine fibrogenesis model (Figure 34). More specifically, in the ethanol-CCl_4 treated mouse model the UGT1A3 and UGT1A4 mRNA levels were tremendously reduced which emphasizes the implication of post-transcriptional regulation (i.e., by miR-34a) in the fibrotic liver tissue which disrupted the UGT1A-mediated glucuronidation capacity incapable to eliminate the accumulating levels of carcinogenic CCl_4-intermediates.

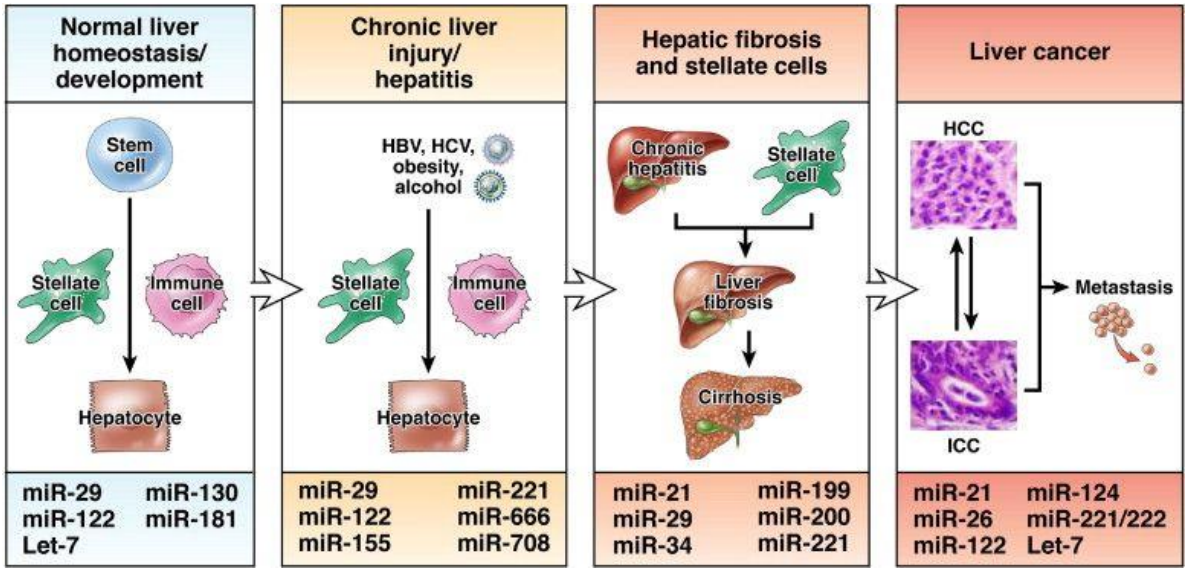

Figure 36. The effect of miRNAs in the liver development, and across liver diseases until liver cancer. The figure shows the different development stages from normal to chronic liver diseases up to hepatic cancer. The stages are outlined from left to right, with stage 1 at the very left. In stage 1, the development of hepatic stem cells to hepatocytes is regulated, among the regulating factors are miRNA such as miR-122 and Let-7. In stage 2, the influence of environmental or other stimuli (e.g. hepatitis B/C viruses, obesity, and alcohol) lead to hepatocyte injury. Relevant miRNAs are among others miR-122 and miR-155. In stage 3, the persistent hepatocyte injury results in chronic inflammation (hepatitis) which can trigger the activation of stellate cells. As a response to the chronic inflammatory conditions and hepatocyte apoptosis/necrosis, stellate cells produce ECM proteins including fibrillar collagens (liver fibrosis). Liver fibrosis can advance to cirrhosis. For instance, the involved miRNAs are miR-34 and miR-199 family members. In stage 4, liver cirrhosis can progress to liver cancer (HCC) which can convert to the intrahepatic cholangiocellular carcinoma (ICC). Finally, HCC or ICC cancer cells can spread to new areas of the body (metastasis). MiRNAs such as miR-122 and Let-7 are downregulated in HCC. The underlying miRNAs outlined in each liver stadium are only exemplary and are far from being complete. The figure was adapted from [113].

HCC emerges as a lethal burden of cirrhosis within a diseased liver [187]. Connolly *et al.* showed in a miRNA profiling study with human primary hepatitis B virus-positive HCC patients that miR-18a is upregulated [188]. In this study, miR-18a reduced the *UGT1A4* expression, which is why miR-18a is identified as a negative regulator of UGT1A4-mediated detoxification of primary and secondary amines, as well as sapogenins that are key in therapeutic drugs [189]. Therefore, the miR-18a-mediated downregulation of *UGT1A4* expression can likely cause drug-induced toxicities, which may be considered during drug administration in patients with HCC.

4.1.3 UGT1A6

The UGT1A6 enzyme was described to exhibit higher specific activity towards complex phenols and primary amines as any other UGT1A isoform [43]. In addition, UGT1A6 belongs to the major tobacco carcinogen detoxifying enzymes able to glucuronidate phenolic benzo(α)pyrene metabolites such as quinones, phenols, and quinols, generated by CYP450-mediated bioactivation [190]. The *in vitro* experiments performed in this work revealed a downregulation of UGT1A6 mRNA expression by miR-15a, miR-16a, miR-18a, miR-25, miR-29a, miR-155, miR-199a-3p, miR-221, miR-486-3p, and miR-519d (Figure 12). This data was further supported by miR-18a, miR-25, miR-155, miR-199a-3p, miR-221, miR-486-3p, and miR-519d that reduced UGT1A6 protein levels (Figure 18). This miRNA-mediated reduction of *UGT1A6* expression may present a likely inducer of increasing OS levels and severe tissue damage due to the accumulation of carcinogenic benzo(α)pyrene metabolites in tissues, forming covalent bonds with intracellular macromolecules, including DNA, protein and/or lipids representing the chemical properties of such reactive metabolites [169]. Thereby, excessive tobacco smokers suffering from advanced liver fibrosis may underlie severe exposure to benzo(α)pyrene metabolite-driven hepatic and non-hepatic tissue damage, in response to miR-199a-3p-mediated reduced UGT1A6 activity. The respective miR-199a-3p could therefere be considered as a significant regulator of the antioxidative balance in fibrotic livers [182]. In a study of our laboratory, Kalthoff *et al*. showed that mice with genetic polymorphisms leading to impaired *UGT1A* expression generated higher OS levels compared to their WT counterparts after benzo(α)pyrene treatment [142]. This further supports the hypothesis of increased OS levels in the presence of *UGT1A6* polymorphisms. Since polymorphisms in the *UGT1A6* gene can modify its expression, the post-transcriptional

regulation by miRNAs in this study is suggested to affect UGT1A6-catalyzed benzo(α)pyrene detoxification. The genotoxic properties of benzo(α)pyrene were studied in the research work by Deng *et al.* [191]. The authors exposed mice to an acute benzo(α)pyrene treatment and observed among all the tested tissues high oxidative stress levels and high DNA damage in the liver, the organ that is primarily involved in the metabolism of carcinogenic benzo(α)pyrene. This finding underscores the need for a rapid UGT1A6-mediated carcinogen glucuronidation from the tissues, to prevent severe liver diseases and hepatocarcinogenesis. Therefore, the upregulation of *UGT1A6*-downregulating miRNAs indicates a significant risk for the elimination of polycyclic aromatic hydrocarbons (PAH), including benzo(α)pyrene which is a ubiquitous food-borne and environmental pollutant found in car exhaust fumes, tabacco smoke, charcoal-grilled meats, and contaminated soil and water [192]. In a case-control study, Su *et al*. found that the environmental exposure to benzo(α)pyrene might increase the risk of HCC, among populations with hepatitis B virus infection and alcohol consumption [193]. Since the expression of miR-221 increased along with the progression of liver fibrosis [182], this miRNA is suggested to facilitate the risk for the development of HCC. Supported by the results in this work, the miR-221-mediated reduction of *UGT1A6* expression may likely result in the impaired UGT1A6-catalyzed benzo(a)pyrene metabolite, drug, and reactive intermediate glucuronidation in fibrotic livers which may promote the OS-induced progression from liver fibrosis to HCC. In addition to PAHs, UGT1A6 glucuronidates ordinary phenol-containing drug paracetamol [45]. The paracetamol elimination is primarily subjected to glucuronidation and sulfation in man. In addition, small amounts of CYP450-produced toxic *N*-acetyl-*p*-benzoquinonimine (NAPQI) are eliminated by the conjugation with glutathione. In the condition of paracetamol overdoses, the NAPQI-intermediate can accumulate in tissues and form covalently bound NAPQI-protein adducts causing severe liver damage and necrotic cell death [194]. The abuse of paracetamol as pain killer in certain diseases may cause fatal hepatoxicity, in response to the miRNA-mediated downregulation of the UGT1A6 activity capable to eliminate paracetamol (and their intermediates) from the body. In response to the miRNA-mediated impaired glucuronidation by UGT1A6, incorrect dosing of paracetamol may overwhelm sulfation and deplete intracellular glutathione levels promoting NAPQI-related development of liver diseases.

During chronic alcohol consumption, the expression of miR-155 is increased in isolated Kupffer cells in which miR-155 induced an inflammatory response (Figure 36) [195]. In this work, the miR-155 overexpression reduced *UGT1A6* expression *in vitro*, which indicates that

miR-155 might, additionally to its reported role, constitute a potential risk factor for the UGT1A6-mediated elimination of potentially harmful substances during the onset or progression of ALD in man.

4.1.4 UGT1A7

The UGT1A7 enzyme is extrahepatically expressed in the orolaryngeal tissue and detoxifies therapeutic drugs and food-borne carcinogens such as PAHs and heterocyclic amines (e.g. PhIP) at their entry point into the body [45]. PhIP is the most abundant heterocyclic amine with well-characterized genotoxicity, reported to form PhIP-DNA adducts in the human colon and mammary gland [196]. These human health-threatening carcinogens are present in processed meat and were described to increase the risk of various cancers such as gastric, colorectal, and esophageal cancers [197]. In this work, miR-4321 reduced the UGT1A7 mRNA expression (Figure 13) that, however, was not supported by a decline in the UGT1A7 protein expression (Figure 19). Since other miRNAs (e.g. miR-183-5p and miR-214-5p) led to a reduction of the UGT1A7 mRNA levels, miRNAs may represent considerable post-transcriptional regulators of *UGT1A7* expression. Therefore, the miRNA-mediated reduction of *UGT1A7* expression may result in the reduced carcinogen glucuronidation in the extrahepatic tissues, promoting macromolecular adduct formation and the tissue damage-derived onset of severe diseases. The functional importance of UGT1A7 in xenobiotic detoxification has been reported before. In 2008, Strassburg *et al*. described the genetic *UGT1A7* variant, *UGT1A7*3*, which contains 3 AA changes (N129K, R131K, and W208R) in the *UGT1A7*-derived exon 1, and an additional promoter polymorphism (-57T>G) which leads to reduced UGT1A7 activity [45]. Furthermore, Strassburg *et al*. performed a case-control study with colorectal cancer (CRC) patients and healthy controls, and found that the *UGT1A7*3* allele exhibited no catalytic activity towards benzo(α)pyrene metabolites, PhIP and other substrates which indicated that *UGT1A7*3* represents the main risk allele of CRC [198]. In addition, the *UGT1A7*3* allele increased the severity of liver cirrhosis and the risk for the development of HCC [199, 200]. This study supports the role of UGT1A7 and shows that an upregulated miRNA (Figure 32) can reduce UGT1A7 mRNA expression in a mouse model of alcoholic liver fibrosis (Figure 34). This result suggests that the miRNA-mediated reduced *UGT1A7* expression can lead to the accumulation of mutagenic carcinogens and other harmful components in the liver and the surrounding tissues which triggers the development

or progression of liver fibrosis/cirrhosis, or CRCs. Experimental evidence for the miR-486-3p-mediated impaired *UGT1A7* expression is provided by the reduction of UGT1A7 mRNA and protein expression in Caco-2 cells (Figure 22, Figure 24), which may significantly repress UGT1A7-glucuronidation in extrahepatic tissues (e.g. the colon) leading to drug-induced toxicities specifically during treatment with medications. As an anti-cancer drug, irinotecan and its toxic active metabolite SN-38 are utilized for the treatment of metastatic CRC [201], in turn, SN-38 is inactivated in the human liver by UGT1A enzymes such as UGT1A7 [202]. However, the presence of SNPs in the first exon of UGT1A7 reduces SN-38 glucuronidation activities and is associated with irinotecan-related toxicities [203]. These findings emphasize the physiological importance of UGT1A7-mediated therapeutic drug metabolism and point to miR-486-3p as a critical regulator of *UGT1A7* expression potentially promoting the accumulation of the toxic SN-38 metabolite in the liver and surrounding tissues, particularly relevant as miR-486-3p was shown to be upregulated in malignant CRC cell lines [204]. In conclusion, the potential upregulation of the *UGT1A7*-downregulating miRNAs such as miR-4321 and miR-486-3p in *UGT1A7*3* carriers may establish a fatal combination and is likely increasing the risk for the development of severe liver disease or cancer.

4.1.5 UGT1A9

UGT1A9 detoxifies propofol [205], flavopiridol [206], mycophenolic acid [207], acetaminophen [208], anticancer drugs [78], and mutagenic arylamines (e.g. PhIP and N-hydroxy-PhIP) [80]. The *UGT1A* expression studies *in vitro* revealed that UGT1A9 mRNA levels were significantly reduced by miR-25 and miR-214-5p (Figure 14). In line with these results, UGT1A9 protein expression was slightly reduced by miR-214-5p in liver cancer HepG2 cells (Figure 20). The downregulation of the UGT1A9-mediated substance glucuronidation by miR-214-5p may increase the risk for the onset of liver diseases since the accumulation of therapeutic drugs and mutagenic xenobiotics in the tissues may initiate severe tissue damage. Thereby, individuals with injured livers or metastatic CRC and upregulated miR-214-5p expression may encounter severe drug-induced toxicities when treated with anticancer drugs, including irinotecan [78]. Iizuka *et al.* showed that miR-214-5p expression correlated with the severity of liver fibrosis in 35 patients with hepatitis C infection which indicated that miR-214-5p may be involved in the progression of liver fibrosis [209]. In line with Iizuka *et al*., this work supports the contribution of miR-214-5p in the

progression of liver fibrosis, because of the potential accumulation of harmful substances in the liver due to the impaired UGT1A9-mediated detoxification of reactive metabolites and other xenobiotics. Consistent with this, further evidence is provided by the experiments using fibrotic mice (Figure 34). In the OS-related condition of liver fibrosis, the UGT1A9 mRNA expression statistically significantly reduced which was potentially attributed to the upregulation of miR-486-3p expression, however, may likely be traced back to other miRNAs such as miR-214-5p dysregulated in the emerging liver fibrosis. A strong indication for the role of miR-214-5p in the progression of liver fibrosis to cirrhosis is provided in this study (chapter 3.8), where the expression of miR-214-5p was detected in liver cirrhosis. This result points to a potential miR-214-5p-mediated impaired *UGT1A9* (and other *UGT1A*) expression through the common UGT1A 3'-UTR, which is attributable to the increase of unconjugated, yet biologically-active compounds readily interacting with intracellular macromolecules causing cell damage and apoptotic/necrotic cell death. In this regard, the miR-214-5p-mediated cellular damage may affect the hepatic as well as extrahepatic tissues, supported by the reduction of *UGT1A* expression in extrahepatic cell lines (chapter 3.5).

4.2 Identification of Novel miRNAs Targeting the Common UGT1A 3'-UTR

Considering the target mRNA 3'-UTR, animal miRNAs form partial complementarity within the MRE. However, perfect complementarity between the miRNA 5'-end nucleotides (nucleotides 2-8), the critical region denoted as the "seed region" and the target mRNA is sufficient for the regulation [110]. In this work, the performed *in vitro* assays determined miR-214-5p, miR-486-3p, and miR-519d as novel *UGT1A* post-transcriptional regulators. The *in silico* analysis to predict the potential binding sites in the UGT1A 3'-UTR revealed the generation of thermodynamically stable mRNA:miRNA duplexes for miR-214-5p and miR-486-3p, based on the 8-nucleotide seed match and additional base pairing near the miRNA 3'-end (Figure 25). The mutagenesis of the 8 nucleotides in the UGT1A 3'-UTR responsible for seed pairing (Figure 26) resulted in a statistically significant recovery of the luciferase activity (Figure 27). This emphasizes the complementary binding of miR-214-5p and miR-486-3p with their predicted MRE within the UGT1A 3'-UTR. Moreover, in this work miR-214-5p and miR-486-3p are identified as two novel regulators of *UGT1A* gene expression due to their hybridization to MREs within the UGT1A 3'-UTR. In other studies, *UGT1A* gene expression

was shown to be regulated by miRNAs [120, 210]. Dluzen *et al.* indicated that miR-491-3p targeted the bioinformatically predicted MRE in the UGT1A 3'-UTR [120]. To confirm the functional implication of the MRE, the authors deleted 4 nucleotides within the UGT1A 3'-UTR-located nucleotide sequence complementary to miR-491-3p's seed region which led to the statistically significant recovery of luciferase activity [120]. In contrast to Dluzen *et al.*, a mutagenesis approach was performed in this work which disrupted the complementary hybridization of the miRNA 5'-end with the UGT1A 3'-UTR MRE and led to similar luciferase recoveries (Figure 27). This result indicates that both strategies (deletion or mutagenesis) lead to the disruption of the nucleotides complementary to the miRNA seed region. Furthermore, this demonstrates that: 1) the MRE-related nucleotides involved in seed pairing are crucial for miRNA activity and 2) a deletion of only 4 nucleotides or the nucleotide mutagenesis are sufficient to inactivate a miR-specific MRE.

Animal miRNAs are reported to form partial complementarity with their target mRNA, whereas plant miRNAs form perfect or near-perfect complementarity with their target mRNAs [211]. Therefore, partial complementarity leads to the regulation of hundreds of target genes by animal miRNAs eliciting pleiotropic effects [96]. Moreover, miR-214-5p and miR-486-3p were recently reported to silence the expression of other genes [212]. Li *et al.* reported that miR-214-5p is a highly expressed miRNA in patients with bone fractures. Under the conditions of bone fractures, miR-214-5p targeted the 3'-UTR of COL4A1 mRNA encoding type IV collagen α-chain 1 which repressed cell survival and extracellular matrix formation of osteoblastic cells. Considering miR-486-3p, it was reported that miR-486-3p is related to cancer [204]. Feng *et al.* reported that miR-486-3p was upregulated in CRC cell lines where it functioned as a negative regulator of apoptosis by binding to the 3'-UTR of BH3-only family proapoptotic protein (BIK) mRNA. The inverse correlation of upregulated miR-486-3p and downregulated BIK increased the CRC cell migration and invasion. Furthermore, it was shown that miR-486-3p contributed to the aggressive behavior of malignant CRC cells. The bioinformatic search for more target mRNAs of miR-214-5p, miR-486-3p, and miR-519d was pursued and predicted RXRα mRNA as a novel target (Figure 29). The experimental validation revealed that RXRα mRNA expression was reduced after miR-214-5p, miR-486-3p, and miR-519d transfection into liver cells (Figure 30). This result suggested that *RXRα* may be considered as another novel target gene regulated by the three candidate miRNAs. In this way, the finding that an animal miRNA is capable of regulating

numerous target mRNAs through partial hybridization to the 3'-UTR was repeatedly supported.

4.3 Hepatoprotective Properties of miR-122

In literature, it is reported that miR-122 comprises 70 % of the liver's total miRNA [213]. Moreover, miR-122 is reported to exert anti-inflammatory and anti-fibrotic properties in the liver [164]. The investigation of the post-transcriptional regulation of *UGT1A* expression *in vitro* pointed to miR-122 as a potential strong inducer of UGT1A-mediated substance detoxification. These results support the hepatoprotective effect of miR-122 and identify *UGT1As* as novel genes induced by miR-122. The miR-122-mediated upregulation of *UGT1A* expression implies that individuals with overexpressed miR-122 are subjected to an enhanced elimination of phase I-activated potentially harmful compounds which may contribute to a considerable reduction of intracellular OS levels by means of an induced UGT1A-mediated detoxification activity. In this study, miR-122 consistently induced the hepatic *UGT1A1*, *UGT1A7*, and *UGT1A9* expression (chapters 3.3, 3.4), which is why this may facilitate the detoxification of SN-38 metabolites [214]. The positive association between a highly active UGT1A enzyme and therapeutic drug metabolism has been reported before [78]. Girard *et al.* explained that *UGT1A9* polymorphisms increased enzyme activity and reduced the irinotecan-induced toxicity. In line with this finding, miR-122 may contribute to the reduction of the unwanted side effects observed with irinotecan medication such as neutropenia and diarrhea due to the tremendous activation of the essential physiological UGT1A enzymes capable to glucuronidate SN-38 metabolites. Of note, Kutay *et al.* reported that miR-122 was downregulated in human primary HCCs [215]. Moreover, Tsai *et al.* developed a miR-122 knockout mouse line and reported that these mice spontaneously developed HCC [213]. These findings suggest that the miR-122-promoted antioxidative balance is disrupted under the conditions of HCC and lacking miR-122 expression which is subjected to a disruption of important cellular metabolic pathways, including the UGT1A-mediated xenobiotic glucuronidation. Against this background, a replacement of miR-122 in subjects with HCC may restore the metabolic antioxidative balance in the liver due to the potential recovery of the UGT1A-mediated glucuronidation of xenobiotic substances. On the other hand, the liver's high miR-122 expression has been reported to be of crucial importance during the infection of hepatitis C virus (HCV). Li *et al.* showed that miR-122 acts as an essential host factor for

HCV infection [216]. The authors described that the 5'-UTR of the HCV genomic RNA has two conserved miR-122 target sites near the internal ribosome entry site which are targeted by miR-122. Hence, the HCV RNA 5'-UTR is protected from nucleolytic degradation which stabilizes this region and stimulates the replication and translation of the viral RNA. In this work, the molecular mechanism of the miR-122-mediated induction of *UGT1A* expression has not been studied in detail. The luciferase data indicate a slight induction of the UGT1A 3'-UTR luciferase activity after miR-122 transfection (Figure 8). However, generally the targeting of miRNAs to the mRNA's 3'-UTR results in post-transcriptional gene silencing which induces mRNA decay and translational inhibition [110]. Considering the molecular mechanism of miR-122 during HCV-mediated liver infection [216], miR-122 might target a sequence which is different from the 3'-UTR to induce gene expression. In literature, the miRNA-mediated induction of gene expression has been reported before. In 2008, Place *et al.* were the first to describe that miR-373 induces mRNA expression by hybridization to complementary sites in the promoters of the target genes which increased RNA polymerase II binding intensity at the transcription start site [217]. Place and colleagues, therefore, regarded miR-373 acting as a TF. An even more interesting mechanism of transcriptional gene activation has been described by Xiao *et al.* [218]. The authors reported that miR-24-1 was capable to remodel the chromatin at enhancer regions in the nucleus which induced the enhancer RNA expression. These literature findings underpin the various mechanisms of miRNAs to induce the target gene expression and lead to the conclusion that one of the above-mentioned mechanisms may be transferable to miR-122, although the underlying mechanisms have yet to be studied.

4.4 Potential Mechanisms for the *UGT1A* Expression Variability

In this work, the miRNA-mediated regulation of UGT1A mRNA expression varied across UGT1A isoforms, even though all UGT1A mRNAs share the common 3'-UTR. This becomes clear when the *in vitro* effects of miR-34a are taken into consideration. Hence, miR-34a increased the UGT1A1 and UGT1A3 mRNA levels, but led to a decrease or no changes in the UGT1A4, UGT1A6, UGT1A7, and UGT1A9 mRNA expression (chapter 3.3). This discrepancy between the different UGT1A isoforms may emphasize more complex mechanisms which can modulate the miRNA-mediated *UGT1A* expression. In numerous studies, an isoform-specific regulation of *UGT1A* expression has been observed. Dluzen *et al.*

studied the post-transcriptional regulation of *UGT1A* expression and revealed a celltype-specific effect after miR-491-3p transfection, showing that UGT1A1 expression and activity decreased in Huh-7 cells, but remained unchanged in HepG2 cells [120]. Similar celltype-specific behavior was also observed in this work when comparing cell line-specific *UGT1A* expression (chapter 3.5). The authors also reported that *UGT1A4* and *UGT1A9* expression were not significantly repressed after miR-491-3p transfection into Huh-7 cells. Dluzen and colleagues computed UGT1A mRNA secondary structures and found that each UGT1A isoform had a unique secondary structure suggesting an impaired hybridization of miR-491-3p to the individual UGT1A mRNA. Later, Wang *et al*. identified miR-298 as a novel post-transcriptional regulator of *UGT1A* expression [210]. In line with the findings by Dluzen *et al*., Wang and colleagues also discovered such an isoform-specific regulation which prompted them to compute UGT1A mRNA secondary structures and report unique miR-298-MRE secondary structures in the UGT1A mRNAs. Regarding these findings, the UGT1A mRNA expression variability may be attributable to such individual UGT1A mRNA secondary structures that likely affects the miRNA-based targeting of MREs in the common UGT1A 3'-UTR. The impaired accessibility of MREs in the UGT1A 3'-UTR may, therefore, affect miRNA activity which points to the importance of mRNA secondary structures. The implication of mRNA secondary structures and miRNA activity has been extensively studied before. Long *et al.* performed an extensive accessibility profiling analysis to study the accessibility of Let-7 miRNA to its complementary sites in the Lin-41 mRNA 3'-UTR [219]. The authors designed Lin-41 mRNA 3'-UTR mutants containing adjacent Let-7-complementary sites with an interspersed 27-nt mutated or designed spacer, and performed *in vivo* experiments that resulted in configurational changes of the target sites and an altered mRNA secondary structure. In fact, Long *et al*. found that Let-7 was most active at structurally accessible target sites, indicating the pivotal contribution of mRNA secondary structures on miRNA activity.

Apart from mRNA secondary structures, the interindividual variability in *UGT1A* gene expression can underlie numerous other regulatory mechanisms. These can include epigenetic modifications, TFs, and polymorphisms (e.g. SNPs). Many epigenetic factors such as DNA methylation, histone modifications and non-coding RNA (e.g. miRNA) regulation can affect drug-metabolizing gene expression and occur as a response to a variety of changes to the environment, diet, patho- or physiological conditions [220, 221]. Histone modifications that occur on the same or another histone tail confer the overall expression status of a DNA

region. Histone acetylation catalyzed by histone acetyltransferases has the highest potential to unfold chromatin, because it neutralizes the basic charge of histone proteins' lysine residues. This results in the disintegration of the DNA and histone interaction which enables the binding of TFs. On the other hand, histone hypoacetylation and hypermethylation is a characterization of silenced DNA sequences [222]. The transfer of a methyl group to the cytosine pyrimidine ring at the 5' position of a CpG site by DNA methyltransferases can silence the transcription on a long-term by alteration of chromatin structure that prevents binding of TFs or co-activators [220]. Interestingly, Oda *et al.* found that the *UGT1A1* promoter was hypermethylated in the kidney and hypomethylated in the liver, indicating the increased expression of *UGT1A1* in the liver, but absent expression in the kidney [223]. Moreover, the authors showed that histone H3 near the *UGT1A1* promoter was hypoacetylated in the kidney, but hyperacetylated in the liver. Mammalian non-coding RNAs were also found to regulate the expression of eukaryotic genomes on different levels (Figure 37) [111].

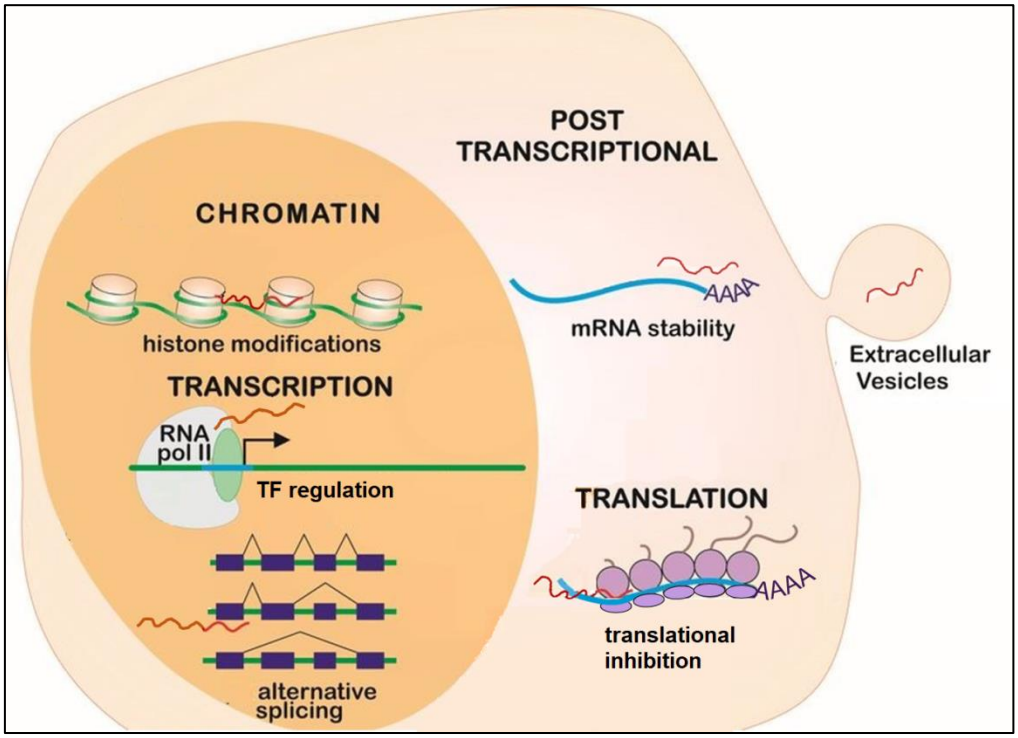

Figure 37. Levels of Gene Expression Regulation by Mammalian microRNA. Mammalian microRNAs regulate the eukaryotic gene expression on different levels. MicroRNAs (represented as red line) are present in the nucleus (ochre) where they can modulate histone modifications and/or DNA methylation. Moreover, microRNAs control the biosynthesis of TFs responsible for transcriptional activation of gene expression and can interact with key splicing factors which can affect mRNA alternative splicing. In the cytoplasm (beige), the interaction of the microRNA 5'-end with MREs in the target mRNA 3'-UTR leads to the degradation of mRNA and can inhibit the mRNA translation. Finally, microRNAs can be incorporated into secreted membrane vesicles (extracellular vesicles) which are then transported between cells to potentially regulate the gene expression of the recipient cell. The figure was modified from [224].

As mentioned before [218], miR-24-1 is capable to translocate into the nucleus and modulate the chromatin structure which can induce the target gene expression. Therefore, the discussed regulatory epigenetic mechanisms may have a considerable impact on *UGT1A* expression, which has in part been supported in this study through the elucidation of the post-transcriptional regulation of RXRα and UGT1A mRNA expression. The TFs HNF1α and 4α, PXR, CAR, and AhR belong to relevant transcriptional regulators of *UGT1A* expression [225, 226]. Hu *et al*. reported that their TF responsive elements are located in the *UGT1A* promoters which implies an individual transcriptional activation of UGT1A mRNA expression [48]. In this work, the isoformic UGT1A mRNA levels revealed variable expression patterns after miR-34a (and other investigated miRNA) transfection which may shed light onto miR-34a-mediated transcriptional activation of UGT1A mRNA expression. As a matter of fact, the relevant heterodimer partner (RXRα) of numerous TFs is regulated by miR-34a. Oda *et al*. reported that miR-34a is a negative regulator of *RXRα* expression in the liver [123], which affected the induction and transactivity of drug-metabolizing enzyme gene expression. As miR-34a can repress *RXRα* expression, the transcriptional activation of each *UGT1A* gene is likely to be affected. Since the RXRα protein forms heterodimers with a considerable number of TFs [52], the miR-34a-mediated downregulation of *RXRα* may be, amongst others, a possible explanation for the *UGT1A* expression variability observed in this work. In this study, the RXRα mRNA expression was reduced by miR-214-5p, miR-486-3p, and miR-519d (Figure 30). This result suggests that the 3 candidate miRNAs impaired the transcriptional activation of UGT1A mRNA expression by downregulation of *RXRα* expression which would, thereby, support the observed *UGT1A* expression variability. However, since the RXRα protein expression was slightly induced rather than reduced the indirect regulation of *UGT1A* expression by miR-214-5p, miR-486-3p, and miR-519d requires further experimental evidence (Figure 31).

Lastly, genetic *UGT1A* polymorphisms can be attributable to the variablitiy in *UGT1A* expression. In this regard, a human variant haplotype containing 10 common occuring *UGT1A* SNPs (UGT1A1*28, UGT1A3 -66T>C, UGT1A3 V47A, UGT1A3 W11R, UGT1A6*2a (S7A/ T181A/ R184S), UGT1A7*3 (N129K/ R131K/ W208R/ -57T>G)) has been described to be present in about 10 % of the white population [139]. Moreover, this haplotype led to reduced UGT1A mRNA and protein expression, as well as transcriptional activation by mutagenic xenobiotics, carcinogens, and endotoxin. The presence of common *UGT1A* promoter polymorphisms was shown to affect the functionality of a TF binding motif

[66]. SNPs in the *UGT1A* promoters, therefore, alter *UGT1A* gene transcription and account for the interindividual variability of *UGT1A* gene expression.

Apart from the variability of UGT1A mRNA expression, a discrepancy between the UGT1A mRNA and protein expression was observed in this study. For instance, UGT1A1 and UGT1A3 mRNA expression was upregulated, whereas the corresponding protein levels were reduced after miR-34a transfection into HepG2 cells (chapters 3.3, 3.4). In literature, this discrepancy has been reported before. In 1999, Olsen and Ambros noted similar relations when studying the impact of regulatory RNA (lin-4) in *C. elegans* larval development [227]. Therefore, Olsen and Ambros observed that lin-4 inhibited the translational elongation and functional LIN-14 protein synthesis in larval development without affecting the abundance of lin-14 mRNA levels. Remarkably, lin-4 and lin-14 mRNA were found in association with polyribosomes which was suggested to impair protein synthesis near a time point of translational initiation [227, 228]. This mechanism may be transferable to this study as well and therefore constitutes a possible explanation for the observed discrepancy between the UGT1A mRNA and protein expression.

4.5 MicroRNAs as Potential Risk Factors for the Development of Liver Fibrosis/Cirrhosis

Continuing excessive alcohol consumption is a major cause of liver cirrhosis [229]. Mainly in Western European countries where liver disease is predominantly evoked by alcohol abuse [230]). In 2010, globally, 493,300 deaths were attributable to liver cirrhosis, and 80,600 deaths were attributable to liver cancer, both liver diseases are *inter alia* caused by excessive alcohol intake [231]. The involvement of miRNAs in the pathogenesis of liver diseases, metabolic disorders and cancer, along with their remarkable stability in plasma or serum makes them reliable prognostic/diagnostic biomarkers for liver diseases or cancer detection [129, 132]. In this study, miR-214-5p, miR-486-3p, and miR-519d regulated *UGT1A* expression to a consistent extent, whereby these miRNAs were chosen for the determination in liver cirrhosis. The circulating levels of miR-214-5p, miR-486-3p, and miR-519d were measured in sera of cirrhotic patients and revealed an upregulation of miR-486-3p (Figure 32). Considering miR-486-3p as a negative regulator of *UGT1A* expression *in vitro*, the miR-486-3p upregulation in liver cirrhosis is likely to impair the UGT1A-mediated detoxification of drugs, environmental carcinogens or other major chemical risk factors capable to generate

cellular damage and increase OS levels in the liver. As miR-486-3p reduced *UGT1A1* and *UGT1A6* expression in HepG2 cells (discussed in chapter 4.1), the impaired elimination of xenobiotic, phenol-containing carcinogens, mutagens, or therapeutic drugs may trigger the onset or development of liver cirrhosis. The consequences of a reduced UGT1A enzyme activity has been explained before. Tang *et al*. reported that genetic variants of the *UGT1A7* gene can lead to a decreased enzyme activity [199]. Moreover, the impaired carcinogen glucuronidation and cellular protection may increase the risk for the development and the functional severity of liver cirrhosis. Given the fact that the cirrhotic patients in this work included a high percentage (75 %) of alcohol-based etiologies [137], it was aimed at creating liver fibrosis in the *htgUGT1A*-WT mouse model by ethanol-CCl_4 treatment. In line with the human study, miR-486-3p was significantly upregulated in fibrotic mice livers (Figure 33), while a significant downregulation of UGT1A mRNA levels was observed (Figure 34). The downregulation of UGT1A mRNA expression in alcoholic liver fibrosis is likely to occur through the upregulation of miR-486-3p. Since the mouse model of alcoholic liver fibrosis mimiced the conditions of liver cirrhosis in the human study, the downregulation of the UGT1A mRNA levels can be translated from the animal to the human situation. Therefore, the reduction of UGT1A mRNA expression may be considered as an additional risk factor for the development or progression of alcohol-induced tissue damage potentially enhancing fibrogenesis. In humans, the excessive alcohol consumption is associated with the “leaky gut” syndrome, which is characterized as elevated intestinal permeability by epithelial cell disruption leading to the increased exposure of the liver to gut-derived compounds via the portal vein [232]. A specific leaky gut-related compound is the bacterial endotoxin lipopolysaccharide (LPS). The increased hepatic exposure to this major cell wall constituent of gram-negative bacteria and other microbial products during ALD leads to hepatic inflammation and oxidative tissue damage [230, 233]. Richardson *et al*. demonstrated that LPS-induced inflammation and the live bacterial infection with gram-negative *Citrobacter rodentium* reduced UGT1A mRNA expression in the livers of treated mice [234]. This highlights that LPS is a critical regulator of *UGT1A* expression during ALD and points to alcohol as: 1) detrimental hepatotoxin able to induce ALD and other severe liver diseases if excessively consumed and 2) chemical drug indirectly capable of silencing UGT1A-glucuronidation in the liver through the exposure of the liver to bacterial LPS. Thus, a steady inflammatory response is generated in liver cirrhosis through an excess of gut-related microbial compounds which further affects hepatic defence mechanisms [233]. In addition to

the increased endotoxin levels, the miR-486-3p-mediated reduction of the UGT1A-glucuronidation activity during ALD may, therefore, cause a detrimental accumulation of gut-related and other toxic compounds (e.g. acetaldehyde) in the liver which is likely promoting liver disease development *in vivo*. Taken together, the overexpression of miR-486-3p in liver fibrosis/cirrhosis suggests that miR-486-3p is likely to represent a significant risk factor for the development or progression of OS-induced liver diseases, indicating a reduced UGT1A-mediated detoxification capacity incapable to maintain the antioxidative balance in cells and subcellular structures in the liver and beyond, further supported by the reduced *UGT1A* expression in extrahepatic cells after miR-486-3p transfection (chapter 3.5).

Even though the miR-486-3p levels increased by only 1.34-fold in fibrotic mice livers, the UGT1A3 and UGT1A4 mRNA expression decreased by three-digit values. Therefore, this tremendous decline in *UGT1A3*/*1A4* transcription may point to other molecular mechanisms which may have been triggered by carcinogen (i.e., ethanol-CCl_4) intoxication. As such, the CCl_4-based intoxication potentially involves the covalent bond formation of the activated free radicals trichloromethyl radical and peroxy trichloromethyl radical with macromolecules, including proteins, lipids and/or nucleic acids causing oxidative modifications, resulting in apoptosis and cell death [235]. Therefore, the significant decrease of UGT1A3 and UGT1A4 mRNA expression is likely the result of the increased oxidative damage-caused hepatocyte cell death, because of the oxidative modifications induced by highly reactive CCl_4-intermediates. In addition, it cannot be excluded that the CCl_4-based intoxication triggered the dysregulation of other miRNAs capable to reduce *UGT1A* expression. Hong *et al*. reported the upregulation of miR-34 and miR-199 family members in CCl_4-induced liver fibrosis in mice [186]. In this study, the results indicate that the huge decline in UGT1A3 and UGT1A4 mRNA expression possibly occurs through the additional upregulation of miR-199a-3p and miR-34a in fibrotic mice. As discussed before (chapter 4.1), miR-199a-3p and miR-34a negatively affect the UGT1A-mediated compound glucuronidation in liver cells. In this way, the miR-199a-3p-mediated impaired UGT1A3-catalyzed glucuronidation of endogenous bile acids and mutagenic carcinogens (CCl_4-intermediates) may promote hepatocyte apoptosis and the onset of liver fibrosis/cirrhosis. Similarly, the miR-34a-mediated downregulation of *UGT1A4* expression can lead to reduced glucuronidation of the building block ‘sapogenins’ used in therapeutic drugs [189]. Eventually, the accumulation of unconjugated therapeutic drugs in tissues may induce drug-induced toxicities in subjects with liver fibrosis/cirrhosis. Moreover, the upregulation of miRNAs in liver fibrosis may affect *UGT1A* expression on the

level of transcriptional induction. Thereby, in literature, it was reported that miR-34a reduced the expression of TFs RXRα and HNF4α, which led in terms of RXRα to a decreased induction and transactivity of drug-metabolizing enzymes [93, 121]. The role of RXRα in the regulation of *UGT1A* transcription was discussed before (chapter 4.4), which implies an impaired transcriptional induction of *UGT1A* expression if RXRα levels are reduced. A considerable activator of *UGT1A* expression is HNF4α, which is a liver-enriched TF responsible for transcriptional activation of several phase I and II enzyme genes, including *UGT1A* genes. Hence, the miR-34a-mediated downregulation of HNF4α negatively affects *UGT1A* expression [236], whereby the miR-mediated transcriptional regulation in ALD-mice must be taken into account.

Since the upregulation of multiple miRNAs is likely in human diseases, the determination of relevant miRNAs is suggested in future studies, in order to understand potential miRNA-based regulatory networks and a possible cooperative targeting of 2 or more miRNAs to the UGT1A 3'-UTR, as this effect was reported to markedly repress the target gene's activity [237]. Moreover, future experiments may include long-term studies in mice (or patients) for the final classification of miR-486-3p as a risk factor likely to contribute to the onset of severe OS-induced liver diseases. Future experiments are suggested to include the *htgUGT1A*-WT mouse model for the analysis of miR-486-3p expression along the development of liver fibrosis. In contrast to the current approach, the miR-486-3p expression levels can be determined in a time-dependent manner. Thereby, the potential upregulation of miR-486-3p across the liver stages (normal liver>alcoholic hepatitis (ALD)>liver fibrosis>liver cirrhosis), may underscore the role of miR-486-3p in the disturbance of the metabolic antioxidative balance in the liver, due to the impaired UGT1A-mediated xenobiotic metabolism. This time- and liver stage-dependent approach may unravel the role of miR-486-3p *in vivo* and help to evaluate this miRNA as a potential risk factor (or biomarker) for the determination of liver fibrosis/cirrhosis. In terms of clinical studies involving cirrhotic patients, the expression levels of miR-486-3p may be determined in the serum from portal venous blood, to compare the miRNA expression levels with the liver vein. This approach may answer the question whether miR-486-3p originates from the liver and exhibits its UGT1A-regulating effects at levels of increasing liver injury.

Apart from miR-486-3p, miR-214-5p was determined in cirrhotic patients, although no expression was measured in healthy subjects. The detection of miR-214-5p in cirrhotic patients may, therefore, support the findings in literature where upregulated miR-214-5p

expression was linked to the advance of liver fibrosis [209]. In our study, the miR-214-5p expression in cirrhotic patients may display a relation between the upregulated miR-214-5p and the disturbance of the UGT1A-mediated antioxidative balance, which is a possible trigger for the development of liver cirrhosis. In line with previous findings [209], the progression of liver fibrosis to cirrhosis is likely the result of the miR-214-5p-mediated reduction of *UGT1A1* and *UGT1A9* expression in the liver, as well as *UGT1A4*, *UGT1A7*, and *UGT1A9* expression in the colon, further supported by the miRNA-mediated reduction of *UGT1A* expression at the entry point of xenobiotics (i.e., the esophagus) (Figure 21, 23). This miR-214-5p-mediated repression of physiological UGT1A enzymes capable to eliminate structurally diverse endo- and xenobiotic substances increases the risk for tissue damage associated with the increment of OS levels, eventually promoting the development or progression of liver cirrhosis.

4.6 Potential miRNA-Based Therapeutic Strategies

Recent *in vivo* studies found that modified antisense oligonucleotides (antimiRs), able to inhibit endogenous miRNAs, may become an entirely new class of drugs. The special properties of miRNAs such as their size and the known nucleotide sequences have attracted the attention of the pharmaceutical industry [238]. AntimiRs are single-stranded oligonucleotides that antagonize miRNA in reverse orientation and silence them irreversibly, in competition to the cellular mRNA target [166]. In this study, miRNA-specific inhibitors (antimiRs) were co-transfected *in vitro* to investigate the molecular mechanisms of the selected miRNAs, i.e. miR-214-5p and miR-486-3p (Figure 28). The silencing of the overexpressed miR-214-5p and miR-486-3p resulted in the statistically significant recovery of luciferase activity which indicates a specific downregulation of UGT1A 3'-UTR luciferase activity by these identified miRNAs, binding to their bioinformatically predicted target sites (Figure 25). Moreover, this experimental approach supported the selective binding of antimiRs to the miRNA target which eliminated their function. To date, numerous miRNAs were shown to be of therapeutic promise, whereby miRNA-targeting antimiR therapeutics are investigated for the future therapy [239]. Despite the yet-existing drawbacks such as dosing or the hybridization-dependent toxicities, miRNA-based drugs might represent a promising new class of drugs with great potential. Furthermore, future miRNA-based therapeutic strategies

aiming to prevent the downregulation of UGT1A enzymes may constitute an additional option in the treatment of OS-associated liver diseases.

4.7 Conclusion

In conclusion, miR-214-5p, miR-486-3p, and miR-519d were identified as post-transcriptional regulators of *UGT1A* gene expression. The overexpression of miR-214-5p, miR-486-3p, and miR-519d in cancer cell lines led to a significant downregulation of UGT1A mRNA and protein levels. Above all, this is the first work showing miR-214-5p and miR-486-3p-mediated post-transcriptional regulation of *UGT1A* expression by targeting specific binding sites in the common UGT1A 3'-UTR. The overexpression of miR-486-3p in cirrhotic patients and *htgUGT1A*-WT mice with alcoholic liver fibrosis suggests that miR-486-3p is likely to represent a so far unidentified risk factor for the development or progression of liver fibrosis/cirrhosis by means of a reduced UGT1A-mediated detoxification activity capable of protecting cells and subcellular structures from oxidative damage associated with inflammatory disease conditions.

5 References

1. Remmer H. The role of theliver in drug metabolism. *Am J Med.* 49, 617-29 (1970).
2. Internisten im Netz. *Funktion der Leber*. 2019, October 31; Available from: https://www.internisten-im-netz.de/fachgebiete/leber-galle-bauchspeicheldruese/leber/funktion-der-leber.html.
3. Zhang D, Zhu M, Humphreys WG. *Drug metabolism in drug design and development: basic concepts and practice*. Hoboken, N.J.: Wiley-Interscience. (2008).
4. Jancova P, Anzenbacher P, Anzenbacherova E. Phase II drug metabolizing enzymes. *Biomed Pap Med Fac Univ Palacky Olomouc Czech Repub.* 154(2), 103-16 (2010).
5. Carriere V, Chambaz J, Rousset M. Intestinal responses to xenobiotics. *Toxicol In Vitro.* 15(4-5), 373-8 (2001).
6. Rowland A, Miners JO, Mackenzie PI. The UDP-glucuronosyltransferases: their role in drug metabolism and detoxification. *Int J Biochem Cell Biol.* 45(6), 1121-32 (2013).
7. Sanchez-Valle V, Chavez-Tapia NC, Uribe M, Mendez-Sanchez N. Role of oxidative stress and molecular changes in liver fibrosis: a review. *Curr Med Chem.* 19(28), 4850-60 (2012).
8. Cichoz-Lach H, Michalak A. Oxidative stress as a crucial factor in liver diseases. *World J Gastroenterol.* 20(25), 8082-91 (2014).
9. Lee J, Giordano S, Zhang J. Autophagy, mitochondria and oxidative stress: cross-talk and redox signalling. *Biochem J.* 441(2), 523-40 (2012).
10. Turrens JF. Mitochondrial formation of reactive oxygen species. *J Physiol.* 552(Pt 2), 335-44 (2003).
11. Zangar RC, Davydov DR, Verma S. Mechanisms that regulate production of reactive oxygen species by cytochrome P450. *Toxicol Appl Pharmacol.* 199(3), 316-31 (2004).
12. Ksenzenko M, Konstantinov AA, Khomutov GB, Tikhonov AN, Ruuge EK. Effect of electron transfer inhibitors on superoxide generation in the cytochrome bc1 site of the mitochondrial respiratory chain. *FEBS Lett.* 155(1), 19-24 (1983).
13. Edeas M, Attaf D, Mailfert AS, Nasu M, Joubet R. Maillard reaction, mitochondria and oxidative stress: potential role of antioxidants. *Pathol Biol (Paris).* 58(3), 220-5 (2010).
14. Solis Herruzo JA, Solis Munoz P. Melatonin and oxidative stress. *Rev Esp Enferm Dig.* 101(7), 453-9 (2009).
15. Deavall DG, Martin EA, Horner JM, Roberts R. Drug-induced oxidative stress and toxicity. *J Toxicol.* 2012(645460 (2012).
16. Kasai H, Nishimura S. Hydroxylation of deoxyguanosine at the C-8 position by ascorbic acid and other reducing agents. *Nucleic Acids Res.* 12(4), 2137-45 (1984).
17. Di Luzio NR. A mechanism of the acute ethanol-induced fatty liver and the modification of liver injury by antioxidants. *Am J Pharm Sci Support Public Health.* 15(1 Pt 1), 50-63 (1966).
18. Niemela O, Parkkila S, Yla-Herttuala S, Halsted C, Witztum JL, Lanca A, Israel Y. Covalent protein adducts in the liver as a result of ethanol metabolism and lipid peroxidation. *Lab Invest.* 70(4), 537-46 (1994).
19. Cesaratto L, Vascotto C, Calligaris S, Tell G. The importance of redox state in liver damage. *Ann Hepatol.* 3(3), 86-92 (2004).
20. Apostolova N, Blas-Garcia A, Esplugues JV. Mitochondria sentencing about cellular life and death: a matter of oxidative stress. *Curr Pharm Des.* 17(36), 4047-60 (2011).
21. Mello T, Ceni E, Surrenti C, Galli A. Alcohol induced hepatic fibrosis: role of acetaldehyde. *Mol Aspects Med.* 29(1-2), 17-21 (2008).
22. Beier JI, McClain CJ. Mechanisms and cell signaling in alcoholic liver disease. *Biol Chem.* 391(11), 1249-64 (2010).
23. Nordmann R, Ribiere C, Rouach H. Implication of free radical mechanisms in ethanol-induced cellular injury. *Free Radic Biol Med.* 12(3), 219-40 (1992).
24. Devi BG, Henderson GI, Frosto TA, Schenker S. Effect of ethanol on rat fetal hepatocytes: studies on cell replication, lipid peroxidation and glutathione. *Hepatology.* 18(3), 648-59 (1993).
25. McKillop IH, Schrum LW. Alcohol and liver cancer. *Alcohol.* 35(3), 195-203 (2005).
26. De Minicis S, Brenner DA. Oxidative stress in alcoholic liver disease: role of NADPH oxidase complex. *J Gastroenterol Hepatol.* 23 Suppl 1, S98-103 (2008).
27. Gonzalez FJ. Role of cytochromes P450 in chemical toxicity and oxidative stress: studies with CYP2E1. *Mutat Res.* 569(1-2), 101-10 (2005).
28. Donohue TM Jr. Alcohol-induced steatosis in liver cells. *World J Gastroenterol.* 13(37), 4974-8 (2007).

29. Rao RK, Seth A, Sheth P. Recent Advances in Alcoholic Liver Disease I. Role of intestinal permeability and endotoxemia in alcoholic liver disease. *Am J Physiol Gastrointest Liver Physiol.* 286(6), G881-4 (2004).
30. Bataller R, Brenner DA. Liver fibrosis. *J Clin Invest.* 115(2), 209-18 (2005).
31. Li S, Tan HY, Wang N, Feng Y, Wang X, Feng Y. Recent Insights Into the Role of Immune Cells in Alcoholic Liver Disease. *Front Immunol.* 10(1328) (2019).
32. Tiniakos DG, Vos MB, Brunt EM. Nonalcoholic fatty liver disease: pathology and pathogenesis. *Annu Rev Pathol.* 5, 145-71 (2010).
33. Perz JF, Armstrong GL, Farrington LA, Hutin YJ, Bell BP. The contributions of hepatitis B virus and hepatitis C virus infections to cirrhosis and primary liver cancer worldwide. *J Hepatol.* 45(4), 529-38 (2006).
34. Xiong J, Wang J, Huang J, Sun W, Wang J, Chen D. Non-alcoholic steatohepatitis-related liver cirrhosis is increasing in China: a ten-year retrospective study. *Clinics (Sao Paulo).* 70(8), 563-8 (2015).
35. Giannini E, Borro P, Botta F, Chiarbonello B, Fasoli A, Malfatti F, Romagnoli P, Testa E, Risso D, Lantieri PB, Antonucci A, Boccato M, Milone S, Testa R. Cholestasis is the Main Determinant of Abnormal CA 19–9 Levels in Patients with Liver Cirrhosis. *The International Journal of Biological Markers.* 15(3), 226-230 (2000).
36. Sid B, Verrax J, Calderon PB. Role of oxidative stress in the pathogenesis of alcohol-induced liver disease. *Free Radic Res.* 47(11), 894-904 (2013).
37. Anzenbacher P, Zanger UM, John W. *Metabolism of drugs and other xenobiotics*. Weinheim: Viley-VCH. (2012).
38. Radominska-Pandya A, Czernik PJ, Little JM, Battaglia E, Mackenzie PI. Structural and functional studies of UDP-glucuronosyltransferases. *Drug Metab Rev.* 31(4), 817-99 (1999).
39. Mackenzie PI. Expression of chimeric cDNAs in cell culture defines a region of UDP glucuronosyltransferase involved in substrate selection. *J Biol Chem.* 265(6), 3432-5 (1990).
40. Burchell B, Coughtrie MW. UDP-glucuronosyltransferases. *Pharmacol Ther.* 43(2), 261-89 (1989).
41. Mackenzie PI, Rodbourne L, Stranks S. Steroid UDP glucuronosyltransferases. *J Steroid Biochem Mol Biol.* 43(8), 1099-105 (1992).
42. Mackenzie PI, Bock KW, Burchell B, Guillemette C, Ikushiro S, Iyanagi T, Miners JO, Owens IS, Nebert DW. Nomenclature update for the mammalian UDP glycosyltransferase (UGT) gene superfamily. *Pharmacogenet Genomics.* 15(10), 677-85 (2005).
43. Tukey RH, Strassburg CP. Human UDP-glucuronosyltransferases: metabolism, expression, and disease. *Annu Rev Pharmacol Toxicol.* 40, 581-616 (2000).
44. Wooster R, Ebner T, Sutherland L, Clarke D, Burchell B. Drug and xenobiotic glucuronidation catalysed by cloned human liver UDP-Glucuronosyltransferases stably expressed in tissue culture cell lines. *Toxicology.* 82(1-3), 119-29 (1993).
45. Strassburg CP, Kalthoff S, Ehmer U. Variability and function of family 1 uridine-5'-diphosphate glucuronosyltransferases (UGT1A). *Crit Rev Clin Lab Sci.* 45(6), 485-530 (2008).
46. Mackenzie PI, Hu DG, Gardner-Stephen DA. The regulation of UDP-glucuronosyltransferase genes by tissue-specific and ligand-activated transcription factors. *Drug Metab Rev.* 42(1), 99-109 (2010).
47. Troberg J, Jarvinen E, Muniz M, Sneitz N, Mosorin J, Hagstrom M, Finel M. Dog UDP-glucuronosyltransferase enzymes of subfamily 1A: cloning, expression, and activity. *Drug Metab Dispos.* 43(1), 107-18 (2015).
48. Hu DG, Meech R, McKinnon RA, Mackenzie PI. Transcriptional regulation of human UDP-glucuronosyltransferase genes. *Drug Metab Rev.* 46(4), 421-58 (2014).
49. Gardner-Stephen DA, Mackenzie PI. Liver-enriched transcription factors and their role in regulating UDP glucuronosyltransferase gene expression. *Curr Drug Metab.* 9(5), 439-52 (2008).
50. Gregory PA, Lewinsky RH, Gardner-Stephen DA, Mackenzie PI. Coordinate regulation of the human UDP-glucuronosyltransferase 1A8, 1A9, and 1A10 genes by hepatocyte nuclear factor 1alpha and the caudal-related homeodomain protein 2. *Mol Pharmacol.* 65(4), 953-63 (2004).
51. Fiorucci S, Zampella A, Distrutti E. Development of FXR, PXR and CAR agonists and antagonists for treatment of liver disorders. *Curr Top Med Chem.* 12(6), 605-24 (2012).
52. Dawson MI, Xia Z. The retinoid X receptors and their ligands. *Biochim Biophys Acta.* 1821(1), 21-56 (2012).
53. Ramadoss P, Marcus C, Perdew GH. Role of the aryl hydrocarbon receptor in drug metabolism. *Expert Opin Drug Metab Toxicol.* 1(1), 9-21 (2005).
54. Murray IA, Patterson AD, Perdew GH. Aryl hydrocarbon receptor ligands in cancer: friend and foe. *Nat Rev Cancer.* 14(12), 801-14 (2014).

55. Yueh MF, Huang YH, Hiller A, Chen S, Nguyen N, Tukey RH. Involvement of the xenobiotic response element (XRE) in Ah receptor-mediated induction of human UDP-glucuronosyltransferase 1A1. *J Biol Chem.* 278(17), 15001-6 (2003).
56. Furukawa M, Xiong Y. BTB protein Keap1 targets antioxidant transcription factor Nrf2 for ubiquitination by the Cullin 3-Roc1 ligase. *Mol Cell Biol.* 25(1), 162-71 (2005).
57. Wu KC, Cui JY, Klaassen CD. Effect of graded Nrf2 activation on phase-I and -II drug metabolizing enzymes and transporters in mouse liver. *PLoS One.* 7(7), e39006 (2012).
58. Kalthoff S, Ehmer U, Freiberg N, Manns MP, Strassburg CP. Interaction between oxidative stress sensor Nrf2 and xenobiotic-activated aryl hydrocarbon receptor in the regulation of the human phase II detoxifying UDP-glucuronosyltransferase 1A10. *J Biol Chem.* 285(9), 5993-6002 (2010).
59. Nakamura A, Nakajima M, Yamanaka H, Fujiwara R, Yokoi T. Expression of UGT1A and UGT2B mRNA in human normal tissues and various cell lines. *Drug Metab Dispos.* 36(8), 1461-4 (2008).
60. Bosma PJ, Seppen J, Goldhoorn B, Bakker C, Oude Elferink RP, Chowdhury JR, Chowdhury NR, Jansen PL. Bilirubin UDP-glucuronosyltransferase 1 is the only relevant bilirubin glucuronidating isoform in man. *J Biol Chem.* 269(27), 17960-4 (1994).
61. Fang JL, Lazarus P. Correlation between the UDP-glucuronosyltransferase (UGT1A1) TATAA box polymorphism and carcinogen detoxification phenotype: significantly decreased glucuronidating activity against benzo(a)pyrene-7,8-dihydrodiol(-) in liver microsomes from subjects with the UGT1A1*28 variant. *Cancer Epidemiol Biomarkers Prev.* 13(1), 102-9 (2004).
62. Strassburg CP. Gilbert-Meulengracht's syndrome and pharmacogenetics: is jaundice just the tip of the iceberg? *Drug Metab Rev.* 42(1), 168-81 (2010).
63. Court MH, Zhang X, Ding X, Yee KK, Hesse LM, Finel M. Quantitative distribution of mRNAs encoding the 19 human UDP-glucuronosyltransferase enzymes in 26 adult and 3 fetal tissues. *Xenobiotica.* 42(3), 266-77 (2012).
64. Lankisch TO, Gillman TC, Erichsen TJ, Ehmer U, Kalthoff S, Freiberg N, Munzel PA, Manns MP, Strassburg CP. Aryl hydrocarbon receptor-mediated regulation of the human estrogen and bile acid UDP-glucuronosyltransferase 1A3 gene. *Arch Toxicol.* 82(9), 573-82 (2008).
65. Mojarrabi B, Butler R, Mackenzie PI. cDNA cloning and characterization of the human UDP glucuronosyltransferase, UGT1A3. *Biochem Biophys Res Commun.* 225(3), 785-90 (1996).
66. Erichsen TJ, Aehlen A, Ehmer U, Kalthoff S, Manns MP, Strassburg CP. Regulation of the human bile acid UDP-glucuronosyltransferase 1A3 by the farnesoid X receptor and bile acids. *J Hepatol.* 52(4), 570-8 (2010).
67. Green MD, Tephly TR. Glucuronidation of amine substrates by purified and expressed UDP-glucuronosyltransferase proteins. *Drug Metab Dispos.* 26(9), 860-7 (1998).
68. Green MD, Tephly TR. Glucuronidation of amines and hydroxylated xenobiotics and endobiotics catalyzed by expressed human UGT1.4 protein. *Drug Metab Dispos.* 24(3), 356-63 (1996).
69. Erichsen TJ, Ehmer U, Kalthoff S, Lankisch TO, Muller TM, Munzel PA, Manns MP, Strassburg CP. Genetic variability of aryl hydrocarbon receptor (AhR)-mediated regulation of the human UDP glucuronosyltransferase (UGT) 1A4 gene. *Toxicol Appl Pharmacol.* 230(2), 252-60 (2008).
70. Bock KW, Kohle C. UDP-glucuronosyltransferase 1A6: structural, functional, and regulatory aspects. *Methods Enzymol.* 400, 57-75 (2005).
71. Harding D, Fournel-Gigleux S, Jackson MR, Burchell B. Cloning and substrate specificity of a human phenol UDP-glucuronosyltransferase expressed in COS-7 cells. *Proc Natl Acad Sci U S A.* 85(22), 8381-5 (1988).
72. Krishnaswamy S, Duan SX, Von Moltke LL, Greenblatt DJ, Court MH. Validation of serotonin (5-hydroxtryptamine) as an in vitro substrate probe for human UDP-glucuronosyltransferase (UGT) 1A6. *Drug Metab Dispos.* 31(1), 133-9 (2003).
73. Bock KW, Forster A, Gschaidmeier H, Bruck M, Munzel P, Schareck W, Fournel-Gigleux S, Burchell B. Paracetamol glucuronidation by recombinant rat and human phenol UDP-glucuronosyltransferases. *Biochem Pharmacol.* 45(9), 1809-14 (1993).
74. Ciotti M, Basu N, Brangi M, Owens IS. Glucuronidation of 7-ethyl-10-hydroxycamptothecin (SN-38) by the human UDP-glucuronosyltransferases encoded at the UGT1 locus. *Biochem Biophys Res Commun.* 260(1), 199-202 (1999).
75. Guillemette C, Ritter JK, Auyeung DJ, Kessler FK, Housman DE. Structural heterogeneity at the UDP-glucuronosyltransferase 1 locus: functional consequences of three novel missense mutations in the human UGT1A7 gene. *Pharmacogenetics.* 10(7), 629-44 (2000).
76. Vogel A, Kneip S, Barut A, Ehmer U, Tukey RH, Manns MP, Strassburg CP. Genetic link of hepatocellular carcinoma with polymorphisms of the UDP-glucuronosyltransferase UGT1A7 gene. *Gastroenterology.* 121(5), 1136-44 (2001).

77. Ohno S, Nakajin S. Determination of mRNA expression of human UDP-glucuronosyltransferases and application for localization in various human tissues by real-time reverse transcriptase-polymerase chain reaction. *Drug Metab Dispos.* 37(1), 32-40 (2009).
78. Girard H, Villeneuve L, Court MH, Fortier LC, Caron P, Hao Q, von Moltke LL, Greenblatt DJ, Guillemette C. The novel UGT1A9 intronic I399 polymorphism appears as a predictor of 7-ethyl-10-hydroxycamptothecin glucuronidation levels in the liver. *Drug Metab Dispos.* 34(7), 1220-8 (2006).
79. Albert C, Vallee M, Beaudry G, Belanger A, Hum DW. The monkey and human uridine diphosphate-glucuronosyltransferase UGT1A9, expressed in steroid target tissues, are estrogen-conjugating enzymes. *Endocrinology.* 140(7), 3292-302 (1999).
80. Yueh MF, Nguyen N, Famourzadeh M, Strassburg CP, Oda Y, Guengerich FP, Tukey RH. The contribution of UDP-glucuronosyltransferase 1A9 on CYP1A2-mediated genotoxicity by aromatic and heterocyclic amines. *Carcinogenesis.* 22(6), 943-50 (2001).
81. Barbier O, Girard H, Inoue Y, Duez H, Villeneuve L, Kamiya A, Fruchart JC, Guillemette C, Gonzalez FJ, Staels B. Hepatic expression of the UGT1A9 gene is governed by hepatocyte nuclear factor 4alpha. *Mol Pharmacol.* 67(1), 241-9 (2005).
82. Gardner-Stephen DA, Mackenzie PI. Hepatocyte nuclear factor1 transcription factors are essential for the UDP-glucuronosyltransferase 1A9 promoter response to hepatocyte nuclear factor 4alpha. *Pharmacogenet Genomics.* 17(1), 25-36 (2007).
83. Munzel PA, Schmohl S, Heel H, Kalberer K, Bock-Hennig BS, Bock KW. Induction of human UDP glucuronosyltransferases (UGT1A6, UGT1A9, and UGT2B7) by t-butylhydroquinone and 2,3,7,8-tetrachlorodibenzo-p-dioxin in Caco-2 cells. *Drug Metab Dispos.* 27(5), 569-73 (1999).
84. Lee RC, Feinbaum RL, Ambros V. The C. elegans heterochronic gene lin-4 encodes small RNAs with antisense complementarity to lin-14. *Cell.* 75(5), 843-54 (1993).
85. Reinhart BJ, Slack FJ, Basson M, Pasquinelli AE, Bettinger JC, Rougvie AE, Horvitz HR, Ruvkun G. The 21-nucleotide let-7 RNA regulates developmental timing in Caenorhabditis elegans. *Nature.* 403(6772), 901-6 (2000).
86. Bartel DP. MicroRNAs: genomics, biogenesis, mechanism, and function. *Cell.* 116(2), 281-97 (2004).
87. Hutvagner G, Zamore PD. A microRNA in a multiple-turnover RNAi enzyme complex. *Science.* 297(5589), 2056-60 (2002).
88. Brennecke J, Hipfner DR, Stark A, Russell RB, Cohen SM. bantam encodes a developmentally regulated microRNA that controls cell proliferation and regulates the proapoptotic gene hid in Drosophila. *Cell.* 113(1), 25-36 (2003).
89. Xu P, Vernooy SY, Guo M, Hay BA. The Drosophila microRNA Mir-14 suppresses cell death and is required for normal fat metabolism. *Curr Biol.* 13(9), 790-5 (2003).
90. Chen CZ, Li L, Lodish HF, Bartel DP. MicroRNAs modulate hematopoietic lineage differentiation. *Science.* 303(5654), 83-6 (2004).
91. Palatnik JF, Allen E, Wu X, Schommer C, Schwab R, Carrington JC, Weigel D. Control of leaf morphogenesis by microRNAs. *Nature.* 425(6955), 257-63 (2003).
92. Friedlander MR, Lizano E, Houben AJ, Bezdan D, Banez-Coronel M, Kudla G, Mateu-Huertas E, Kagerbauer B, Gonzalez J, Chen KC, LeProust EM, Marti E, Estivill X. Evidence for the biogenesis of more than 1,000 novel human microRNAs. *Genome Biol.* 15(4), R57 (2014).
93. Chen Y, Xiao J, Zhang X, Bian X. MicroRNAs as key mediators of hepatic detoxification. *Toxicology.* 368-369, 80-90 (2016).
94. Stenvang J, Petri A, Lindow M, Obad S, Kauppinen S. Inhibition of microRNA function by antimiR oligonucleotides. *Silence.* 3(1), 1 (2012).
95. Friedman RC, Farh KK, Burge CB, Bartel DP. Most mammalian mRNAs are conserved targets of microRNAs. *Genome Res.* 19(1), 92-105 (2009).
96. Selbach M, Schwanhausser B, Thierfelder N, Fang Z, Khanin R, Rajewsky N. Widespread changes in protein synthesis induced by microRNAs. *Nature.* 455(7209), 58-63 (2008).
97. Manvati S, Mangalhara KC, Khan J, Pathania GL, Kaul S, Kaushik M, Arora A, Dhar PK. Deciphering the role of microRNA - A step by step guide. *Gene Expr Patterns.* 25-26, 59-65 (2017).
98. Ruby JG, Jan CH, Bartel DP. Intronic microRNA precursors that bypass Drosha processing. *Nature.* 448(7149), 83-6 (2007).
99. Lee Y, Kim M, Han J, Yeom KH, Lee S, Baek SH, Kim VN. MicroRNA genes are transcribed by RNA polymerase II. *Embo j.* 23(20), 4051-60 (2004).
100. Borchert GM, Lanier W, Davidson BL. RNA polymerase III transcribes human microRNAs. *Nat Struct Mol Biol.* 13(12), 1097-101 (2006).
101. Han J, Lee Y, Yeom KH, Nam JW, Heo I, Rhee JK, Sohn SY, Cho Y, Zhang BT, Kim VN. Molecular basis for the recognition of primary microRNAs by the Drosha-DGCR8 complex. *Cell.* 125(5), 887-901 (2006).

102. Lund E, Guttinger S, Calado A, Dahlberg JE, Kutay U. Nuclear export of microRNA precursors. *Science.* 303(5654), 95-8 (2004).
103. MacRae IJ, Ma E, Zhou M, Robinson CV, Doudna JA. In vitro reconstitution of the human RISC-loading complex. *Proc Natl Acad Sci U S A.* 105(2), 512-7 (2008).
104. Bernstein E, Caudy AA, Hammond SM, Hannon GJ. Role for a bidentate ribonuclease in the initiation step of RNA interference. *Nature.* 409(6818), 363-6 (2001).
105. Ma E, MacRae IJ, Kirsch JF, Doudna JA. Autoinhibition of human dicer by its internal helicase domain. *J Mol Biol.* 380(1), 237-43 (2008).
106. Cullen BR. Transcription and processing of human microRNA precursors. *Mol Cell.* 16(6), 861-5 (2004).
107. Khvorova A, Reynolds A, Jayasena SD. Functional siRNAs and miRNAs exhibit strand bias. *Cell.* 115(2), 209-16 (2003).
108. Meister G, Landthaler M, Patkaniowska A, Dorsett Y, Teng G, Tuschl T. Human Argonaute2 mediates RNA cleavage targeted by miRNAs and siRNAs. *Mol Cell.* 15(2), 185-97 (2004).
109. Winter J, Jung S, Keller S, Gregory RI, Diederichs S. Many roads to maturity: microRNA biogenesis pathways and their regulation. *Nat Cell Biol.* 11(3), 228-34 (2009).
110. Felekkis K, Touvana E, Stefanou C, Deltas C. microRNAs: a newly described class of encoded molecules that play a role in health and disease. *Hippokratia.* 14(4), 236-40 (2010).
111. Carthew RW, Sontheimer EJ. Origins and Mechanisms of miRNAs and siRNAs. *Cell.* 136(4), 642-55 (2009).
112. Brennecke J, Stark A, Russell RB, Cohen SM. Principles of microRNA-target recognition. *PLoS Biol.* 3(3), e85 (2005).
113. Wang XW, Heegaard NH, Orum H. MicroRNAs in liver disease. *Gastroenterology.* 142(7), 1431-43 (2012).
114. Xin X, Zhang Y, Liu X, Xin H, Cao Y, Geng M. MicroRNA in hepatic fibrosis and cirrhosis. *Front Biosci (Landmark Ed).* 19, 1418-24 (2014).
115. Szabo G, Csak T. Role of MicroRNAs in NAFLD/NASH. *Dig Dis Sci.* 61(5), 1314-24 (2016).
116. Murakami Y, Yasuda T, Saigo K, Urashima T, Toyoda H, Okanoue T, Shimotohno K. Comprehensive analysis of microRNA expression patterns in hepatocellular carcinoma and non-tumorous tissues. *Oncogene.* 25(17), 2537-45 (2006).
117. Vuppalanchi R, Liang T, Goswami CP, Nalamasu R, Li L, Jones D, Wei R, Liu W, Sarasani V, Janga SC, Chalasani N. Relationship between differential hepatic microRNA expression and decreased hepatic cytochrome P450 3A activity in cirrhosis. *PLoS One.* 8(9), e74471 (2013).
118. Bala S, Petrasek J, Mundkur S, Catalano D, Levin I, Ward J, Alao H, Kodys K, Szabo G. Circulating microRNAs in exosomes indicate hepatocyte injury and inflammation in alcoholic, drug-induced, and inflammatory liver diseases. *Hepatology.* 56(5), 1946-57 (2012).
119. Han ZB, Chen HY, Fan JW, Wu JY, Tang HM, Peng ZH. Up-regulation of microRNA-155 promotes cancer cell invasion and predicts poor survival of hepatocellular carcinoma following liver transplantation. *J Cancer Res Clin Oncol.* 138(1), 153-61 (2012).
120. Dluzen DF, Sun D, Salzberg AC, Jones N, Bushey RT, Robertson GP, Lazarus P. Regulation of UDP-glucuronosyltransferase 1A1 expression and activity by microRNA 491-3p. *J Pharmacol Exp Ther.* 348(3), 465-77 (2014).
121. Takagi S, Nakajima M, Kida K, Yamaura Y, Fukami T, Yokoi T. MicroRNAs regulate human hepatocyte nuclear factor 4alpha, modulating the expression of metabolic enzymes and cell cycle. *J Biol Chem.* 285(7), 4415-22 (2010).
122. Takagi S, Nakajima M, Mohri T, Yokoi T. Post-transcriptional regulation of human pregnane X receptor by micro-RNA affects the expression of cytochrome P450 3A4. *J Biol Chem.* 283(15), 9674-80 (2008).
123. Oda Y, Nakajima M, Tsuneyama K, Takamiya M, Aoki Y, Fukami T, Yokoi T. Retinoid X receptor alpha in human liver is regulated by miR-34a. *Biochem Pharmacol.* 90(2), 179-87 (2014).
124. Papageorgiou I, Freytsis M, Court MH. Transcriptome association analysis identifies miR-375 as a major determinant of variable acetaminophen glucuronidation by human liver. *Biochem Pharmacol.* 117, 78-87 (2016).
125. Wang H, Peng R, Wang J, Qin Z, Xue L. Circulating microRNAs as potential cancer biomarkers: the advantage and disadvantage. *Clin Epigenetics.* 10(59) (2018).
126. Calin GA, Sevignani C, Dumitru CD, Hyslop T, Noch E, Yendamuri S, Shimizu M, Rattan S, Bullrich F, Negrini M, Croce CM. Human microRNA genes are frequently located at fragile sites and genomic regions involved in cancers. *Proc Natl Acad Sci U S A.* 101(9), 2999-3004 (2004).
127. Croce CM. Causes and consequences of microRNA dysregulation in cancer. *Nat Rev Genet.* 10(10), 704-14 (2009).

128. Nazarenko I, Rupp AK, Altevogt P. Exosomes as a potential tool for a specific delivery of functional molecules. *Methods Mol Biol.* 1049, 495-511 (2013).
129. Mitchell PS, Parkin RK, Kroh EM, Fritz BR, Wyman SK, Pogosova-Agadjanyan EL, Peterson A, Noteboom J, O'Briant KC, Allen A, Lin DW, Urban N, Drescher CW, Knudsen BS, Stirewalt DL, Gentleman R, Vessella RL, Nelson PS, Martin DB, Tewari M. Circulating microRNAs as stable blood-based markers for cancer detection. *Proc Natl Acad Sci U S A.* 105(30), 10513-8 (2008).
130. Shen J, Stass SA, Jiang F. MicroRNAs as potential biomarkers in human solid tumors. *Cancer Lett.* 329(2), 125-36 (2013).
131. Kroh EM, Parkin RK, Mitchell PS, Tewari M. Analysis of circulating microRNA biomarkers in plasma and serum using quantitative reverse transcription-PCR (qRT-PCR). *Methods.* 50(4), 298-301 (2010).
132. Wang K, Zhang S, Marzolf B, Troisch P, Brightman A, Hu Z, Hood LE, Galas DJ. Circulating microRNAs, potential biomarkers for drug-induced liver injury. *Proc Natl Acad Sci U S A.* 106(11), 4402-7 (2009).
133. Huang YH, Liang KH, Chien RN, Hu TH, Lin KH, Hsu CW, Lin CL, Pan TL, Ke PY, Yeh CT. A Circulating MicroRNA Signature Capable of Assessing the Risk of Hepatocellular Carcinoma in Cirrhotic Patients. *Sci Rep.* 7(1), 523 (2017).
134. Szabo G, Bala S. MicroRNAs in liver disease. *Nat Rev Gastroenterol Hepatol.* 10(9), 542-52 (2013).
135. Braconi C, Henry JC, Kogure T, Schmittgen T, Patel T. The role of microRNAs in human liver cancers. *Semin Oncol.* 38(6), 752-63 (2011).
136. Arrese M, Eguchi A, Feldstein AE. Circulating microRNAs: emerging biomarkers of liver disease. *Semin Liver Dis.* 35(1), 43-54 (2015).
137. Jansen C, Eischeid H, Goertzen J, Schierwagen R, Anadol E, Strassburg CP, Sauerbruch T, Odenthal M, Trebicka J. The role of miRNA-34a as a prognostic biomarker for cirrhotic patients with portal hypertension receiving TIPS. *PLoS One.* 9(7), e103779 (2014).
138. Austermann C, Schierwagen R, Mohr R, Anadol E, Klein S, Pohlmann A, Jansen C, Strassburg CP, Schwarze-Zander C, Boesecke C, Rockstroh JK, Odenthal M, Trebicka J. microRNA-200a: A stage-dependent biomarker and predictor of steatosis and liver cell injury in human immunodeficiency virus patients. *Hepatol Commun.* 1(1), 36-45 (2017).
139. Ehmer U, Kalthoff S, Fakundiny B, Pabst B, Freiberg N, Naumann R, Manns MP, Strassburg CP. Gilbert syndrome redefined: a complex genetic haplotype influences the regulation of glucuronidation. *Hepatology.* 55(6), 1912-21 (2012).
140. Hoek JB, Pastorino JG. Ethanol, oxidative stress, and cytokine-induced liver cell injury. *Alcohol.* 27(1), 63-8 (2002).
141. Kong LB, Ren WG, Mi HM, Zhao SX, Zhang YG, Nan YM. [Establishment of a complex alcoholic liver fibrosis mouse model and investigation of OPN and TGF-beta1 hepatic expression]. *Zhonghua Gan Zang Bing Za Zhi.* 21(3), 207-12 (2013).
142. Kalthoff S, Landerer S, Reich J, Strassburg CP. Protective effects of coffee against oxidative stress induced by the tobacco carcinogen benzo[alpha]pyrene. *Free Radic Biol Med.* 108, 66-76 (2017).
143. Chang T-H, Huang H-Y, Hsu JB-K, Weng S-L, Horng J-T, Huang H-D. An enhanced computational platform for investigating the roles of regulatory RNA and for identifying functional RNA motifs. *BMC Bioinformatics.* 14(2), S4 (2013).
144. Krek A, Grun D, Poy MN, Wolf R, Rosenberg L, Epstein EJ, MacMenamin P, da Piedade I, Gunsalus KC, Stoffel M, Rajewsky N. Combinatorial microRNA target predictions. *Nat Genet.* 37(5), 495-500 (2005).
145. Betel D, Wilson M, Gabow A, Marks DS, Sander C. The microRNA.org resource: targets and expression. *Nucleic Acids Research.* 36(suppl_1), D149-D153 (2008).
146. Rehmsmeier M, Steffen P, Hochsmann M, Giegerich R. Fast and effective prediction of microRNA/target duplexes. *Rna.* 10(10), 1507-17 (2004).
147. Kubista M, Andrade JM, Bengtsson M, Forootan A, Jonak J, Lind K, Sindelka R, Sjoback R, Sjogreen B, Strombom L, Stahlberg A, Zoric N. The real-time polymerase chain reaction. *Mol Aspects Med.* 27(2-3), 95-125 (2006).
148. Sahi J, Grepper S, Smith C. Hepatocytes as a tool in drug metabolism, transport and safety evaluations in drug discovery. *Curr Drug Discov Technol.* 7(3), 188-98 (2010).
149. Szultka-Mlynska M, Buszewski B. Study of in-vitro metabolism of selected antibiotic drugs in human liver microsomes by liquid chromatography coupled with tandem mass spectrometry. *Anal Bioanal Chem.* 408(29), 8273-8287 (2016).
150. Bradford MM. A rapid and sensitive method for the quantitation of microgram quantities of protein utilizing the principle of protein-dye binding. *Anal Biochem.* 72, 248-54 (1976).
151. Hnasko TS, Hnasko RM. The Western Blot. *Methods Mol Biol.* 1318, 87-96 (2015).

152. Dalby B, Cates S, Harris A, Ohki EC, Tilkins ML, Price PJ, Ciccarone VC. Advanced transfection with Lipofectamine 2000 reagent: primary neurons, siRNA, and high-throughput applications. *Methods.* 33(2), 95-103 (2004).
153. Felgner PL, Gadek TR, Holm M, Roman R, Chan HW, Wenz M, Northrop JP, Ringold GM, Danielsen M. Lipofection: a highly efficient, lipid-mediated DNA-transfection procedure. *Proc Natl Acad Sci U S A.* 84(21), 7413-7 (1987).
154. Yang JP, Huang L. Time-dependent maturation of cationic liposome-DNA complex for serum resistance. *Gene Ther.* 5(3), 380-7 (1998).
155. McNabb DS, Reed R, Marciniak RA. Dual luciferase assay system for rapid assessment of gene expression in Saccharomyces cerevisiae. *Eukaryot Cell.* 4(9), 1539-49 (2005).
156. Castell JV, Jover R, Martínez-Jiménez CP, Gómez-Lechón MJ. Hepatocyte cell lines: their use, scope and limitations in drug metabolism studies. *Expert Opin Drug Metab Toxicol.* 2(2), 183-212 (2006).
157. Donato MT, Lahoz A, Castell JV, Gómez-Lechón MJ. Cell lines: a tool for in vitro drug metabolism studies. *Curr Drug Metab.* 9(1), 1-11 (2008).
158. Knowles BB, Howe CC, Aden DP. Human hepatocellular carcinoma cell lines secrete the major plasma proteins and hepatitis B surface antigen. *Science.* 209(4455), 497-9 (1980).
159. Donato MT, Tolosa L, Gómez-Lechón MJ. Culture and Functional Characterization of Human Hepatoma HepG2 Cells. *Methods Mol Biol.* 1250, 77-93 (2015).
160. Wong ML, Medrano JF. Real-time PCR for mRNA quantitation. *Biotechniques.* 39(1), 75-85 (2005).
161. Luo X, Gu X, Li L. Development of a simple and efficient method of harvesting and lysing adherent mammalian cells for chemical isotope labeling LC-MS-based cellular metabolomics. *Anal Chim Acta.* 1037, 97-106 (2018).
162. Brunelle JL, Green R. One-dimensional SDS-polyacrylamide gel electrophoresis (1D SDS-PAGE). *Methods Enzymol.* 541, 151-9 (2014).
163. Goldman A, Harper S, Speicher DW. Detection of Proteins on Blot Membranes. *Curr Protoc Protein Sci.* 86, 10.8.1-10.8.11 (2016).
164. Bandiera S, Pfeffer S, Baumert TF, Zeisel MB. miR-122--a key factor and therapeutic target in liver disease. *J Hepatol.* 62(2), 448-57 (2015).
165. Sabolovic N, Humbert AC, Radominska-Pandya A, Magdalou J. Resveratrol is efficiently glucuronidated by UDP-glucuronosyltransferases in the human gastrointestinal tract and in Caco-2 cells. *Biopharm Drug Dispos.* 27(4), 181-9 (2006).
166. Aravalli RN. Development of MicroRNA Therapeutics for Hepatocellular Carcinoma. *Diagnostics (Basel).* 3(1), 170-91 (2013).
167. Moya M, Gómez-Lechón MJ, Castell JV, Jover R. Enhanced steatosis by nuclear receptor ligands: a study in cultured human hepatocytes and hepatoma cells with a characterized nuclear receptor expression profile. *Chem Biol Interact.* 184(3), 376-87 (2010).
168. Tanaka T, Dancheck BL, Trifiletti LC, Birnkrant RE, Taylor BJ, Garfield SH, Thorgeirsson U, De Luca LM. Altered localization of retinoid X receptor alpha coincides with loss of retinoid responsiveness in human breast cancer MDA-MB-231 cells. *Mol Cell Biol.* 24(9), 3972-82 (2004).
169. Attia SM. Deleterious effects of reactive metabolites. *Oxid Med Cell Longev.* 3(4), 238-53 (2010).
170. Varkonyi-Gasic E, Wu R, Wood M, Walton EF, Hellens RP. Protocol: a highly sensitive RT-PCR method for detection and quantification of microRNAs. *Plant Methods.* 3(12) (2007).
171. Chen C, Ridzon DA, Broomer AJ, Zhou Z, Lee DH, Nguyen JT, Barbisin M, Xu NL, Mahuvakar VR, Andersen MR, Lao KQ, Livak KJ, Guegler KJ. Real-time quantification of microRNAs by stem-loop RT-PCR. *Nucleic Acids Res.* 33(20), e179 (2005).
172. Davis S, Lollo B, Freier S, Esau C. Improved targeting of miRNA with antisense oligonucleotides. *Nucleic Acids Res.* 34(8), 2294-304 (2006).
173. Garzon R, Marcucci G, Croce CM. Targeting microRNAs in cancer: rationale, strategies and challenges. *Nat Rev Drug Discov.* 9(10), 775-89 (2010).
174. Bhogal RH, Hodson J, Bartlett DC, Weston CJ, Curbishley SM, Haughton E, Williams KT, Reynolds GM, Newsome PN, Adams DH, Afford SC. Isolation of primary human hepatocytes from normal and diseased liver tissue: a one hundred liver experience. *PLoS One.* 6(3), e18222 (2011).
175. Ritter JK, Crawford JM, Owens IS. Cloning of two human liver bilirubin UDP-glucuronosyltransferase cDNAs with expression in COS-1 cells. *J Biol Chem.* 266(2), 1043-7 (1991).
176. Marcuello E, Altes A, Menoyo A, Del Rio E, Gomez-Pardo M, Baiget M. UGT1A1 gene variations and irinotecan treatment in patients with metastatic colorectal cancer. *Br J Cancer.* 91(4), 678-82 (2004).
177. Bosma PJ, Chowdhury JR, Bakker C, Gantla S, de Boer A, Oostra BA, Lindhout D, Tytgat GN, Jansen PL, Oude Elferink RP, et al. The genetic basis of the reduced expression of bilirubin UDP-glucuronosyltransferase 1 in Gilbert's syndrome. *N Engl J Med.* 333(18), 1171-5 (1995).

178. Wasserman E, Myara A, Lokiec F, Goldwasser F, Trivin F, Mahjoubi M, Misset JL, Cvitkovic E. Severe CPT-11 toxicity in patients with Gilbert's syndrome: two case reports. *Ann Oncol.* 8(10), 1049-51 (1997).
179. Trottier J, Verreault M, Grepper S, Monté D, Bélanger J, Kaeding J, Caron P, Inaba TT, Barbier O. Human UDP-glucuronosyltransferase (UGT)1A3 enzyme conjugates chenodeoxycholic acid in the liver. *Hepatology.* 44(5), 1158-70 (2006).
180. Liedtke C, Luedde T, Sauerbruch T, Scholten D, Streetz K, Tacke F, Tolba R, Trautwein C, Trebicka J, Weiskirchen R. Experimental liver fibrosis research: update on animal models, legal issues and translational aspects. *Fibrogenesis Tissue Repair.* 6(1), 19 (2013).
181. Billington D, Evans CE, Godfrey PP, Coleman R. Effects of bile salts on the plasma membranes of isolated rat hepatocytes. *Biochem J.* 188(2), 321-7 (1980).
182. Ogawa T, Enomoto M, Fujii H, Sekiya Y, Yoshizato K, Ikeda K, Kawada N. MicroRNA-221/222 upregulation indicates the activation of stellate cells and the progression of liver fibrosis. *Gut.* 61(11), 1600-9 (2012).
183. Copple BL, Jaeschke H, Klaassen CD. Oxidative stress and the pathogenesis of cholestasis. *Semin Liver Dis.* 30(2), 195-204 (2010).
184. Xu T, Li L, Hu HQ, Meng XM, Huang C, Zhang L, Qin J, Li J. MicroRNAs in alcoholic liver disease: Recent advances and future applications. *J Cell Physiol.* 234(1), 382-394 (2018).
185. Noetel A, Kwiecinski M, Elfimova N, Huang J, Odenthal M. microRNA are Central Players in Anti- and Profibrotic Gene Regulation during Liver Fibrosis. *Front Physiol.* 3(49) (2012).
186. Hong JS, Lee DH, Yook YW, Na D, Jang YJ, Kim JH, Lee YS. MicroRNA signatures associated with thioacetamide-induced liver fibrosis in mice. *Biosci Biotechnol Biochem.* 81(7), 1348-1355 (2017).
187. Tarao K, Nozaki A, Ikeda T, Sato A, Komatsu H, Komatsu T, Taguri M, Tanaka K. Real impact of liver cirrhosis on the development of hepatocellular carcinoma in various liver diseases-meta-analytic assessment. *Cancer Med.* 8(3), 1054-1065 (2019).
188. Connolly E, Melegari M, Landgraf P, Tchaikovskaya T, Tennant BC, Slagle BL, Rogler LE, Zavolan M, Tuschl T, Rogler CE. Elevated expression of the miR-17-92 polycistron and miR-21 in hepadnavirus-associated hepatocellular carcinoma contributes to the malignant phenotype. *Am J Pathol.* 173(3), 856-64 (2008).
189. Bachran C, Bachran S, Sutherland M, Bachran D, Fuchs H. Saponins in tumor therapy. *Mini Rev Med Chem.* 8(6), 575-84 (2008).
190. Baird WM, Hooven LA, Mahadevan B. Carcinogenic polycyclic aromatic hydrocarbon-DNA adducts and mechanism of action. *Environ Mol Mutagen.* 45(2-3), 106-14 (2005).
191. Deng C, Dang F, Gao J, Zhao H, Qi S, Gao M. Acute benzo[a]pyrene treatment causes different antioxidant response and DNA damage in liver, lung, brain, stomach and kidney. *Heliyon.* 4(11), e00898 (2018).
192. Phillips DH. Polycyclic aromatic hydrocarbons in the diet. *Mutat Res.* 443(1-2), 139-47 (1999).
193. Su Y, Zhao B, Guo F, Bin Z, Yang Y, Liu S, Han Y, Niu J, Ke X, Wang N, Geng X, Jin C, Dai Y, Lin Y. Interaction of benzo[a]pyrene with other risk factors in hepatocellular carcinoma: a case-control study in Xiamen, China. *Ann Epidemiol.* 24(2), 98-103 (2014).
194. Larson AM. Acetaminophen hepatotoxicity. *Clin Liver Dis.* 11(3), 525-48, vi (2007).
195. Bala S, Marcos M, Kodys K, Csak T, Catalano D, Mandrekar P, Szabo G. Up-regulation of microRNA-155 in macrophages contributes to increased tumor necrosis factor {alpha} (TNF{alpha}) production via increased mRNA half-life in alcoholic liver disease. *J Biol Chem.* 286(2), 1436-44 (2011).
196. Gooderham NJ, Creton S, Lauber SN, Zhu H. Mechanisms of action of the carcinogenic heterocyclic amine PhIP. *Toxicol Lett.* 168(3), 269-77 (2007).
197. Jakszyn P, Agudo A, Ibáñez R, García-Closas R, Pera G, Amiano P, González CA. Development of a food database of nitrosamines, heterocyclic amines, and polycyclic aromatic hydrocarbons. *J Nutr.* 134(8), 2011-4 (2004).
198. Strassburg CP, Vogel A, Kneip S, Tukey RH, Manns MP. Polymorphisms of the human UDP-glucuronosyltransferase (UGT) 1A7 gene in colorectal cancer. *Gut.* 50(6), 851-6 (2002).
199. Tang KS, Lee CM, Teng HC, Huang MJ, Huang CS. UDP-glucuronosyltransferase 1A7 polymorphisms are associated with liver cirrhosis. *Biochem Biophys Res Commun.* 366(3), 643-8 (2008).
200. Tseng CS, Tang KS, Lo HW, Ker CG, Teng HC, Huang CS. UDP-glucuronosyltransferase 1A7 genetic polymorphisms are associated with hepatocellular carcinoma risk and onset age. *Am J Gastroenterol.* 100(8), 1758-63 (2005).
201. Fujita K, Kubota Y, Ishida H, Sasaki Y. Irinotecan, a key chemotherapeutic drug for metastatic colorectal cancer. *World J Gastroenterol.* 21(43), 12234-48 (2015).
202. Mathijssen RH, van Alphen RJ, Verweij J, Loos WJ, Nooter K, Stoter G, Sparreboom A. Clinical pharmacokinetics and metabolism of irinotecan (CPT-11). *Clin Cancer Res.* 7(8), 2182-94 (2001).

203. Villeneuve L, Girard H, Fortier LC, Gagné JF, Guillemette C. Novel functional polymorphisms in the UGT1A7 and UGT1A9 glucuronidating enzymes in Caucasian and African-American subjects and their impact on the metabolism of 7-ethyl-10-hydroxycamptothecin and flavopiridol anticancer drugs. *J Pharmacol Exp Ther.* 307(1), 117-28 (2003).
204. Feng L, Jing L, Han J, Wang G, Liu Y, Zhang X, Wang Y, Wang F, Ma H, Liu Y. MicroRNA 486-3p directly targets BIK and regulates apoptosis and invasion in colorectal cancer cells. *Onco Targets Ther.* 11, 8791-8801 (2018).
205. Kansaku F, Kumai T, Sasaki K, Yokozuka M, Shimizu M, Tateda T, Murayama N, Kobayashi S, Yamazaki H. Individual differences in pharmacokinetics and pharmacodynamics of anesthetic agent propofol with regard to CYP2B6 and UGT1A9 genotype and patient age. *Drug Metab Pharmacokinet.* 26(5), 532-7 (2011).
206. Ramírez J, Iyer L, Journault K, Bélanger P, Innocenti F, Ratain MJ, Guillemette C. In vitro characterization of hepatic flavopiridol metabolism using human liver microsomes and recombinant UGT enzymes. *Pharm Res.* 19(5), 588-94 (2002).
207. Bernard O, Guillemette C. The main role of UGT1A9 in the hepatic metabolism of mycophenolic acid and the effects of naturally occurring variants. *Drug Metab Dispos.* 32(8), 775-8 (2004).
208. Mutlib AE, Goosen TC, Bauman JN, Williams JA, Kulkarni S, Kostrubsky S. Kinetics of acetaminophen glucuronidation by UDP-glucuronosyltransferases 1A1, 1A6, 1A9 and 2B15. Potential implications in acetaminophen-induced hepatotoxicity. *Chem Res Toxicol.* 19(5), 701-9 (2006).
209. Iizuka M, Ogawa T, Enomoto M, Motoyama H, Yoshizato K, Ikeda K, Kawada N. Induction of microRNA-214-5p in human and rodent liver fibrosis. *Fibrogenesis Tissue Repair.* 5(1), 12 (2012).
210. Wang P, Nie YL, Wang SJ, Yang LL, Yang WH, Li JF, Li XT, Zhang LR. Regulation of UGT1A expression by miR-298 in human livers from the Han Chinese population and in human cell lines. *Epigenomics.* 10(1), 43-57 (2018).
211. Li Z, Xu R, Li N. MicroRNAs from plants to animals, do they define a new messenger for communication? *Nutr Metab (Lond).* 15(68) (2018).
212. Li QS, Meng FY, Zhao YH, Jin CL, Tian J, Yi XJ. Inhibition of microRNA-214-5p promotes cell survival and extracellular matrix formation by targeting collagen type IV alpha 1 in osteoblastic MC3T3-E1 cells. *Bone Joint Res.* 6(8), 464-471 (2017).
213. Tsai WC, Hsu SD, Hsu CS, Lai TC, Chen SJ, Shen R, Huang Y, Chen HC, Lee CH, Tsai TF, Hsu MT, Wu JC, Huang HD, Shiao MS, Hsiao M, Tsou AP. MicroRNA-122 plays a critical role in liver homeostasis and hepatocarcinogenesis. *J Clin Invest.* 122(8), 2884-97 (2012).
214. Lankisch TO, Vogel A, Eilermann S, Fiebeler A, Krone B, Barut A, Manns MP, Strassburg CP. Identification and characterization of a functional TATA box polymorphism of the UDP glucuronosyltransferase 1A7 gene. *Mol Pharmacol.* 67(5), 1732-9 (2005).
215. Kutay H, Bai S, Datta J, Motiwala T, Pogribny I, Frankel W, Jacob ST, Ghoshal K. Downregulation of miR-122 in the rodent and human hepatocellular carcinomas. *J Cell Biochem.* 99(3), 671-8 (2006).
216. Li Y, Masaki T, Yamane D, McGivern DR, Lemon SM. Competing and noncompeting activities of miR-122 and the 5' exonuclease Xrn1 in regulation of hepatitis C virus replication. *Proc Natl Acad Sci U S A.* 110(5), 1881-6 (2013).
217. Place RF, Li LC, Pookot D, Noonan EJ, Dahiya R. MicroRNA-373 induces expression of genes with complementary promoter sequences. *Proc Natl Acad Sci U S A.* 105(5), 1608-13 (2008).
218. Xiao M, Li J, Li W, Wang Y, Wu F, Xi Y, Zhang L, Ding C, Luo H, Li Y, Peng L, Zhao L, Peng S, Xiao Y, Dong S, Cao J, Yu W. MicroRNAs activate gene transcription epigenetically as an enhancer trigger. *RNA Biol.* 14(10), 1326-1334 (2017).
219. Long D, Lee R, Williams P, Chan CY, Ambros V, Ding Y. Potent effect of target structure on microRNA function. *Nat Struct Mol Biol.* 14(4), 287-94 (2007).
220. Peng L, Zhong X. Epigenetic regulation of drug metabolism and transport. *Acta Pharm Sin B.* 5(2), 106-12 (2015).
221. Zanger UM, Schwab M. Cytochrome P450 enzymes in drug metabolism: regulation of gene expression, enzyme activities, and impact of genetic variation. *Pharmacol Ther.* 138(1), 103-41 (2013).
222. Bianchi M, Renzini A, Adamo S, Moresi V. Coordinated Actions of MicroRNAs with other Epigenetic Factors Regulate Skeletal Muscle Development and Adaptation. *Int J Mol Sci.* 18(4), (2017).
223. Oda S, Fukami T, Yokoi T, Nakajima M. Epigenetic regulation is a crucial factor in the repression of UGT1A1 expression in the human kidney. *Drug Metab Dispos.* 41(10), 1738-43 (2013).
224. Fernandes JCR, Acuña SM, Aoki JI, Floeter-Winter LM, Muxel SM. Long Non-Coding RNAs in the Regulation of Gene Expression: Physiology and Disease. *Noncoding RNA.* 5(1), (2019).
225. Honkakoski P, Negishi M. Regulation of cytochrome P450 (CYP) genes by nuclear receptors. *Biochem J.* 347(Pt 2), 321-37 (2000).

226. Zhou J, Zhang J, Xie W. Xenobiotic nuclear receptor-mediated regulation of UDP-glucuronosyl-transferases. *Curr Drug Metab.* 6(4), 289-98 (2005).
227. Olsen PH, Ambros V. The lin-4 regulatory RNA controls developmental timing in Caenorhabditis elegans by blocking LIN-14 protein synthesis after the initiation of translation. *Dev Biol.* 216(2), 671-80 (1999).
228. Wightman B, Ha I, Ruvkun G. Posttranscriptional regulation of the heterochronic gene lin-14 by lin-4 mediates temporal pattern formation in C. elegans. *Cell.* 75(5), 855-62 (1993).
229. Osna NA, Donohue TM Jr., Kharbanda KK. Alcoholic Liver Disease: Pathogenesis and Current Management. *Alcohol Res.* 38(2), 147-161 (2017).
230. Seitz HK, Bataller R, Cortez-Pinto H, Gao B, Gual A, Lackner C, Mathurin P, Mueller S, Szabo G, Tsukamoto H. Alcoholic liver disease. *Nat Rev Dis Primers.* 4(1), 16 (2018).
231. Rehm J, Samokhvalov AV, Shield KD. Global burden of alcoholic liver diseases. *J Hepatol.* 59(1), 160-8 (2013).
232. Bishehsari F, Magno E, Swanson G, Desai V, Voigt RM, Forsyth CB, Keshavarzian A. Alcohol and Gut-Derived Inflammation. *Alcohol Res.* 38(2), 163-171 (2017).
233. Fukui H. Gut-liver axis in liver cirrhosis: How to manage leaky gut and endotoxemia. *World J Hepatol.* 7(3), 425-42 (2015).
234. Richardson TA, Sherman M, Kalman D, Morgan ET. Expression of UDP-glucuronosyltransferase isoform mRNAs during inflammation and infection in mouse liver and kidney. *Drug Metab Dispos.* 34(3), 351-3 (2006).
235. Weber LW, Boll M, Stampfl A. Hepatotoxicity and mechanism of action of haloalkanes: carbon tetrachloride as a toxicological model. *Crit Rev Toxicol.* 33(2), 105-36 (2003).
236. Kamiyama Y, Matsubara T, Yoshinari K, Nagata K, Kamimura H, Yamazoe Y. Role of human hepatocyte nuclear factor 4alpha in the expression of drug-metabolizing enzymes and transporters in human hepatocytes assessed by use of small interfering RNA. *Drug Metab Pharmacokinet.* 22(4), 287-98 (2007).
237. Megiorni F, Cialfi S, Dominici C, Quattrucci S, Pizzuti A. Synergistic post-transcriptional regulation of the Cystic Fibrosis Transmembrane conductance Regulator (CFTR) by miR-101 and miR-494 specific binding. *PLoS One.* 6(10), e26601 (2011).
238. van Rooij E, Purcell AL, Levin AA. Developing microRNA therapeutics. *Circ Res.* 110(3), 496-507 (2012).
239. Titze-de-Almeida R, David C, Titze-de-Almeida SS. The Race of 10 Synthetic RNAi-Based Drugs to the Pharmaceutical Market. *Pharm Res.* 34(7), 1339-1363 (2017).

Publications

1. Steffen Landerer, Sandra Kalthoff, Stefan Paulusch, Christian P. Strassburg. UDP-glucuronosyltransferase polymorphisms affect diethylnitrosamine-induced carcinogenesis in humanized transgenic mice. *Cancer Sci.* (2020).
2. Steffen Landerer, Sandra Kalthoff, Stefan Paulusch, Christian P. Strassburg. A Gilbert syndrome-associated haplotype protects against fatty liver disease in humanized transgenic mice. *Sci Rep.* 10(1):8689, (2020).
3. Sandra Kalthoff, Stefan Paulusch, Alexander Rupp, Stefan Holdenrieder, Gunther Hartmann, Christian P. Strassburg. The coffee ingredients caffeic acid and caffeic acid phenylethyl ester protect against irinotecan-induced leukopenia and oxidative stress response. *Br J Pharmacol.* 177(18), 4193-4208 (2020).
4. Richard H. Little, Stuart D. Woodcock, Rosaria Campilongo, Rowena K.Y. Fung, Robert Heal, Libby Humphries, Alba Pacheco-Moreno, Stefan Paulusch, Egidio Stigliano, Eleni Vikeli, Danny Ward, Jacob G. Malone. Differential regulation of genes for cyclic-di-GMP metabolism orchestrates adaptive changes during rhizosphere colonization by *Pseudomonas fluorescens*. *Front Microbiol.* 10:1089, (2019).